Long-term Changes in the Indo-Sri Lankan Upwelling System, a Perspective to Study the Impact of Climate Change in a Tropical Ocean

by

PARVATHY V S

(2015-20-011)

THESIS

Submitted in partial fulfillment of the

requirements for the degree of

B.Sc. – M.Sc. (Integrated) Climate Change Adaptation

Faculty of Agriculture

Kerala Agricultural University

ACADEMY OF CLIMATE CHANGE EDUCATION AND RESEARCH

VELLANIKKARA, THRISSUR – 680 656

KERALA, INDIA

2020

DECLARATION

I, Parvathy, V. S. (2014 – 20 – 105) hereby declare that this thesis entitled **"Long-term Changes in the Indo-Sri Lankan Upwelling System, a Perspective to Study the Impact of Climate Change in a Tropical Ocean"** is a bonafide record of research work done by me during the course of research and the thesis has not previously formed the basis for the award to me of any degree, diploma, associateship, fellowship or other similar title, of any other University or Society.

Place: Vellanikkara — Parvathy V S

Date: — (2015-20-011)

CERTIFICATE

Certified that this thesis entitled **"Long-term Changes in the Indo-Sri Lankan Upwelling System, a Perspective to Study the Impact of Climate Change in a Tropical Ocean"** is a record of research work done independently by Miss. Parvathy, V.S. under my guidance and supervision and that it has not previously formed the basis for the award of any degree, diploma, fellowship or associateship to her.

Place: Vellanikkara
Date:

Mr. Muraleedharan K.R.
Principal Scientist
Physical Oceanography Department
CSIR-National Institute of
Oceanography (NIO),
Regional Center, Kochi
Ernakulam-682018

CERTIFICATE

We, the undersigned members of the advisory committee of Miss. Parvathy, V.S., a candidate for the degree of **B.Sc – M.Sc (Integrated) Climate Change Adaptation** agree that the thesis entitled **"Long-term Changes in the Indo-Sri Lankan Upwelling System, a Perspective to Study the Impact of Climate Change in a Tropical Ocean"** may be submitted by Miss. Parvathy, V.S. in partial fulfillment of the requirement for the degree.

Mr. Muraleedharan K.R.
Principal Scientist
Physical Oceanography Department
CSIR-National Institute of
Oceanography (NIO),
Regional Center, Kochi
Ernakulam-682018

Dr. P.O. Nameer
(Member, Advisory Committee)
Special Officer
Academy of Climate Change Education
and Research (ACCER),
Kerala Agricultural University
Vellanikkara, Thrissure-680656

Dr. Madhu N.V.
Senior Scientist
CSIR-National Institute of
Oceanography (NIO),
Regional Center, Kochi
Ernakulam-682018

Dr. Phiros Shah
Assistant Professor
Kerala University of Fisheries and Ocean
Studies (KUFOS)
Panangad
Ernakulam-682506

(EXTERNAL EXAMINER)

ACKNOWLEDGEMENT

First and foremost, I would like to thank ***Almighty God*** *for giving me the strength, knowledge, ability and opportunity to undertake this research study and to persevere and complete it satisfactorily.*

I would like to express my sincere gratitude and obligation to ***Mr. Muraleedharan K.R.,*** *Pricnipal Scientist, Physical Oceanography Department, CSIR-National Institute of Oceanography (NIO), Regional Centre (RC), Kochi, and my mentor, for his sincere guidance, motivation, patience and unconditional support, which enabled me to complete my M.Sc thesis work successfully.*

I would like to convey my sincere gratitude to my advisory committee members, ***Dr. P.O. Nameer,*** *Special Officer, Academy of Climate Change Education and Research (ACCER), KAU,* ***Dr. Madhu N.V.,*** *Senior Scientist, NIO-RC, Kochi, and* ***Dr. Phiros Shah,*** *Assistant Professor, Kerala University of Fisheries and Ocean Studies for sparing their valuable time to help me conduct my thesis smoothly and for their constant encouragement.*

I extend my sincere gratitude to ***Dr. Dinesh Kumar,*** *Scientist in Charge and Chief Scientist, NIO-RC, Kochi for letting me undertake this work at the institute. I respectfully thank* ***Dr. C. Revichandran,*** *Chief Scientist, NIO-RC, Kochi.*

I express my heartfelt thanks to ***Mr. Sebin John,*** *Project Scientist-C, India Meteorological Department, New Delhi, for being my unofficial mentor. I sincerely thank* ***Mr. Abdul Azeez S.,*** *Project Associate, NIO-RC, Kochi, for his valuable help and guidance.*

I would like to extend my heartfelt thanks to ***Mrs. Seena G.,*** *PhD Scholar, NIO-RC, Kochi and Project Associates at NIO-RC, Kochi,* ***Ms. Manju K. G.*** *and* ***Mr. Ravikumar C. Nair,*** *for their support and encouragement.*

I would also like to convey my sincere thanks to ***Mr. Panini Dasgupta,*** *PhD scholar, Indian Institute of Tropical Meteorology (IITM), Pune, for his valuable help. I am thankful to* ***Ms. Saranya J. S, Ms. Athira K. S., Ms. Resna K., Ms. Swathy S.*** *and each and every one of my batchmates for their cooperation and moral support. I also thank* ***Mr. Jineesh V. K.,*** *Assistant Professor, ACCER, for his constant support.*

*I am grateful to **Academy of Climate Change Education and Research** for providing me the opportunity to undertake this work. I would like to thank all the teaching and non-teaching staffs of ACCER for their help and support. I am greatly indebted to the **National Institute of Oceanography** and the Director for providing me all the resources needed for my research programme. I thank each and every staffs of NIO-RC, Kochi for their cooperation.*

*Last, but not the least, I express my everlasting gratitude to **my parents and my big brother** for being my strength and inspiration and for every opportunities that they have paved for me with their sacrifices.*

Parvathy V S

TABLE OF CONTENTS

LIST OF TABLES

LIST OF FIGURES

SYMBOLS AND ABBREVIATIONS

APDRC	Asia-Pacific Data Research Center
AVHRR	Advanced Very High Resolution Radiometer
CbPM	Carbon-based Productivity Model
CMFRI	Central Marine Fisheries Research Institute
CWC	Central Water Commission
D26	Depth of 26°C isotherm
ECMWF	European Center for Medium-Range Weather Forecast
ENSO	El Nino Southern Oscillation
FVCOM	Finite Volume Community Ocean Model
GOF	Global Ocean Forecasting System
HYCOM	Hybrid Coordinate Ocean Model
IOD	Indian Ocean Dipole
ITF	Indonesian Throughflow
LTA	Local Temperature Anomaly
MHW	Marine Heat Wave
MJO	Madden Julian Oscillation
MPI	Message Passing Interface
MSL	Mean Sea Level
NCODA	Navy Coupled Ocean Data Assimilation
NOAA	National Oceanic and Atmospheric Administration
NPP	Net Primary Productivity
ONI	Oceanic Nino Index
OTCZ	Oceanic Tropical Convergence Zone
RMSD	Root Mean Square Deviation
SLA	Sea Level Anomaly
SSHA	Sea Surface Height Anomaly
SSS	Sea Surface Salinity
SST	Sea Surface Temperature

CHAPTER 1

INTRODUCTION

70% of the earth's surface is occupied by vast oceans which contribute about 46.2% of the total annual global Net Primary Productivity (NPP) (Field et al, 1998). About 54.8 million people worldwide are dependent on fisheries and aquaculture for their livelihood and income, with Asia accounting for more than 87%. During 2005 to 2010, on an average, about 52% of the total marine fish catch was reported from areas including the Eastern Central Atlantic, Northeast Pacific, Eastern Central Pacific, Southwest Atlantic, Southeast Pacific and Northwest Pacific. These are the areas which showed highest variability in total fish catch, many of which is known to have upwelling phenomena, hence characterized by high natural variability (FAO, 2012).

Among the several types of upwelling, induced by different factors, wind-driven upwelling is the most important. In the Northern Hemisphere (Southern Hemisphere), the surface winds are expected to move the surface water to the right (left) with the net transport of water at an angle of 90° to the wind direction which is termed as Ekman transport. The surface winds induce upwelling via Ekman transport. Coastal upwelling, equatorial upwelling and ice-edge upwelling are the three main forms of wind-driven upwelling (Kampf and Chapman, 2016). Coastal upwelling occurs near the coast when the surface winds blowing parallel to the coast induce offshore Ekman transport, bringing up the subsurface water to the surface. Equatorial upwelling is generated by the prevailing trade winds which result in divergence at the equator due to the change in the sign of the Coriolis parameter on either sides of the equator. Ice-edge upwelling results from the reducing effect of wind stress on the currents under the sea ice. As the subsurface water is colder and nutrient-rich than the surface water, upwelling supports high biological activity, thereby making the region highly productive. Among the three forms of wind-driven upwelling, coastal upwelling has direct impact on fisheries as most of the major fishing grounds are associated with these coastal upwelling systems. About 25% of the reported marine fish catches are contributed by the five major upwelling systems of the world, which covers only 5% of the total ocean area (Smitha, 2010).

The major upwelling regions over the world include coasts of California, Peru, Chile, northwest and southwest Africa and Portugal which are also known as eastern boundary upwelling regions. Seasonal upwelling is observed along the coasts of Somalia, Oman, Sumatra, South China Sea and along the southwest coast of India. The highest level of productivity is expected to observe at moderate upwelling intensity (Optimal Environmental Window hypothesis). When the intensity of upwelling is high, the biota will be advected offshore while low intensity upwelling brings up insufficient nutrients to the surface, both resulting in low productivity (Cury and Roy, 1989).

Global climate change seems to have an impact on the upwelling since it is expected to affect the global wind patterns. Bakun (1990) suggested an enhancement of offshore Ekman transport and associated upwelling due to climate change and global warming which would result in the intensification of the upwelling favorable winds. Hsieh and Boer (1992) stated that the Bakun hypothesis cannot be true globally. The impact of climate change varies regionally, even in the regions with similar oceanographic processes, which implies that the upwelling processes can be impacted by several other regional factors. For instance, El Nino Southern Oscillation (ENSO) is known to have an impact on the upwelling along the Peru coast, declining the Peruvian anchovy population, thereby impacting the global annual fish catch. Hence it is important to study upwelling phenomena regionally.

In the case of Indian Ocean, upwelling is usually observed in three regions: off the coasts of Somalia-Oman, Sumatra and southwest coast of India, all being seasonal phenomena associated with the summer monsoon winds. The upwelling in the western Indian Ocean accounts for the relatively cooler Sea Surface Temperature (SST) at the region during the period. It is observed that despite the cooling brought by the upwelling, the warming due to increased CO2 emission has become dominant after 1995 (Kumar et al., 2009). Indian Ocean Dipole (IOD) as well as El Nino Southern Oscillation (ENSO) are expected to have impacts on the Indian Ocean SST. The western Indian Ocean has been observed to be warming for more than a century, thereby triggering more number of IOD events (Rao et al., 2012). Frolicher et al. (2018) stated that under present global warming scenario, the incidence of Marine Heat Waves (MHW) will become more frequent across the globe, with the maximum increase expected in the tropics. The continuing warming and increased incidence of marine heat waves in the tropics might have an impact on the upwelling processes in the Indian Ocean. Praveen et al. (2016) observed a shift

in both the magnitude and direction of winds over the western Arabian Sea which demarcates it into two zones of increased and decreased southwesterly winds along the Oman coast and the Somali coast respectively. They also suggested an enhancement in the marine productivity in the western Arabian Sea due to the net upwelling increase along the Oman coast as a result of the enhanced winds. The mentioned changes in the southwesterly winds can bring about changes in the southeastern Arabian Sea upwelling also. This study is focused on the long-term variability in the upwelling along the southwest coast of India.

India has a long coastline of about 7600 km which is known to have large fishery potential. Majority of the coastal population in the country is mainly dependent on these coastal waters for their livelihood. Hence the coastal upwelling along the southwest coast of India is of great importance when it comes to fisheries in India and its economy. When compared globally, southeastern Arabian Sea upwelling is much smaller in both intensity and extent and is produced as a result of monsoon winds, which reverse its direction seasonally. The southwest monsoon winds being parallel to the west coast and southern tip of the Indian Subcontinent, induce upwelling along the west coast of India, with maximum upwelling observed between Kollam and Kochi, which progressively weakens northwards (Smitha et al., 2008). Southeastern Arabian Sea upwelling is observed to commence in June, coincident with the onset of summer monsoon, peaks by July-August and dissipates by September. The west coast of India contributes to majority of the Indian marine fisheries with both the northwest and southwest coast contributing almost equally (CMFRI Annual Report 2017-18). CMFRI Annual Report 2018-19 pointed out an enhancement in the chlorophyll concentration in southeastern Arabian Sea region which seemed to overlap with the upwelling period. And also, the southwest coast of India is the region where the unique phenomenon of mudbank is observed to occur in association with the summer monsoon, making the coast highly productive and providing the fishermen safe fishing grounds. The mudbank is considered to occur as a result of coastal upwelling. Hence the marine fish catch of India is expected to be dependent on the upwelling process along the southwest coast.

Upwelling intensity cannot be measured directly and hence certain indices are used. Since coastal upwelling is generated by offshore Ekman transport, it is used as the primary indicator of coastal upwelling. Sea Surface Temperature (SST) at the coastal region is another indicator as the process brings cold subsurface water to the surface, creating a difference in

coastal and offshore SST. Upwelling is also indicated by the reduction in the sea level height and the upward movement of isotherms.

The main objective of this study is to understand the long-term changes in the southwesterly winds during the summer monsoon and the upwelling intensity along the southwest coast of India and also to identify the major factors which control spatio-temporal variability of the coastal upwelling system.

Finite Volume Community Ocean Model (FVCOM) was ran for 'with wind' and 'without wind' condition to understand the role of wind on the upwelling along the southwest coast of India. The model results confirmed that the upwelling along the region is primarily caused by the wind during the summer monsoon season. The study also revealed the influence of wind speed and direction on the upwelling intensity. The upwelling indices for a period of 19 years, from 2000 to 2018 were analyzed to understand the trend in upwelling intensity. No significant trends are observed in the upwelling intensity except for the inter-annual variations. Oceanic Nino Indiex and the annual rainfall of India are analyzed to understand the probable reason for the inter-annual variations. The SST and wind speed over the southeast Arabian Sea during the monsoon season did not show considerable changes for the past two decades but the Mean Sea Level has observed to rise during the period.

CHAPTER 2

Review of Literature

2.1. UPWELLING

Upwelling is the process by which water from the subsurface water is brought to the surface to replace the surface water which has been displaced by horizontal flow. The upwelled water will be colder and nutrient-rich than the surface water and hence it enhances the production of phytoplanktons through the process of photosynthesis. This makes the upwelling region highly productive.

Two important upwelling processes are observed in the ocean, one being the slow upwelling of cold abyssal water to compensate the surface water sinking in the Polar Regions and the other being the upwelling of subsurface waters to balance the surface water displacement due to winds (Smitha and Sajeev, 2010). Coastal upwelling, open ocean upwelling and equatorial upwelling are the three major types of upwelling observed globally. Coastal upwelling occurs near the coast when the surface winds take the surface water away from the shore. In the Northern Hemisphere, the coastal upwelling is induced by along-shore wind component when the seaward side of the coast is towards the right of an observer looking in the downwind direction (Garvine, 1971). The surface water moves to the right (left) in the Northern Hemisphere (Southern Hemisphere), with the net transport of water at an angle of 90° to the direction of wind which is termed as Ekman transport. When the Ekman transport moves the surface water offshore, the colder, denser and nutrient-rich water from the bottom replaces the surface water and paves way to coastal upwelling. Wind induced divergence of surface waters causes upwelling in the open ocean which is referred to as open ocean upwelling. Downwelling, the process of sinking of surface waters, adjacent to the upwelling region is the characteristics of open ocean upwelling. Equatorial upwelling occurs when the easterlies blowing along the Inter-Tropical Convergence Zone (ITCZ) in both Atlantic and Pacific basins move the surface water away from the equator, bringing dense, nutrient-rich water from below to the surface, leading to enhanced primary production. Of all types of upwelling, coastal upwelling is most significant since it is directly related to fisheries. From the five major upwelling systems of the world, which

covers only 5% of the total ocean area, about 25% of the total global marine fish catches are reported (Smitha and Sajeev, 2010).

The process of upwelling has been observed to occur most favourably when the coast is on the left-hand (right-hand) side of a person who looks in the wind direction in the Northern Hemisphere (Southern Hemisphere) and upwelling is intense when the wind blows at an angle of 21.5° with the coast (Hidaka and Series, 1954).

The major coastal upwelling zones over the globe occur along the coasts of California, northwestern Africa, southwestern Africa and Peru of western South America (Bakun, 2016). Among these upwelling zones, upwelling along the Peruvian coast which is in the Pacific basin is particularly impacted by the El Nino Southern Oscillation (ENSO) (Bakun *et al.*, 2015). ENSO suppresses the upwelling along the Peruvian coast due to the warm water that flows from the western Pacific, declining the fish catch along the coast.

2.2. UPWELLING IN THE INDIAN OCEAN

Due to the reversal of winds between summer and winter, a reversal of upwelling and downwelling is observed in the Indian Ocean, with a predominantly downwelling band north of 5°N in January which gradually become predominantly upwelling band in July (Xie and Hsieh, 1995). In the Indian Ocean, upwelling is observed mainly at three locations: along the coasts of Java and Sumatra, Somalia-Oman and southwest India which are considered small scale when compared to the major global coastal upwelling zones. All these upwelling systems are associated with the southwest monsoon.

The establishment of an intense low-level wind jet during the summer monsoon, known as the Findlater Jet induces open ocean upwelling in the northern Indian Ocean along the Somalia-Oman coasts. This upwelling is also influenced by the reflected Rossby waves, the absence of which triggers the weakening of the westward zonal current during the boreal fall, thereby hindering the flow of warmer water to the upwelling region, reducing the SST by about 0.4°C. Changes in the SST alters the along-shore winds over the region which in turn influence the coastal upwelling (Tozuka et al., 2014).

The equatorial Indian Ocean upwelling occurs along the coasts of Sumatra and Java during the summer monsoon, from June to October by the influence of southeasterly monsoon

winds from Australia, which eventually ceases with the reversal of winds. The upwelling generated by the equatorial easterlies is enhanced by the strong local along-shore wind that is observed during May to October. The propagation of equatorial and coastal Kelvin waves also have an impact on the upwelling occurring in this region (Chen *et al.*, 2016).

Weak-to-moderate upwelling occurs along the southwest coast of India with the southwest monsoon onset, starting from the southern tip of India, gradually reaching up to Goa by July-August. The southwest monsoon winds which usually blow from the southwest direction over most parts of the Arabian Sea become north-northwesterly along the west coast of India due to the influence of Western Ghats, resulting in offshore Ekman transport and associated upwelling (Smitha *et al.*, 2008). This is less intense than those occurring at other parts of the Indian Ocean but still it accounts for about 53% of the total Arabian Sea fish yield (Jayaram *et al.*, 2010).

2.3. UPWELLING OFF SOUTHWEST COAST OF INDIA

Along the southwest coast of India, upwelling is an annually recurring phenomenon during the southwest monsoon. The major cause of the upwelling is the divergence caused by the southward positive wind stress curl along the Indian coast (McCreary et al., 1993). Along the eastern boundary of the Arabian Sea, the wind stress component due to summer monsoon winds which is almost directly onshore is towards the equator, resulting in an offshore component of Ekman transport. The upwelling can be identified by surface cooling, coastal sea level fall and rapid upward movement of isotherms occurring from May to September (Smitha and Sajeev, 2010).

According to the study conducted by McCreary et al. in 1993, the upwelling along the southwest coast of India is observed to commence in June, by the beginning of the summer monsoon and its signals are first observed in the southern latitudes which gradually spreads towards the North along with coastally trapped Kelvin waves. It is also observed that cooling occurs in the entire southwest coast and south of India and peaks by July-August with the minimum Sea Surface Temperature (SST) at the southern tip of India and the cooling dissipates by the end of the summer monsoon, by September. Gupta et al. (2016), in the study conducted over the southeastern Arabian Sea shelf, states that the upwelling initiates in the deeper layers

during January-March and it progresses to the upper layers in the following months (June-September). The intensification takes about 4 months (from April to July) while it collapses within a month.

The study conducted by Smitha et al. (2014) along the southwest coast of India for the years 2009 and 2010 states that offshore Ekman mass transport can be evidenced by February/March but the intensity and the chlorophyll concentration is found to be highest during the time of summer monsoon which emphasize the importance of wind speed in coastal upwelling process. The maximum upwelling along the southwest coast of India is observed to occur between 8°N and 14°N. During the period between October and February, the southern tip of India experience strong upwelling while it is moderate along the southwest coast.

The west coast of India contributes to majority of the Indian marine fisheries, with both the northwest and southwest coast contributing almost equally (CMFRI Annual Report 2017-18). CMFRI Annual Report 2018-19 pointed out an enhancement in the chlorophyll concentration in southeastern Arabian Sea region which seemed to overlap with the upwelling period.

2.4. SEA LEVEL HEIGHT VARIABILITY

Two pairs of upwelling and downwelling Kelvin waves are observed to evolve in the Equatorial Indian Ocean and Bay of Bengal which propagate eastward alternately along the equator during a year. The first and second upwelling Kelvin waves originate in the west and east Equatorial Indian Ocean respectively while the first and second downwelling Kelvin waves originate in the Central Equatorial Indian Ocean. They bifurcate into two branches, one propagating northward and the other southward as they hit the Sumatra coast. Among these Kelvin waves, the second downwelling Kelvin wave is the most pronounced as it reaches all the way to the southeast Arabian Sea, travelling along the Bay of Bengal coastal wave guide. This is favoured by the equatorward flowing East India Coastal Current while the first upwelling and downwelling Kelvin waves are opposed by clockwise rotating eddy circulation at the head of Bay of Bengal and poleward flowing East India Coastal Current. The annual variations in the equatorial zonal winds are expected to reflect in the Sea Surface Height Anomaly (SSHA) through the eastward propagating Kelvin waves (Rao et al, 2010). During El Nino years, the second downwelling Kelvin wave is observed to be absent while the second upwelling Kelvin

wave is observed to strengthen. The second upwelling Kelvin Wave will be weak during La Nina years. Sreenivas et al. (2012), in their study concluded that the seasonal sea level changes in the coastal Bay of Bengal and the central Bay of Bengal are governed by the corresponding characteristic Kelvin waves and by the Rossby waves radiated from the eastern boundary in the last season, respectively.

Swapna et al. (2017) pointed out that during the last 3-4 decades, the sea level in the north Indian Ocean is observed to be on rise, especially in the Arabian Sea. The reason for this rise is attributed to the enhanced heat storage due to reduced southward ocean heat transport as a result of weakening monsoon circulation.

At the Cochin coast, the monthly mean sea level variation is about 20 cm annually and the sea level at Veraval, Marmagao and Cochin is observed to decrease during the monsoon period when the rainfall is considerably high which suggest that the contribution of rain runoff to the sea level change is small (Shetye, 2016).

2.5. EL NINO SOUTHERN OSCILLATION

El Nino Southern Oscillation is a coupled ocean-atmospheric phenomenon observed in the Pacific Ocean characterized by a see-saw pattern of reversing surface air pressure (known as the Southern Oscillation) and the corresponding changes in the SST pattern (known as the El Nino).

In a normal year, the easterly trade winds over the tropical Pacific take surface water westwards, warming it further, causing upwelling in the Peru coast and accumulation of warm water in the western Pacific. When the trade winds weaken or reverse the direction, the warm water from the western Pacific flows eastwards giving rise to an El Nino event, hindering the upwelling along the Peru coast. After a mature phase of El Nino, a basin-wide warming is expected to occur in the Indian Ocean (Nigam and Shen, 1993). The Rossby waves produced during an ENSO event which propagate from the east, along with the simultaneous presence of upwelling and shallow thermocline induces an SST variability in the western tropical South Indian Ocean (Xie et al., 2002). This SST variability induces changes in the Indo-Pacific Walker circulation thereby causing delay in the Indian Summer Monsoon (Annamalai et al., 2005).

While the El Nino is considered as the warm extreme of ENSO, La Nina is the cold extreme. La Nina is an intensified situation of the normal condition which is characterized by enhanced upwelling along the Peru coast. During prolonged La Nina events in 1973-76 and 1998-2001, the southwest tropical Indian Ocean showed maximum cooling which was influenced not only by thermodynamics or heat flux but mainly by the westward propagating upwelling Rossby waves and local Ekman transport which favors the upwelling (Singh, Chowdary and Gnanaseelan, 2013).

The study conducted by Miyakawa et al. (2017) on the abrupt termination of the super-intense 1997/1998 El Nino revealed the extensive interaction between El Nino and Madden Julian Oscillation (MJO). They reconfirmed the existing theory that the easterly winds over the central to east Pacific is extensively enhanced by the main MJO convective envelope situated near the Maritime Continent which in turn strengthen the surface upwelling, thereby terminating the El Nino.

2.6. INDIAN OCEAN DIPOLE

Indian Ocean Dipole (IOD) is a coupled ocean-atmospheric phenomenon in which the western basin of the Indian Ocean becomes warmer than normal while the eastern basin becomes cooler than normal, resulting in increased rainfall over tropical eastern Africa and the western Indian Ocean and decreased rainfall over the Indonesian archipelago causing severe drought. The surface wind field over the tropical Indian Ocean, mainly the east-to-west component over the equatorial central and eastern part experiences large changes during a dipole mode event (Saji *et al.*, 1999). Two phases of IOD are defined – one being the positive phase where the western Indian Ocean warms while the eastern Indian Ocean cools and the other being the negative phase which is the opposite condition.

The anomalies associated with the IOD are observed to commence around June, intensifying in the following months and peaking dramatically in October. A normal year is characterized by the convergence of southeast trade winds in the South Equatorial Trough resulting in high rainfall over Oceanic Tropical Convergence Zone (OTCZ) while a dipole mode event weakens the convection at OTCZ and the winds converge further downstream causing the rainfall anomalies (Saji *et al.*, 1999).

The growth of an IOD event seems to be affected by the ENSO and the Java-Sumatra upwelling. The stronger than normal easterly winds along the Java coast enhances the upwelling along the coast, increasing the local cooling (Meyers et al., 2006).

The study conducted by Iskandar et al. (2010) on the eddy-induced Chlorophyll in the southeastern Indian Ocean during 2006 IOD event revealed that the surface Chlorophyll-a bloom occurs if the Deep Chlorophyll Maximum is located above the Mixed Layer Depth and otherwise, the bloom is suppressed. Hence the surface Chlorophyll concentration is dependent on Mixed Layer Depth. George et al. (2013) reconfirmed this connection and they also stated that the Deep Chlorophyll maximum is determined by nitracline or thermocline depth, which in turn depend predominantly on Ekman pumping and Rossby waves.

Upwelling occurs along the Sumatra coast during a positive IOD event causing positive Sea Surface Salinity (SSS) anomaly in the region. This anomaly will further be enhanced by the reduced rainfall which is caused as a result of changes in the atmospheric circulation. However, all the positive and negative SSS anomaly peaks do not coincide with the positive and negative dipole events. A few of the positive SSS peaks can occur during, or shortly after El Nino events as the atmospheric patterns associated with them are favourable for creating high SSS values. Similarly, the negative anomaly peaks, which do not coincide with negative dipole events can occur during La Nina events, as the atmospheric circulation patterns at the time can induce higher than normal precipitation over the region thereby reducing the SSS value (Grunseich et al., 2011).

Most of the El Nino events are accompanied by an IOD event as strong El Nino is expected to trigger the development of IOD. During the years when the El Nino anomalies begin to appear early in the preceding winter season, the IOD is observed to be weak, while during the years when the anomalies appear in the spring-summer season, an enhanced positive IOD is observed. This is because the El Nino induces anomalous anti-cyclonic circulation over the southeastern Indian Ocean which brings about some changes in the climatological winds, thereby warming the eastern Indian Ocean (Roxy et al., 2011).

The numerical experiments conducted by Yuan et al. (2011) show that the IOD event reduces the sea level in the eastern Indian Ocean and establishes a stronger eastward pressure gradient across the Indonesian sea. This results in an enhanced Indonesian Throughflow (ITF)

which tends to produce an upper ocean heat content deficit by transporting warm water into the eastern Indian Ocean from the far western Pacific Ocean. The ITF inter-annual variations impact the Pacific ocean-atmosphere coupled system through equatorial wave propagation, which amplifies the upwelling anomalies in the Indonesian seas.

During 2006-2008, three consecutive positive IOD events were reported with the strongest one in 2006. The event during 2007 was weaker and short-lived. 2008 positive IOD event was reported to develop in April, matured in June and terminated in September. The 2008 event ended abruptly, mainly due to the eastern-boundary-reflected upwelling Rossby waves which developed an eastward zonal current along the equator leading to the termination of zonal heat advection, thereby creating a warming tendency in the eastern equatorial Indian Ocean (Iskandar et al., 2013).

Wang and Yuan (2015) studied the negative IOD events and suggested that the downwelling anomalies in the eastern IO during a negative IOD event is terminated by the Rossby waves reflected from the western boundary and the easterly wind anomalies. They also hypothesized that during the 1996-97 negative IOD, the easterly wind anomalies generated by the interactions of the Hadley cell and Walker cell which are induced by the persistent downwelling state in the equatorial IO terminate the downwelling anomalies in the east.

2.7. CLIMATE CHANGE AND GLOBAL UPWELLING

Bakun (1990) suggested an enhancement of offshore Ekman transport and thereby associated upwelling, due to climate change and global warming which would result in the intensification of the upwelling favourable winds. Hsieh and Boer (1992) stated that the Bakun hypothesis cannot be true globally. The impact of climate change varies globally even in regions with similar oceanographic processes. Among the five major upwelling zones over the world, coastal areas of Benguela, Peru, Canary and northern California witnessed an increasing trend in upwelling while a decreasing trend was observed along Chile, southern and central California, and central Somalia coasts (Varela et al., 2015).

As per the study conducted by Xie & Hsieh in 1995, the upwelling in the upwelling regions as well as the downwelling in the downwelling regions seemed to intensify during the

period from 1950 to 1988, mainly in boreal winter rather than in boreal summer and the anomaly corresponds to the intensified wind.

Manjusha et al. (2013), from the study conducted along the southwest coast of India, pointed out that while different species of pelagic fishes respond to the prevailing environmental conditions in different ways, the herbivorous small pelagic fishes are expected to benefit from the current global warming trend. The results also showed nearly 50% increase in the coastal upwelling along the southwest coast of India during southwest monsoon.

Praveen et al. (2016) observed a shift in both the magnitude and direction of winds over the western Arabian Sea which demarcates it into two zones of increased and decreased southwesterly winds along the Oman coast and the Somali coast respectively. They also suggested an enhancement in the marine productivity in the western Arabian Sea due to the net upwelling increases along the Oman coast as a result of the enhanced winds.

2.8. INDIAN OCEAN WARMING

In the study conducted by Cadet (1985) on the Southern Oscillation over the Indian Ocean, a cycle with a period of about 40 months in the eastern Indian Ocean and about 30 months in the western part is described, the origin of which is marked by high pressure, low cloudiness and strong zonal winds. The zonal winds decreases and the SST and air temperature increase in the following 7-8 months. The minimum pressure is reached when the cycle reaches half way. It is also noticed in this study that some of the Indian Ocean warming events (in the year when El Nino related warming occurs) coincide with the Pacific Ocean warming while some are not associated with the Pacific Ocean warming events. Preceding a warming event, a decrease of trade wind intensity over the Pacific and Indian Ocean and a reduction in convective activity over the eastern Indian Ocean are expected. The variations in the intensity of each warming event are observed to be more uniform over the Indian Ocean than that of the Pacific Ocean. Since the periodicity differs in the western and eastern parts of the Indian Ocean, certain events that are significant in the western part will be insignificant in the eastern part. Some results also showed that the anomalies propagate to the east over the Indian Ocean.

The Indian Ocean has been observed to be warming throughout the past five decades and the Western Indian Ocean for more than a century. During summer monsoon, due to the strong monsoon winds and the associated upwelling, the western Indian Ocean generally has cooler sea

surface temperatures than the rest of the Indian Ocean. The Indian Ocean warm pool has been observed to be warming and expanding. Rao et al. (2012) proposed a coupled ocean-atmosphere feedback mechanism which suggested that the warming of the Indian Ocean is expected to enhance the convection over the west central equatorial Indian Ocean and thereby strengthens the anomalous easterlies. This can trigger more number of IOD events. And also, the downwelling oceanic Rossby waves triggered by the anticyclonic wind stress curl is expected to deepen the thermocline, thereby further warming the Indian Ocean and expanding the Indian Ocean Warm Pool.

A study conducted by Kumar et al. (2009) revealed a decadal scale variability in the annual mean SST of the Arabian Sea basin which is driven by upwelling. The SST anomaly cycle shows a slow warming trend in the period between 1960-1995 and then a disruption is observed afterwards, which cannot be attributed to the natural changes in solar activity. Hence it is assumed that despite the cooling brought by the upwelling, the warming due to increased CO_2 emission has become dominant after 1995.

El Nino results in low-level easterly anomalies over the western Indian Ocean leading to warming by weakening the mean westerlies while La Nina does not show any significant cooling anomalies (Roxy et al., 2014). Rapid warming of Indian Ocean enhances the ocean stratification and thereby hinders the mixing of nutrients from the subsurface layers to the euphotic zone. As a result, during the past six decades, a decline of about 20% in the marine phytoplankton was pointed out by Roxy et al. (2016), with large declining rate during the last 16 years.

Dong and McPhaden (2016) pointed out an interhemispheric SST gradient in the Indian Ocean during the recent global warming hiatus, with an increased warming trend in the region south of 10°S and relatively weaker trend in the northern part. The main reason for this gradient is attributed to the enhanced Indonesian Throughflow (ITF) which is expected to reduce the vertical mixing by depressing the thermocline in the southern part, thereby hindering the cooling of the surface water. When compared to the pre-hiatus decade, the enhanced ITF and the associated thermocline deepening is responsible for 70% of the recent warming trend. The positive wind stress curl between 10°S and 20°S and the negative wind stress curl between the equator and 10°S due to changes in Walker circulation induced anomalous downwelling and anomalous upwelling respectively in the respective regions. Also, the intensified coastal

upwelling along the Somalia coast due to anomalous southwesterly wind stress adds up to the condition.

2.9. MARINE HEAT WAVES

Frolicher et al. (2018) stated that under present global warming scenario, the incidence of Marine Heat Waves (MHW) will become more frequent across the globe, with the maximum increase expected in the tropics and the Arctic Ocean while in the Southern Ocean, it is the lowest. They also stated the global warming as the reason for 87% of the MHW occurring recently. Oliver et al. (2018) found that the occurrence of MHW and their duration have increased by 34% and 17% globally which contributed to 54% increase in the annual MHW days. Rahmstorf and Coumou (2011) stated that the Moscow MHW in 2010 occurred only due to climate warming. In 2013-2015, northeast Pacific region experienced a large MHW which is reported to be the strongest MHW since 1982. Cheung and Frolicher (2020) stated that MHW can double the magnitude of impact of long-term climate change on the fish stocks by 2050.

CHAPTER 3

MATERIALS AND METHODS

3.1. STUDY AREA

The area used for the study is the part of the western Arabian Sea within 5°N & 20°N latitudes 65°E & 80°E longitudes.

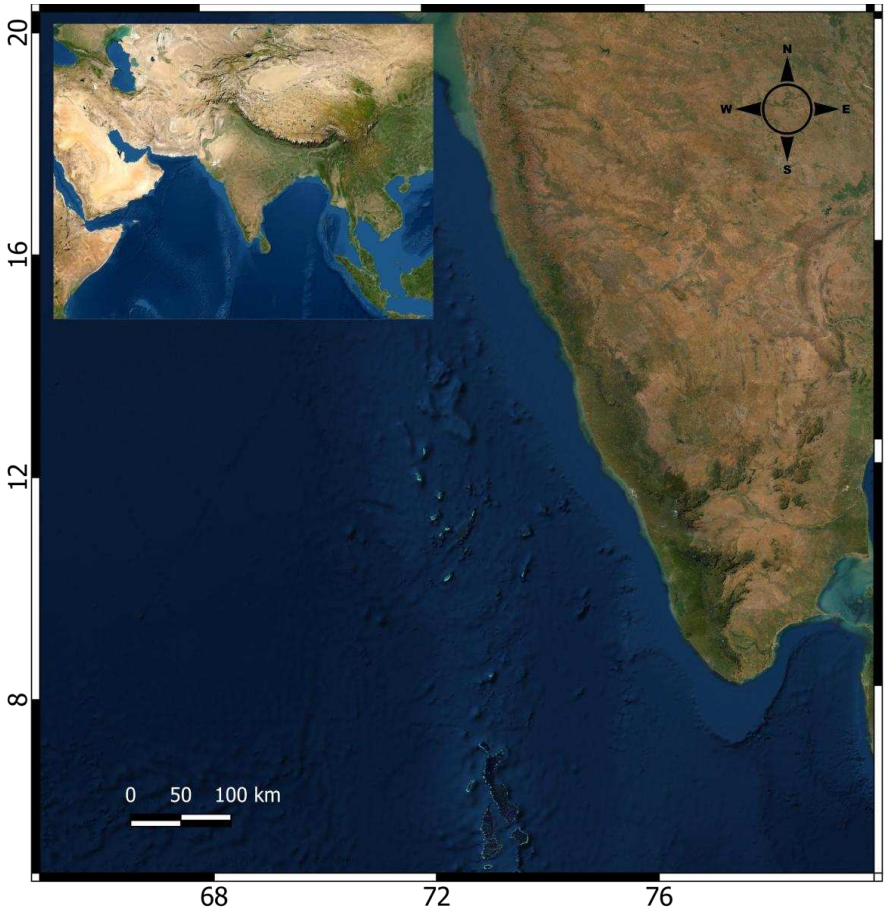

Figure 3.1. Study area – southeast Arabian Sea

The Arabian Sea is characterized by seasonally reversing wind system called the monsoon. During summer, strong south-westerly winds with moisture-laden air blow from the sea towards the land mass, while during winter, the reversal of the winds takes place which results in north-westerly winds with dry air blowing from the land to ocean. The changes in the

wind fields in summer and winter would alter the ocean circulations of the Arabian Sea seasonally.

The coastal areas of the Arabian Sea is one among the highly productive regions in the Indian Ocean as it is expected to have an oceanographic phenomenon termed as upwelling which brings up the cold, nutrient-rich subsurface water to the surface to replace the relatively warmer, nutrient-deficient surface water, making the coastal areas highly productive. The upwelling in the Arabian Sea coast is observed to commence in association with the onset of summer monsoon. Under favourable conditions of SST and nutrients, Arabian Sea is observed to have phytoplankton blooms.

This study is focussed on the upwelling along the southwest coast of India where the upwelling is usually found to begin prior to the southwest monsoon onset and retain till September.

3.2 DATA

3.2.1 Surface winds

Monthly means of surface wind vectors (u and v components) at 10 meter height from 1979 to 2018 from ERA-Interim, a global atmospheric reanalysis product was collected from European Centre for Medium-Range Weather Forecast (ECMWF). The data has a spatial resolution of ~80 km on 60 levels in the vertical from the surface up to 0.1 hPa.

3.2.2 Sea Surface Temperature

Monthly Sea Surface Temperature (SST) for the period 1985 to 1999 from Pathfinder AVHRR with a spatial resolution of 9 km and for the period 2000 to 2018 derived from MODIS-Terra and MODIS-Aqua channels in the mid-IR region (3.8-4.1 um) with a spatial resolution of 4.63 km are obtained from APDRC. The mid-IR channels are useful in the high water vapor, low-latitude regions and are less susceptible to aerosol contamination.

3.2.3 Ocean Temperature

Daily ocean temperature from Hybrid Coordinate Ocean Model (HYCOM) Analysis and Reanalysis products of Global Ocean Forecasting System 3.1 (GOFS 3.1) with a spatial

resolution of 0.08º lon x 0.04 º lat and 0.08º respectively are collected from https://www.hycom.org for the period 2000 to 2018. For data assimilation, the system uses the Navy Coupled Ocean Data Assimilation (NCODA) system.

3.2.4 Sea Level Height Anomaly

Sea level height anomaly (SSHA) processed from all altimeter missions: Jason-3, Sentinel-3A, Hy-2A, Saral/AltiKa, Cryosat-2, Jason-2, Jason-1, T/P, ENVISAT, GFO, ERS1/2 with a spatial resolution of 0.25°, from 1993 to 2018 is obtained from Copernicus Marine Environment Monitoring Service. The processing system uses the Geophysical Data Records to produce Sea Level Anomaly (SLA) in delayed time. All altimeter fields are interpolated at crossover locations and dates. In order to obtain the gridded SLA, all the flying satellites are merged and an Optimal Interpolation is made.

3.2.5 Carbon-based Productivity Model (CbPM)

Net Primary Production (NPP) from CbPM during 2003-2019 was downloaded from http://sites.science.oregonstate.edu/ocean.productivity/1080.by.2160.monthly.inputData.php.

3.2.6 Fisheries Data

Species-wise annual marine fish catch for Kerala coast (district-wise) from 2007 to 2018 was obtained from Central Marine Fisheries Research Institute (CMFRI).

3.2.7. Oceanic Nino Index (ONI)

ONI for the years 1950-2020 was downloaded from National Oceanic and Atmospheric Administration (NOAA) Climate Prediction Center (CPC) from the site https://origin.cpc.ncep.noaa.gov/products/analysis_monitoring/ensostuff/ONI_v5.php.

3.3. METHODS

3.3.1 Upwelling Indices

Since upwelling intensity cannot be measured directly, various upwelling indices are used to understand the intensity of upwelling.

3.3.1.1 Upwelling index from surface winds

In the Northern Hemisphere (Southern Hemisphere), the surface winds are expected to move the surface water to the right (left) with the net transport of water at an angle of 90° to the wind direction which is termed as Ekman transport. Coastal upwelling is generated when the surface winds blowing parallel to the coast induce offshore Ekman transport, bringing up the subsurface water. Hence offshore Ekman mass transport is taken as primary indicator of upwelling.

Along the southwest coast of India, the surface wind is mostly north-westerly while it is mostly tangential at the southern tip of India and hence for the calculation of offshore Ekman transport, zonal wind and meridional wind components are neglected respectively.

Ekman mass transport due to zonal and meridional wind is calculated using the equation

$$M_u = \frac{\tau_x}{f_c}$$

$$M_v = \frac{\tau_y}{f_c}$$

respectively, where τ_x is the cross-shore wind stress, τ_y is the along-shore wind stress and f_c is the Corriolis parameter which has the value of $2\omega \sin(\emptyset)$, where ω is the angular velocity of the Earth's rotation and has a value of $7.292 * 10^{-5}$, and $\emptyset$ is the latitude. The wind stress is calculated by

$$\tau_x = \rho_{air} C_d |V| u$$

$$\tau_y = \rho_{air} C_d |V| v$$

where ρ_{air} is the density of air, C_d is the dimensionless drag coefficient, $|V|$ is the wind speed and u and v are the zonal and meridional components of the wind. The wind speed is calculated using the equation

$$V = \sqrt{(u^2 + v^2)}$$

The dimensionless drag coefficient for the southeast Arabian Sea is calculated using the formula

$$C_d = \begin{cases} (0.29 + \frac{3.1}{V} + \frac{7.7}{V^2})10^{-3} & \text{if } 3\,m/s < |V| > 6\,m/s \\ (0.06 + 0.07V)10^{-3} & \text{if } 6\,m/s < |V| > 26\,m/s \end{cases}$$

3.3.1.2 Upwelling index from Sea Surface Temperature (SST)

The process of coastal upwelling brings colder nutrient-rich water from the subsurface to the surface and hence there will be anomaly between the coastal and offshore Sea Surface Temperatures (SST). This anomaly is used for understanding the upwelling intensity and is termed as Local Temperature Anomaly (LTA). Upwelling along the southwest coast of India is expected to extend up to about 200-300 km. In this study, LTA is calculated as

$$LTA = T_{offshore} - T_{coastal}$$

where $T_{offshore}$ and $T_{coastal}$ are the SST of offshore and coastal station respectively. During upwelling, LTA will be positive and vice versa. The greater the LTA, the greater is the upwelling intensity.

For calculating LTA, 10 coastal stations are selected with their corresponding offshore stations perpendicular to the coast, at a distance of 1° and 2° from the coast as shown in figure 4.2.

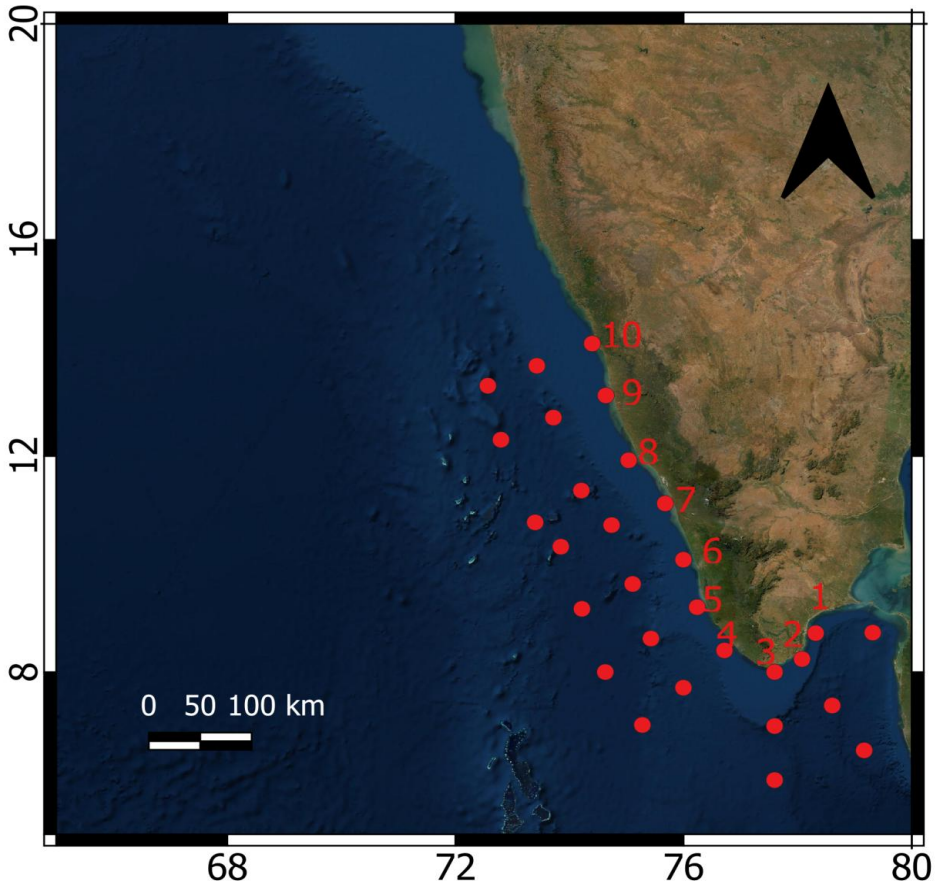

Figure 3.2. Study region showing the coastal and offshore stations selected for LTA calculation.

3.3.1.3 Sea Level Anomaly

Upwelling brings colder, denser water towards the surface which reduces the sea level. Hence sea level height anomaly during southwest monsoon can be a result of upwelling though there are several other factors which affect the sea level variability.

3.3.1.4 Shifting of Isotherms

Ocean temperature data from HYCOM collected from APDRC is used to understand the movement of isotherm at 10 selected locations in the Southeast Arabian Sea as shown in figure 2. At each location, four sub-locations are taken at distances 20km, 50km, 75km and 100km from the coast. The rapid upward movement of isotherms serves as an indicator of upwelling.

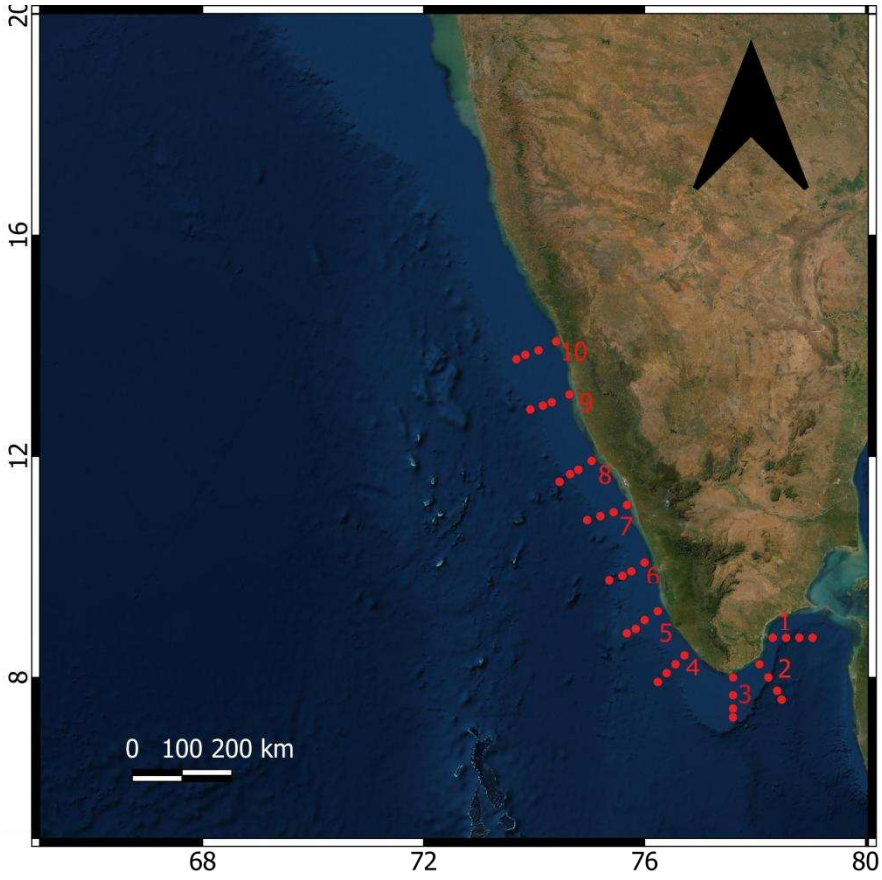

Figure 3.3. study area showing different locations and sub-locations selected for analysis of isotherms

3.3.1.5 Carbon-based Productivity Model (CbPM)

Behrenfeld et al. (2005) were the first to describe the CbPM which was later expanded upon by Westberry et al. (2008). Unlike the traditional approach to Net Primary Production (NPP) modeling, CbPM relates NPP to phytoplankton carbon biomass and growth rate.

$$NPP = carbon * growth\,rate$$

(Behrenfeld et al., 2005)

Phytoplankton biomass is assessed from particulate backscattering coefficients (b_{bp}).

$$carbon = 13000 * (b_{bp} - 0.00035)$$

(Behrenfeld et al., 2005)

Phytoplankton growth rate is a function of nutrient and temperature stress and photoacclimation and is derived from satellite chlorophyll-to-carbon data.

$$growth\,rate = u_{max} * f(N,T) * g(Ig)$$

(Behrenfeld et al., 2005)

where $u_{max} = 2$, $f(N,T)$ is the reduction in growth rate due to suppression of nutrient and temperature and $g(Ig)$ is the growth rate reduction due to light limitation.

$$f(N,T) = \frac{(Chl{:}\,C)_{observed} - \varepsilon}{(Chl{:}\,C)_{max} - \varepsilon}$$

(Westberry et al., 2008)

where $(Chl{:}\,C)_{observed}$ and $(Chl{:}\,C)_{max}$ are the observed and maximum $Chl{:}\,C$ ratio and ε is the minimum $Chl{:}\,C$ ratio when NPP is zero which is ~0.0003.

$$(Chl{:}\,C)_{max} = 0.022 + (0.045 - 0.022) * \mathrm{e}^{-3\mathrm{Ig}}$$

(Behrenfeld et al., 2005)

where $(Chl{:}\,C)_{max}$ is the chlorophyll-to-carbon ration under nutrient replete condition, $(Chl{:}\,C)_{observed}$ is the satellite-derived chlorophyll-to-carbon ratio and Ig is the median mixed layer light level which is calculated as

$$Ig = PAR * \mathrm{e}^{-KPAR*\frac{MLD}{2}}$$

(Behrenfeld et al., 2005)

The evaluation of f(Ig) requires information of Mixed Layer Depth (MLD), Photosynthetically Available Radiation (PAR) and attenuation coefficients for PAR (KPAR) and is calculated using the equation

$$g(Ig) = 1 - \mathrm{e}^{-5Ig}$$

(Westberry et al., 2008)

3.3.2. Modelling Approach

The Finite Volume Community Ocean Model (FVCOM) was used to simulate the temperature profile of southwest coast of India for a period of one year (2014). The model

decomposes primitive equations over unstructured triangular grids, having spatial resolution varying from 20 m (within 10 km area of inlet) to 50 km (in the open ocean) and consist of about 60,000 elements with 21 vertical sigma levels. The maximum model time step of one second is set by the lowest CFL value in the domain to preserve the stability over the simulation (D. F. Hill, 2007). The model was forced by tide at open boundary, which was extracted from Global tidal model and river discharge for the year 2014 was taken from Central Water Commission (CWC). Surface meteorological forcing's such as atmospheric pressure, wind, solar radiation and cloud were taken from European Centre for Medium Weather Forecast (ECMWF). Currents, Salinity and temperature forcing at the open boundary was extracted from hybrid global ocean model data. Global self-consistent, hierarchical high-resolution geography database available at http://www.soest.hawaii.edu/wessel/gshhg/ was utilised for delineating land-water interface, while estuaries and backwaters were incorporated by digitizing LISS-III data. FVCOM model was run in parallel mode on a multiprocessor computer to achieve minimum execution time with the technology of MPI (Message Passing Interface) and the outputs stored in NETCDF format with one hour interval. Several studies showed that wind is the major parameter influencing upwelling phenomena, where the rapid upward shifting of 26^{o} C isotherm is evident. The present modelling study is mainly aimed to understand the fact that whether upwelling prevails in southwest coast of India without wind. FVCOM model have a capability to switch ON and OFF of different parameters. Here we were simulated the model for two conditions 1) real condition with WIND ON 2) experimental condition with WIND OFF. If the real condition is calibrated and validated with in-situ measured data, so that the experimental condition may valid throughout the study.

3.3.2.1. Calibration and validation of the FVCOM Model

3.3.2.1.1. In-situ measurements

Validation/calibration of the water level and current simulations for the southwest monsoon period were carried out using in-situ measurements spanning from 24th July-21st August 2010 in the Cochin estuary and two inlet connected to sea (Cochin and Munambam), while those for transition stage of monsoon were done from 20th September-20th October 2009. Water levels were recorded at 10 minutes interval at 6 different locations using SBE-26 plus water level recorder. Aanderaa RCM-9 current meters were deployed at 4 locations to record

water speed and direction at 10 minutes interval. Salinity profiles at Cochin coastal water were obtained from 8 offshore locations upto 35 m depth using SBE-19 plus CTD (conductivity ± 0.001 S/m) during the year 2014.

3.3.2.1.2. Model validation

The data from in-situ observations were used to evaluate model accuracy. Taylor diagram provides a statistical summary of the model to produce accurate results in terms of correlation, centred Root Mean Square Deviation (RMSD) and variance. The correlation between model and observation is given by the azimuthal position, while the distance from the reference point (observations) is a measure of the centered RMSD. Therefore, an ideal model (being in full agreement with observations) is marked by the reference point (0.1) with coordinates $\phi = 0$ and radius = 1, which means the correlation coefficient is equal to 1 and the modelled and measured variations have the same amplitude. Figure 3.4 represents statistical significance of model by comparing simulated tide, U and V components with the observed data from the various location the Cochin estuary. Both the season, Taylor diagram showed very good correlation (>0.7) of tide and current simulations with a standard deviation < 0.5 and low RMSE (<1.0). Salinity variation in the shelf off Kochi was simulated for the year 2014 and was well-matched with in-situ measurements. The representative months having large, medium and low riverine flux were subjected to statistical significance (Figure 3.5). Throughout the validation, high correction coefficient (≥0.7) was noticed at all stations with a minimum standard deviation and RMSD (<0.3).

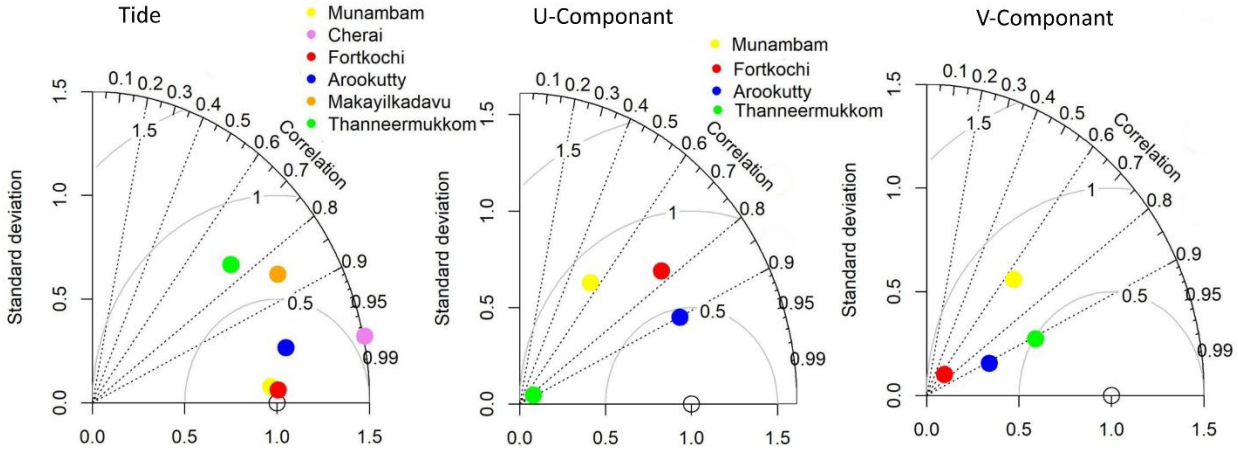

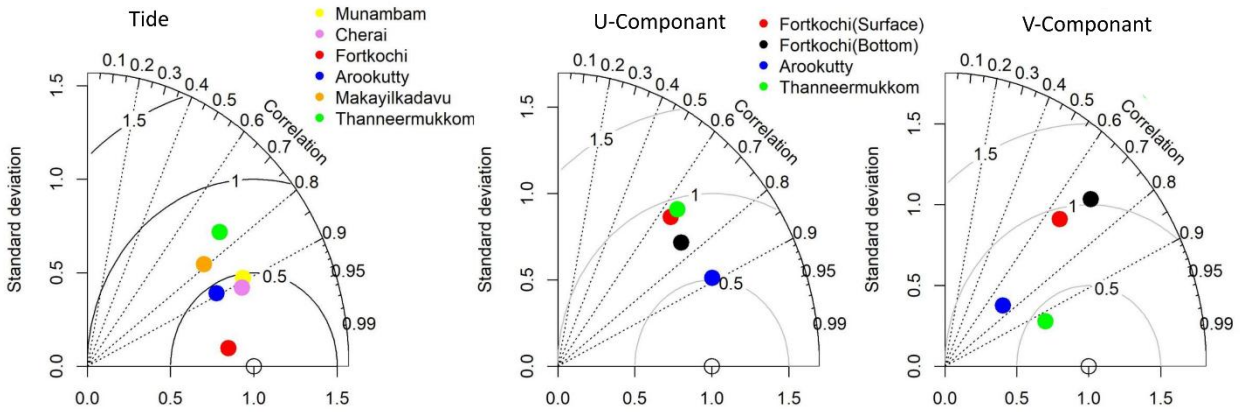

Figure 3.4. Top panel and Bottom panel shows the Taylor diagram generated for monsoon and Post monsoon period respectively.

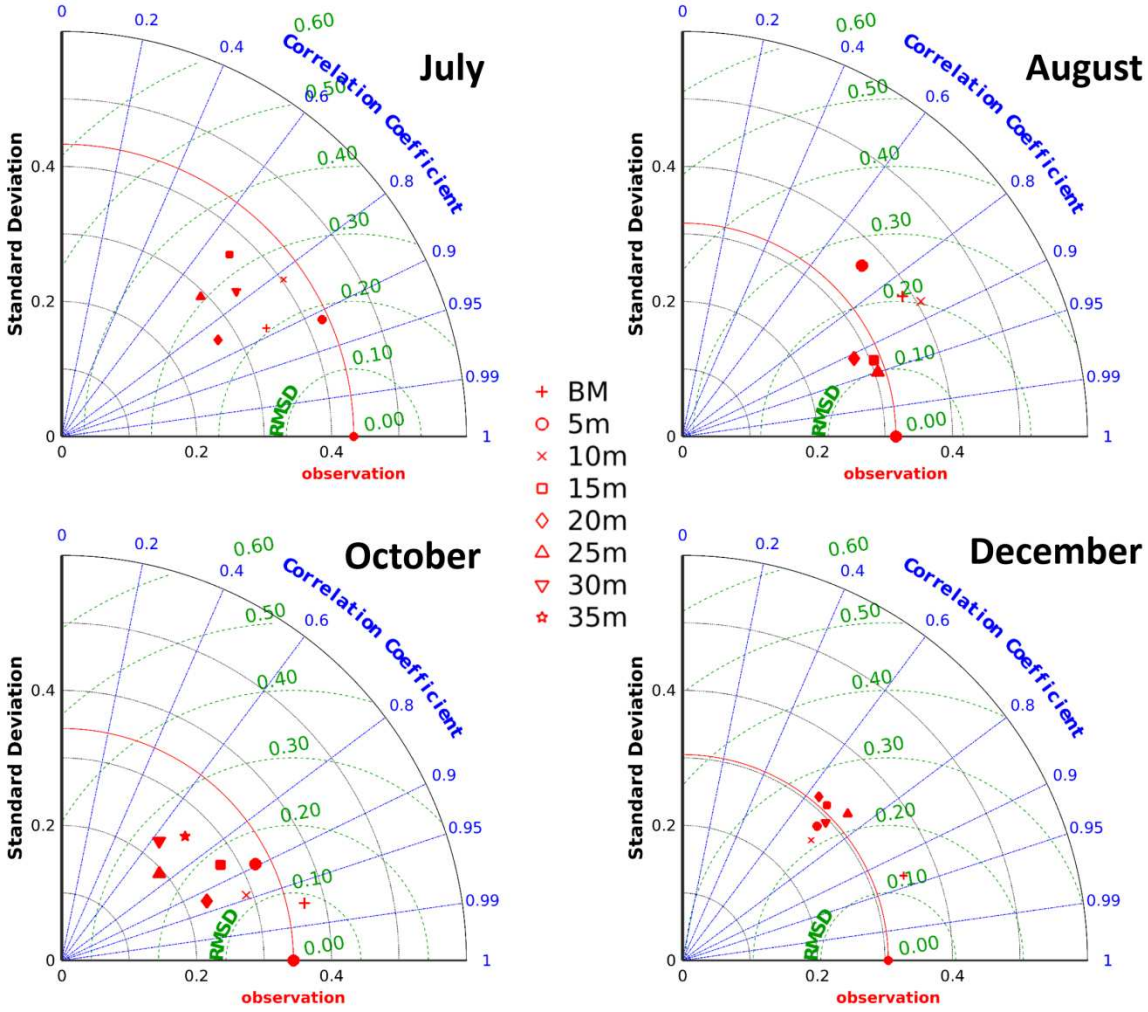

Figure 3.5. Taylor diagram represent statistical significance of model by comparing temperature with the observed data from the various location of the shelf off Kochi for different months in the year 2014.

3.3.3. Oceanic Nino Index (ONI)

To identify ENSO years, the Oceanic Nino Index (ONI) from NOAA was analyzed. From the ONI values calculated for overlapping 3-months periods, the years with values equal to or above +0.5° anomaly for 5 consecutive periods is defined to be an El Nino year and similarly the years with values equal to or below -0.5° anomaly is defined to be La Nina year. And as for the strength, the years with ONI values from 0.5° to 0.9° anomaly for at least 3 consecutive overlapping 3-month period is classified as weak, 1° to 1.4° anomaly as moderate, 1.5° to 1.9° anomaly as strong and years with values greater than 2 as very strong .

CHAPTER 4

RESULTS

4.1. CLIMATOLOGY

4.1.1. Surface Winds and Offshore Ekman Mass Transport

Wind is an important parameter for changing the ocean dynamics, which can drag a water column up to 100 m while passing over ocean surface. Figure 4.1 shows the wind speed, offshore Ekman transport due to meridional wind and zonal wind during January to December. During January and February, along the west coast of India, the mean wind to the North of 12°N is mainly northerly and to the South, it is north-easterly. The mean wind becomes north-westerly along the entire coast of the study area by April. The wind speed along the west coast seems to be in the range of 1-5 ms^{-1} from January to April, and the value decreases with passing months. The wind speed starts to increase from April onwards. In May, the wind speed along the coast is about 3 ms^{-1} with the direction towards the southeast. The direction becomes westerly in June with the speed reaching the range of 5-6 ms^{-1}. In July and August, the wind speed further increases and the direction becomes north-westerly along the southwest coast of India. By September, the wind speed starts to decrease, and the wind direction gradually shifts to north-easterly. The wind direction over the southern tip of India is almost tangential from May till October, after which the direction changes to north-easterly over the entire study area. The strongest wind is observed during the month of July and the maximum is observed at the southern tip of India. The lowest wind is observed during the months of March-April and October-November.

Many studies showed that the upwelling is mainly controlled by the wind acting upon the ocean water. Upwelling along the southwest coast of India is taken to be negative since the upwelling favourable wind along the region is equatorward while the values are considered to be positive along the southern tip of India as the upwelling favourable wind at the region is eastward. Offshore Ekman transport along the Indian coast is observed to be evident from May onwards at the southern coast. Both the spatial extent and strength seem to increase during June-July and reaches up to a maximum of 4500 $kgm^{-1}s^{-1}$ in July along the southern coast. The strength of Ekman transport is observed to decrease northward and it starts to reduce from

August at the southern coast. The offshore Ekman transport becomes negligible along the whole coast by the end of September.

4.1.2. Sea Surface Temperature (SST) and Local Temperature Anomaly (LTA)

Figure 4.2 shows the climatology of Sea Surface Temperature (SST) for the study region. In January and February, average SST along the southwest coast of India is about 28°C. A decreasing tendency of SST is found to the North of 15°N and to the South of 7.5°N. The SST in the entire study region shows an increasing pattern from January onwards. Most of the region shows SST greater than 29°C by May. As an indication of the wind induced upwelling, the SST begins to show a reduction, initially from the southern coastal tip of India. The low SST region gradually expands northward along the coast and the SST over the entire region also shows a decreasing pattern. During July and August, SST near to the coastal region reaches about 24-25°C and the minimum SST region is found to be confined to the coast within the latitudes 7.5°N and 15°N. After August, the water begins warming up, which is evident from figure 4.2.

Figure 4.3 shows the climatology of Local temperature anomaly (LTA) for the 10 different sites and it shows that the peak LTA values occur during summer monsoon period (June-September). The maximum LTA of about 2.5-3°C is usually observed at Site 3, followed by Site 4 (2-2.5°C). At Site 1, the LTA is observed to show negative values during June-September while at Site 2, LTA attain positive values just above zero during June. The LTA was found to be decreasing northward. The peak value at Site 7 reached up to 1.8°C and this value was observed to be slightly higher than that of Site 5 and Site 6 which happens to be about 1.75°C and 1.5°C respectively. That is, there is a slight reduction in the upwelling index between at Site 5 and Site 6.

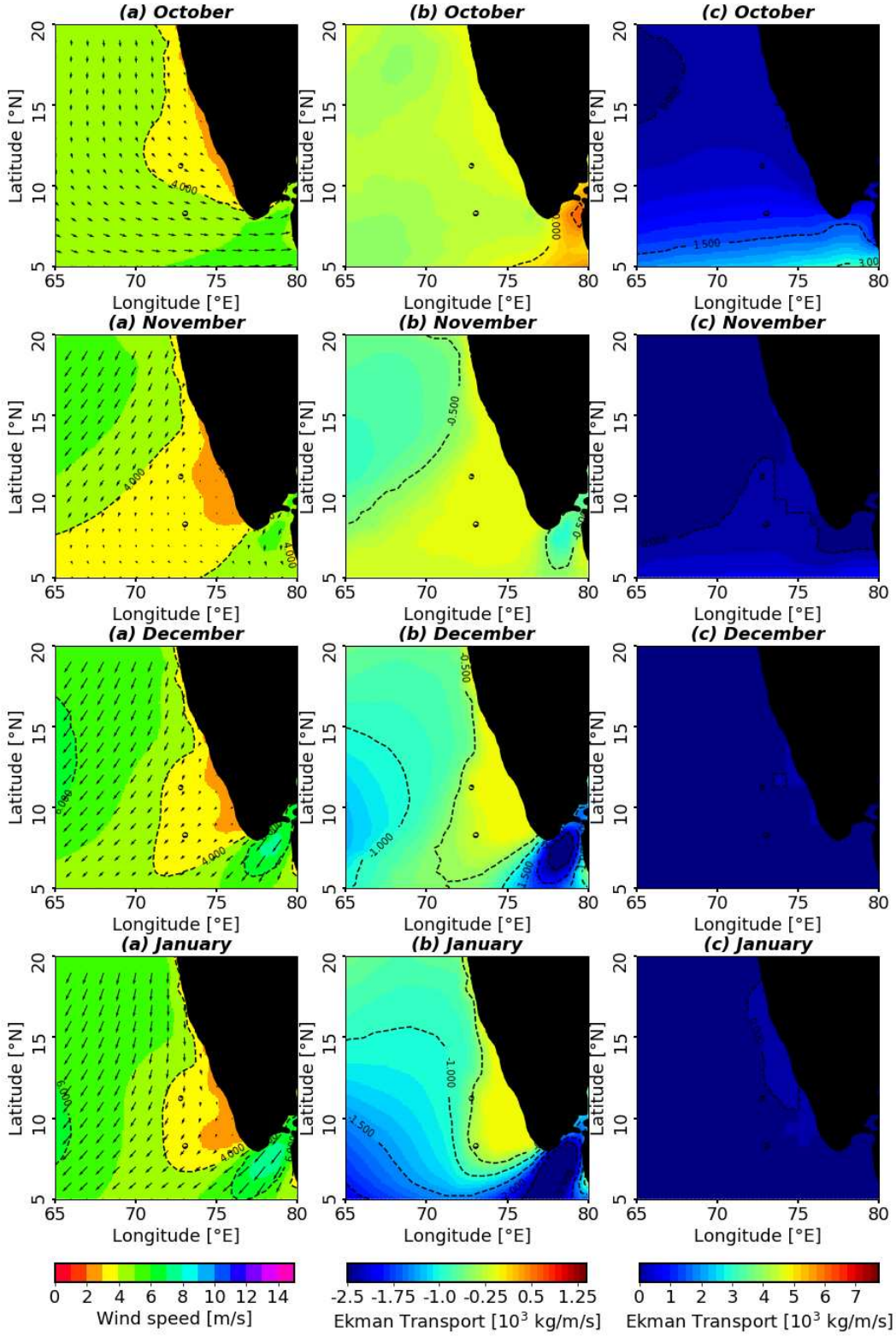

Figure 4.1.A. Climatology of (a) wind speed (in ms^{-1}), (b) Ekman transport due to meridional wind component and (c) Ekman transport due to zonal wind component (in 10^3 $kgm^{-1}s^{-1}$) during October to January

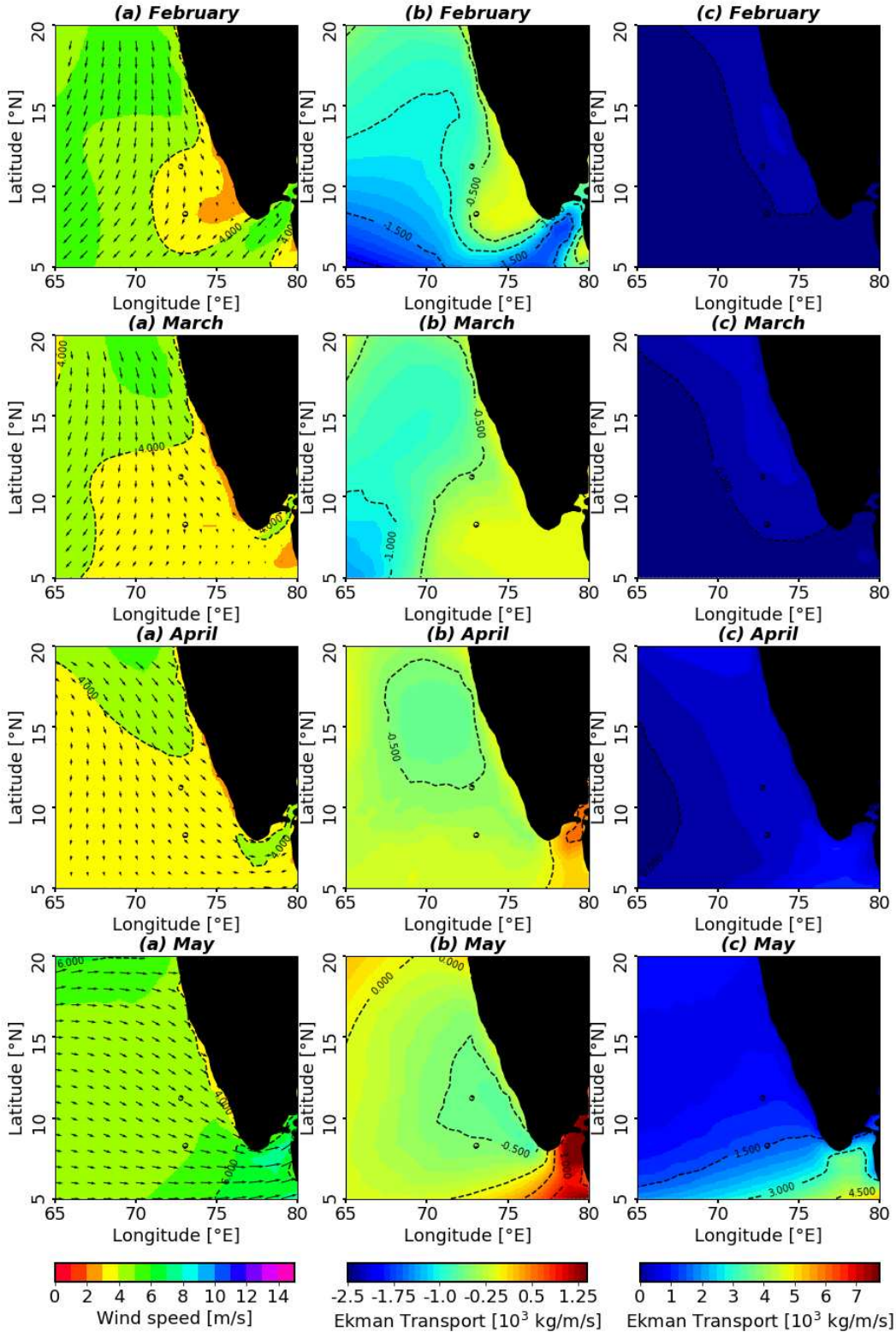

Figure 4.1.B. Climatology of (a) wind speed (in ms^{-1}), (b) Ekman transport due to meridional wind component and (c) Ekman transport due to zonal wind component (in 10^3 $kgm^{-1}s^{-1}$) during February to May

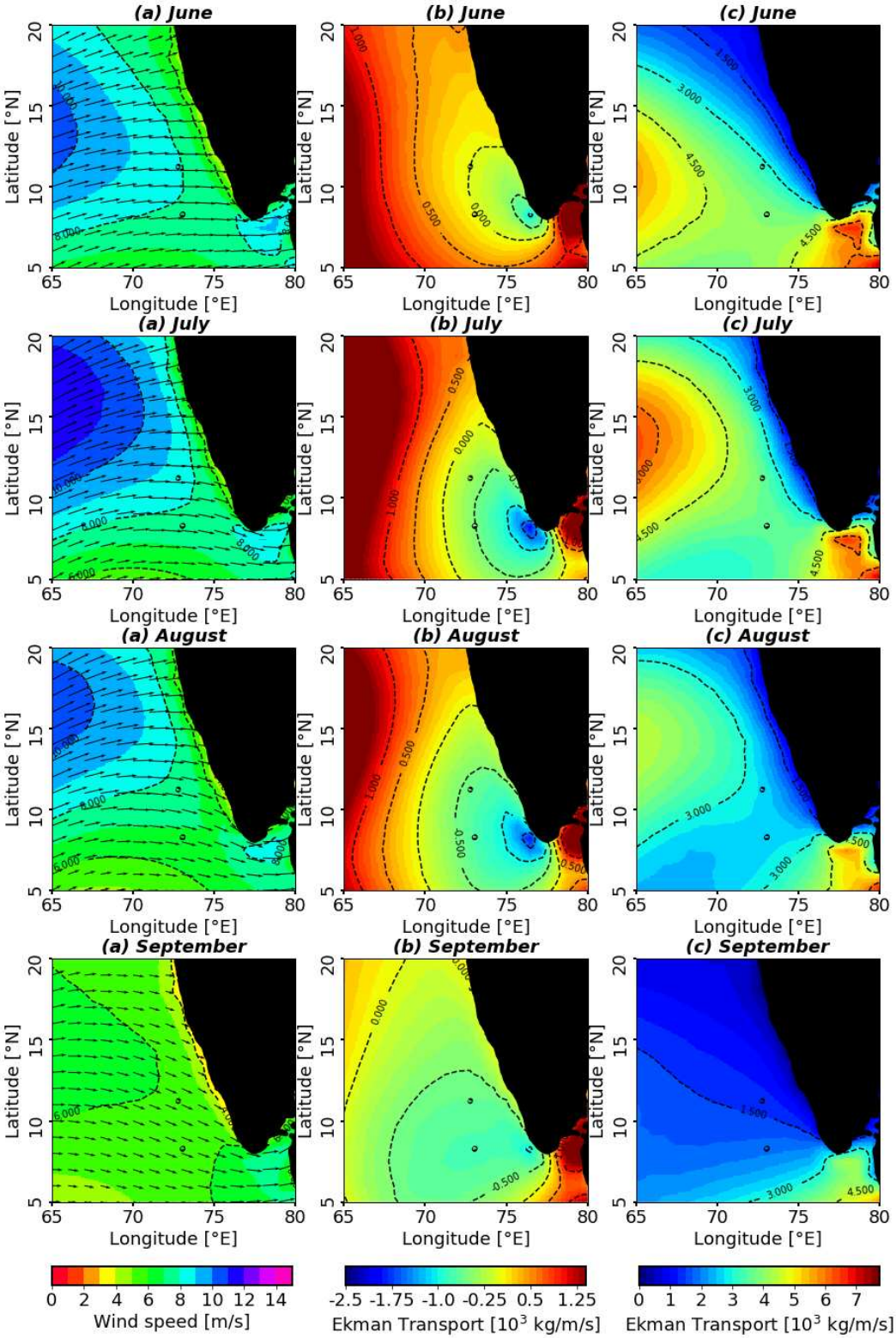

Figure 4.1.C. Climatology of (a) wind speed (in ms^{-1}), (b) Ekman transport due to meridional wind component and (c) Ekman transport due to zonal wind component (in 10^3 $kgm^{-1}s^{-1}$) during June to September

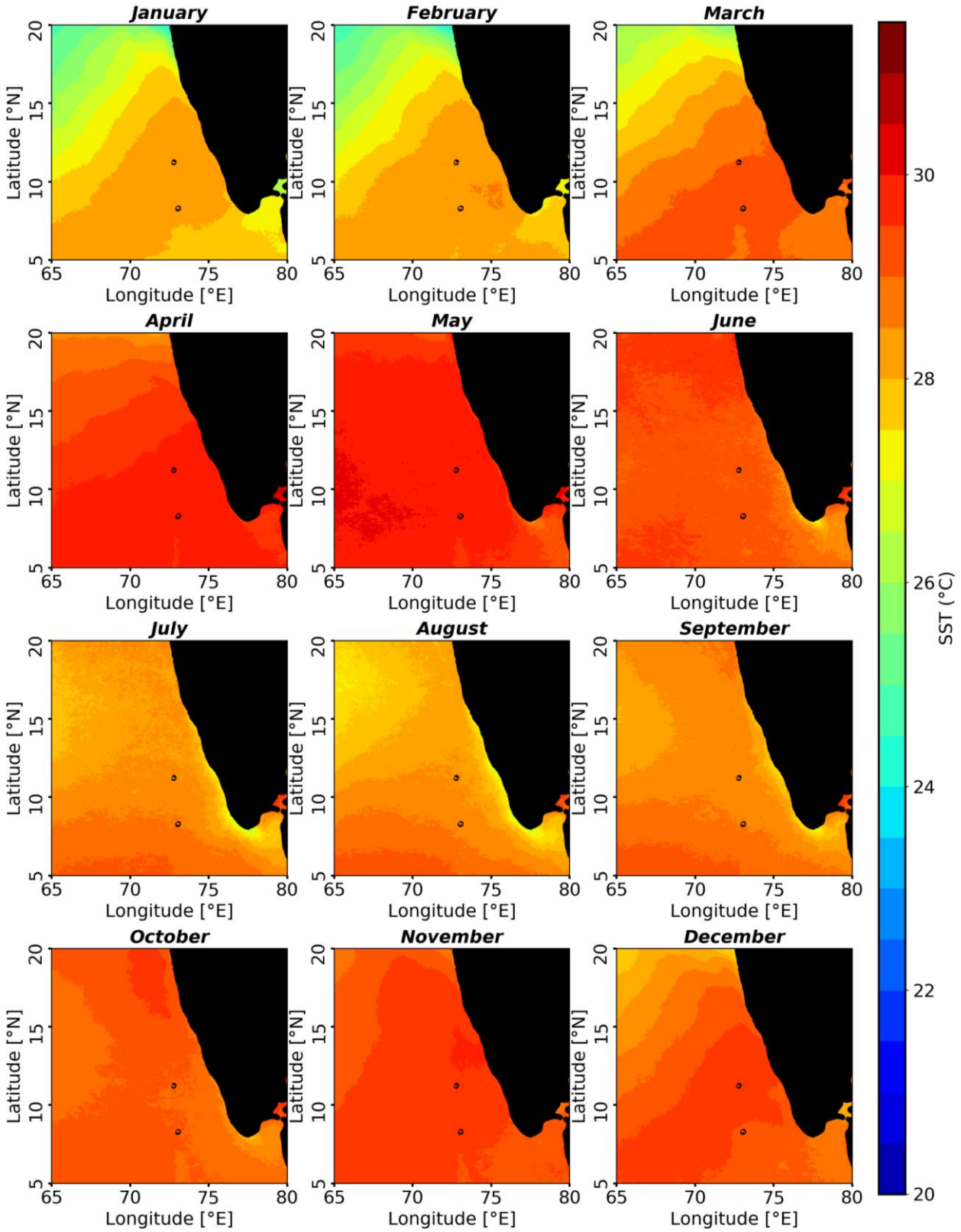

Figure 4.2. SST Climatology during January to December

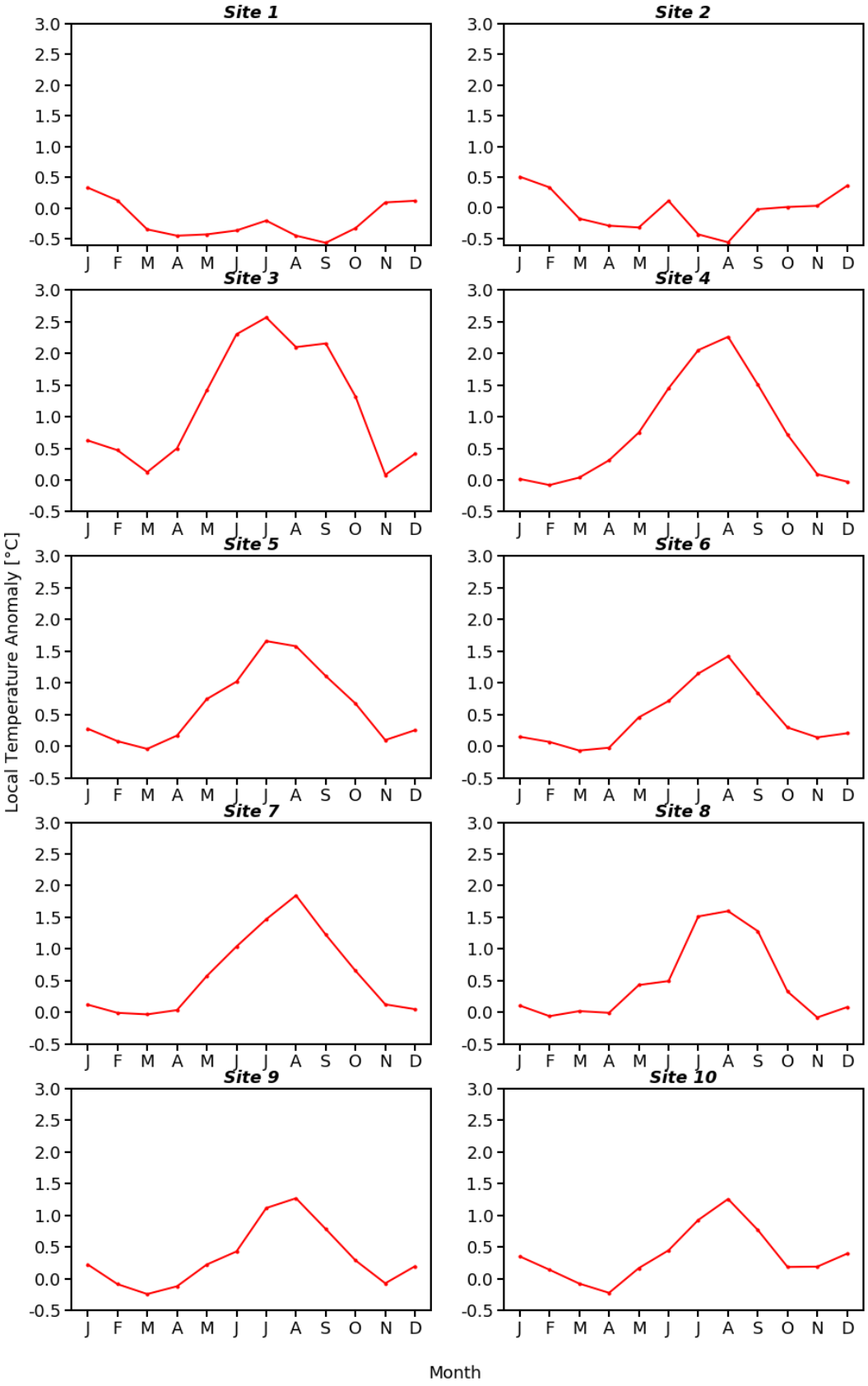

Figure 4.3. LTA Climatology for different sites from January to December

4.1.3. Isotherm Depth

To elucidate the shifting of isotherms, four sub-locations are selected at each site at a distance of about 20 km, 50 km, 75 km and 100 km away from the coast which are also perpendicular to the coast. The 26°C which is taken as the base of the mixed layer is used as the reference in this study. During June to September, upslopping of isotherms are evident at most of the sites with the maximum upslopping observed within 50 km distance from the coast. Beyond 50 km distance from the coast, upslopping is weaker. At Site 1 and Site 2, the isotherms are not clearly visible at 20 km distance from the coast. The upslopping of isotherm become more prominent from Site 1 to Site 3. The strongest upslopping is found at Site 3. At Site 4, the upslopping at 20 km distance from the coast is prominent but at 50 km, the upslopping is weak when compared to Site 5. From Site 1 to Site 5, the isotherms attain minimum depth during the month of July while for the remaining sites, a lag is observed. The upslopping is found to be slightly stronger at Site 7 than that of Site 5 and Site 6. To the north of Site 7, the upslopping again starts to weaken.

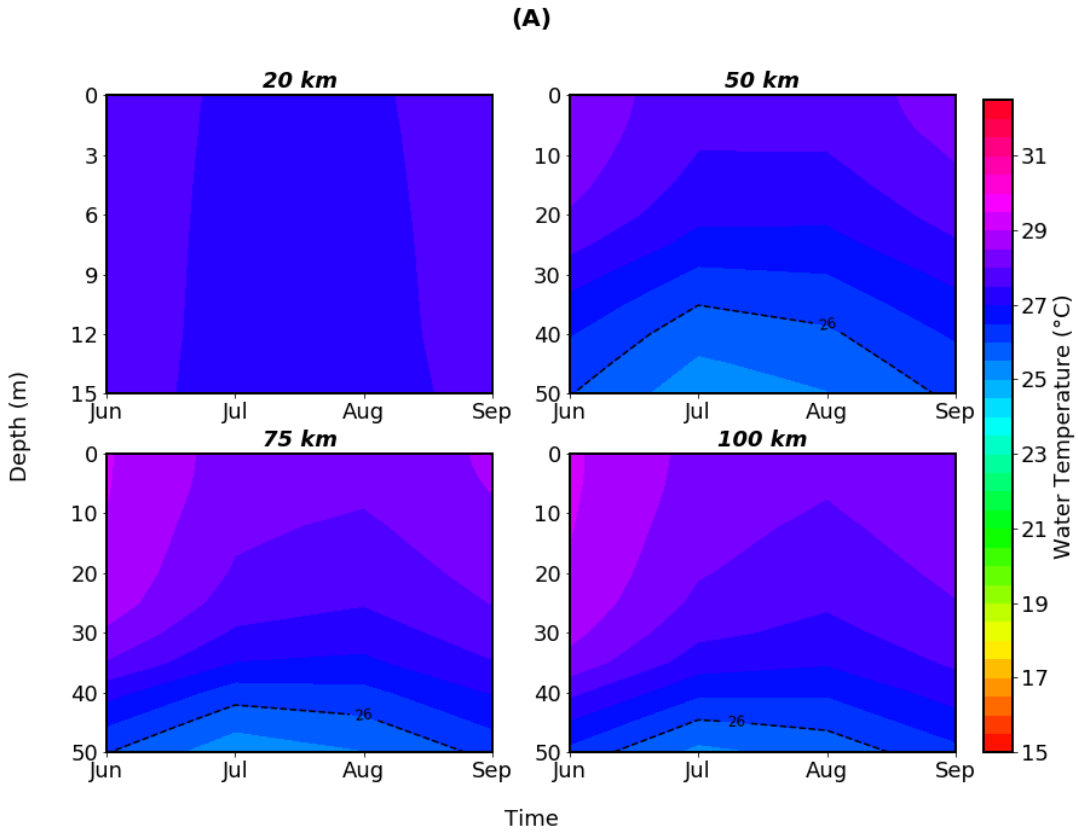

Figure 4.4 (A). Climatology of D26 at 20, 50, 75 and 100 km distances for Site 1

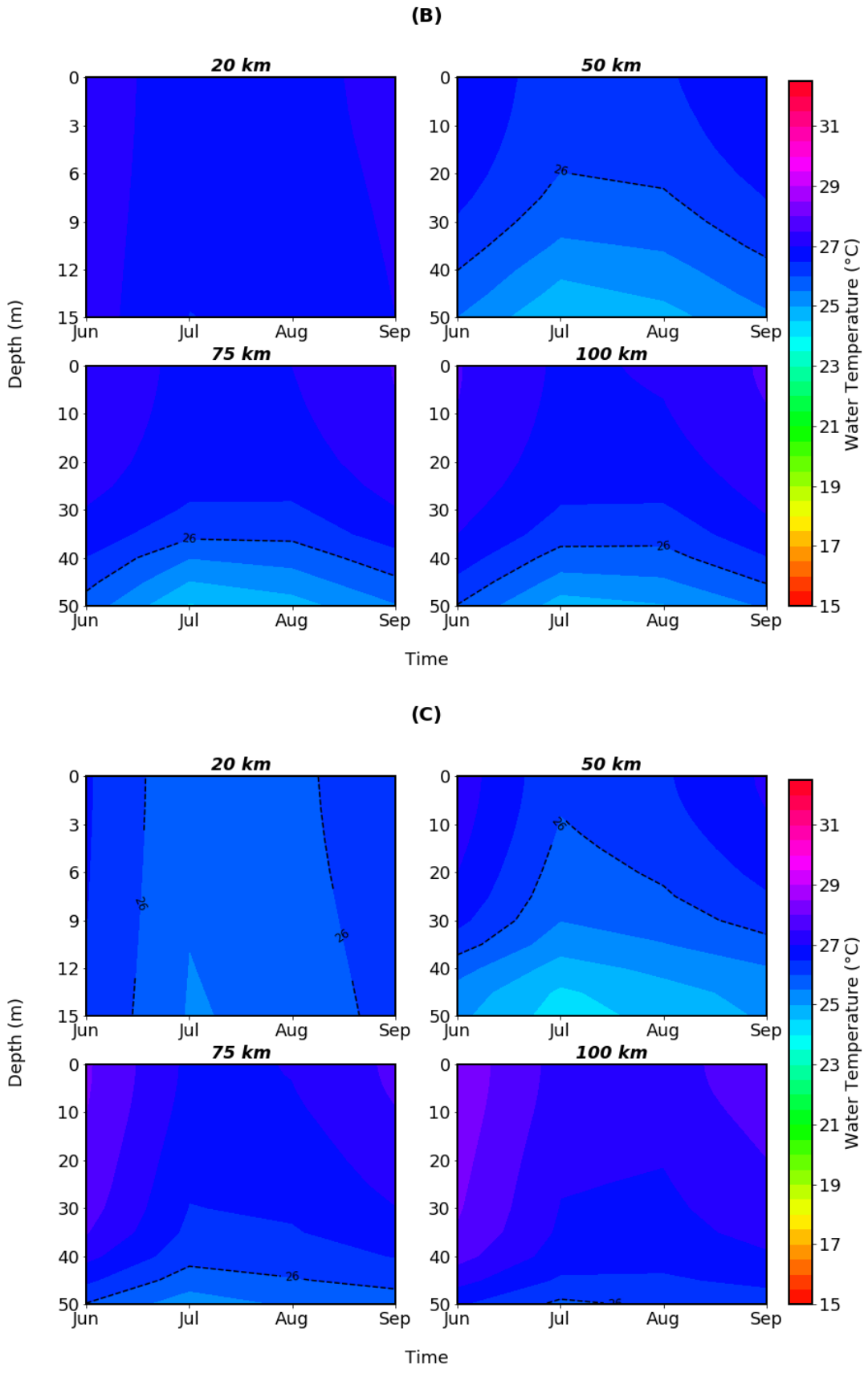

Figure 4.4. Climatology of D26 at 20, 50, 75 and 100 km distances for (B) Site 2 and (C) Site 3

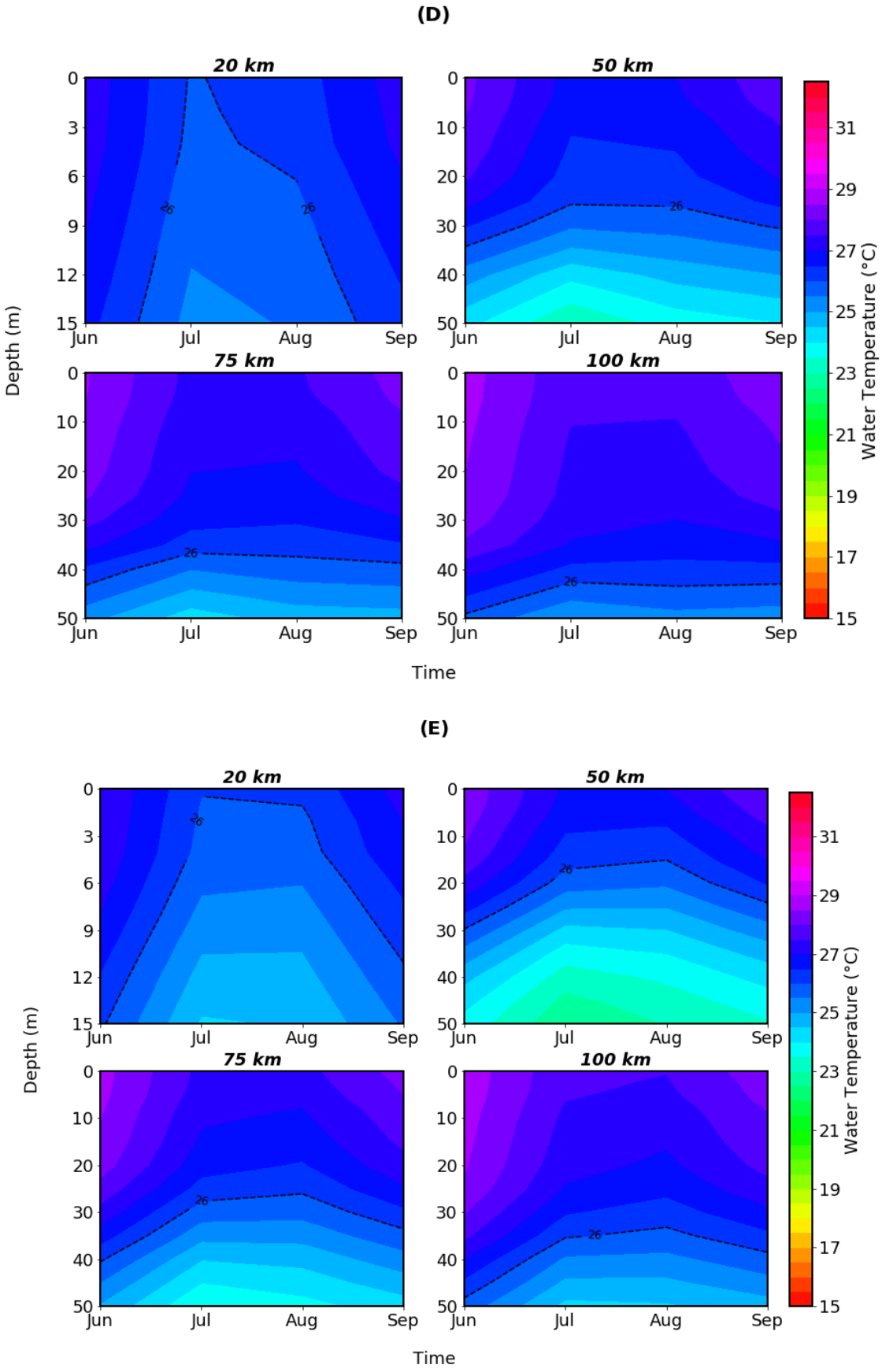

Figure 4.4. Climatology of D26 at 20, 50, 75 and 100 km distances for (D) Site 4 and (E) Site 5

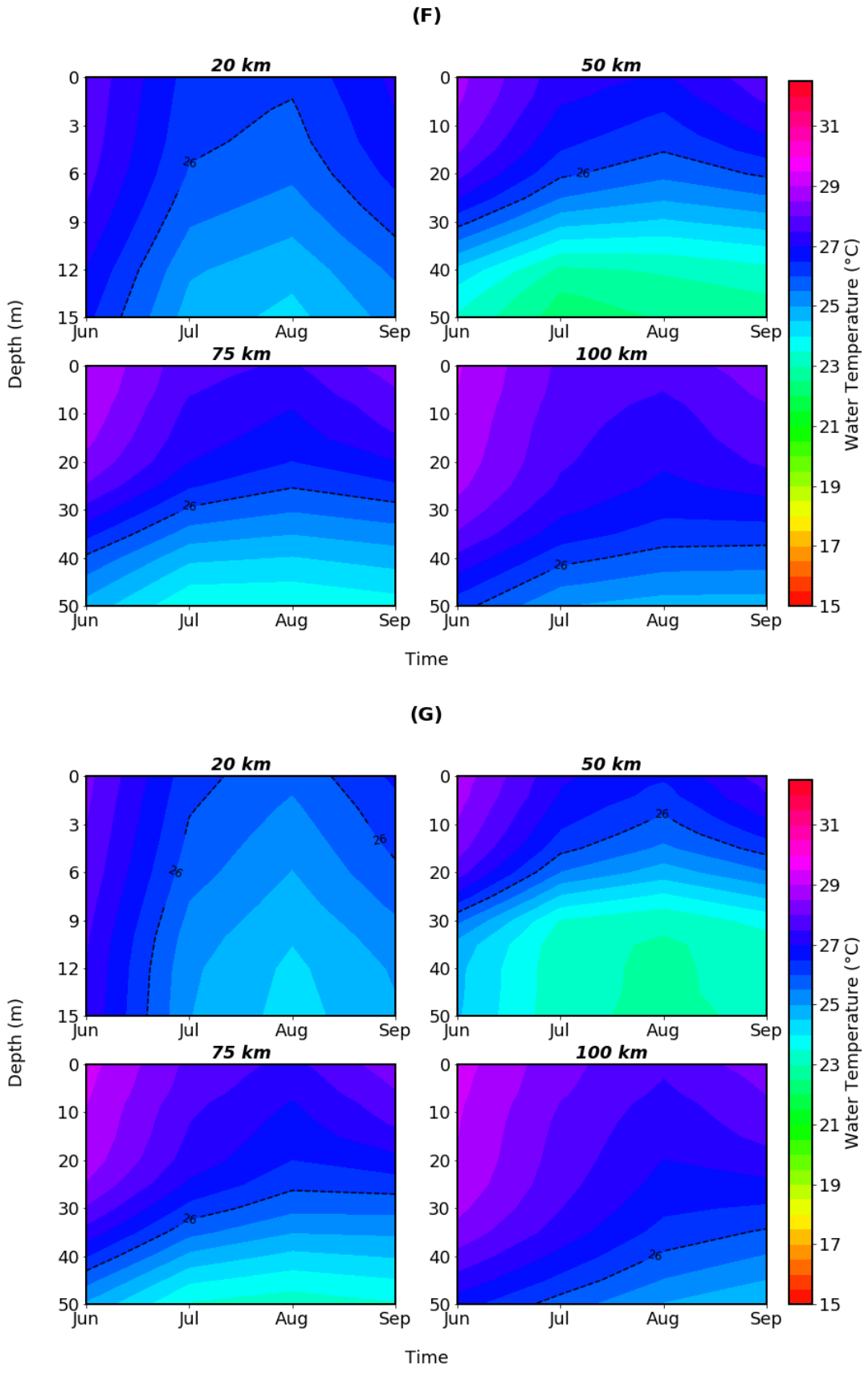

Figure 4.4. Climatology of D26 at 20, 50, 75 and 100 km distances for (F) Site 6 and (G) Site 7

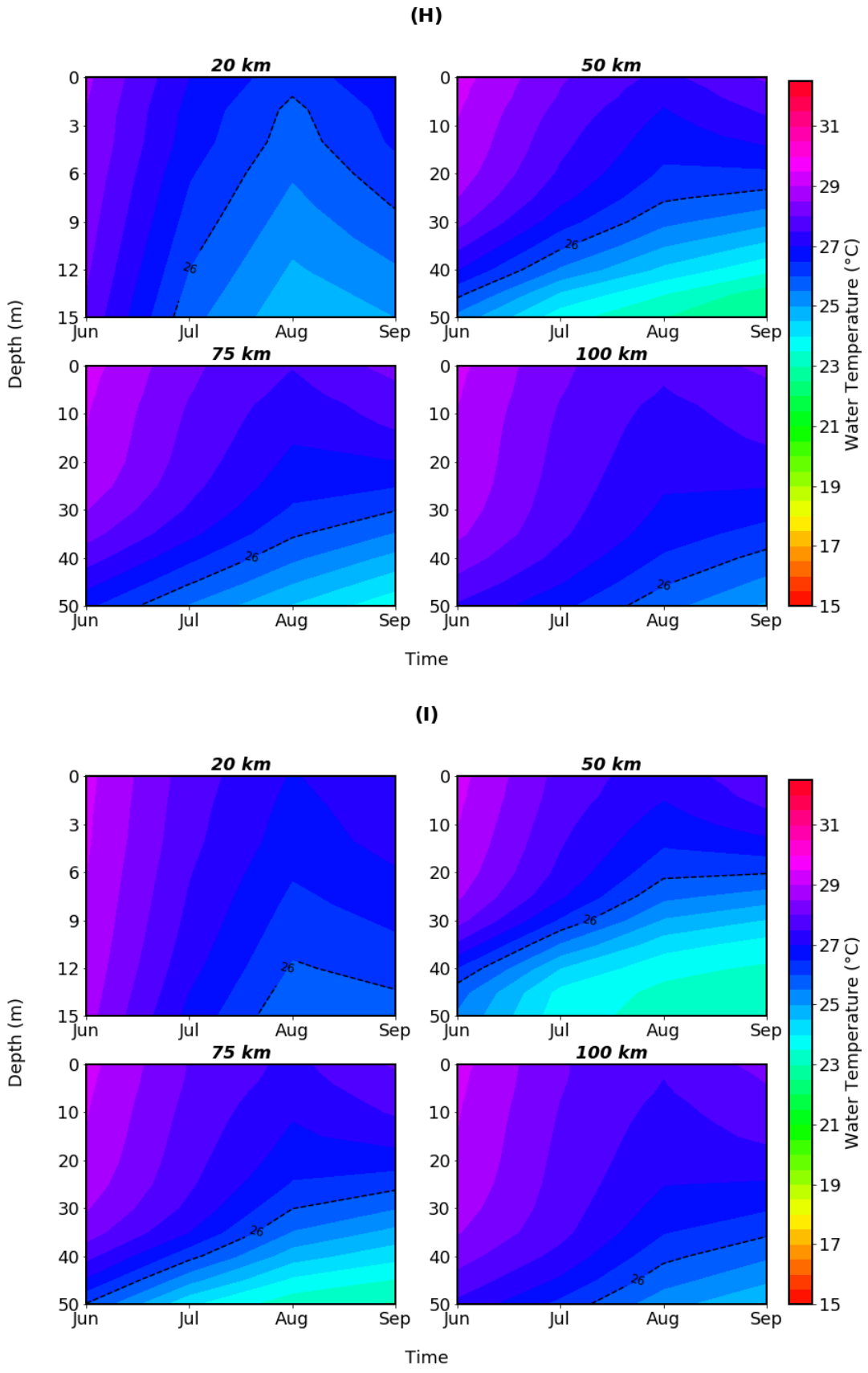

Figure 4.4. Climatology of D26 at 20, 50, 75 and 100 km distances for (H) Site 8 and (I) Site 9

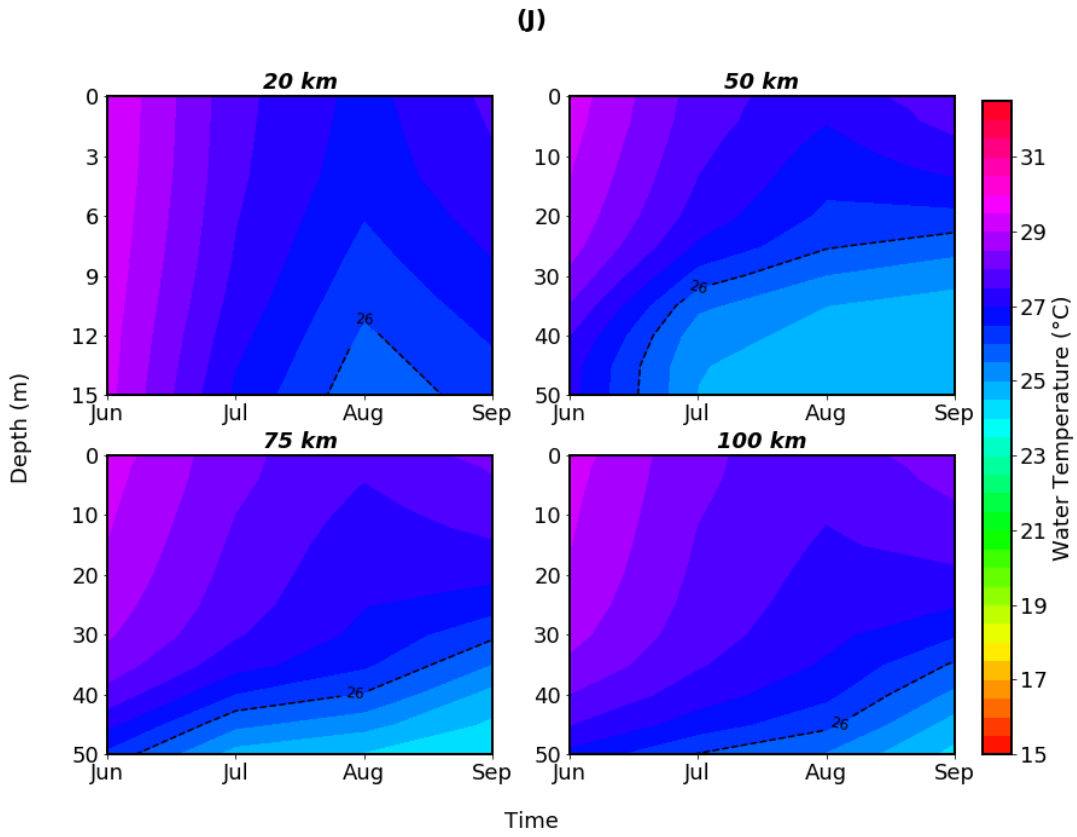

Figure 4.4. Climatology of D26 at 20, 50, 75 and 100 km distances for (J) Site 10

4.1.4. Mean Sea Level (MSL) Anomaly

Figure 4.5 shows the climatology of Mean Sea Level (MSL) Anomaly. During January to May, the MSL anomaly is observed to be positive with a rise of about 15 cm along the southwest coast of India. The sea level shows a decreasing pattern from January onwards. During June, MSL anomaly becomes almost negligible and also begins to appear as negative anomaly, which is found to be more prominent in the coastal region between 7.5°N and 12.5°N. The extent of anomaly along the coast reaches maximum of about -10 cm in August, after which the sea level begins to increase over again. In November, the MSL anomaly gains positive value of about 5 cm along the coast while negative anomaly can still be observed in the offshore regions. The negative anomaly keeps shifting in the offshore direction till January and from February onwards, the MSL rises over the entire study area. The negative MSL anomaly is observed to

start from the southern coastal region and then the region anomaly extends towards north as well as offshore regions.

4.1.5. Carbon based Production Model (CbPM)

Figure 4.6 shows the climatology of Net Primary Production (NPP) along the southwest coast of India. From January to March, NPP increased along the coast to the north of 17°N. The maximum NPP, greater than 1350 $mgCm^{-2}day^{-1}$ was observed in March and afterwards NPP declines. The southwest coast is oligotrophic during the premonsoon season. NPP shows a rising trend along the southern coastal region from May onwards, starting from the south and progressing northwards. The highest NPP along the southwest coast is observed during the month of September with value ranging between (1200-1350 $mgCm^{-2}day^{-1}$). Then the value again starts to decrease afterwards and becomes negligible by beginning of November. But still, higher NPP can be observed at the northern latitudes between 17-20°N. Higher NPP values are found between these latitudes during most of the months.

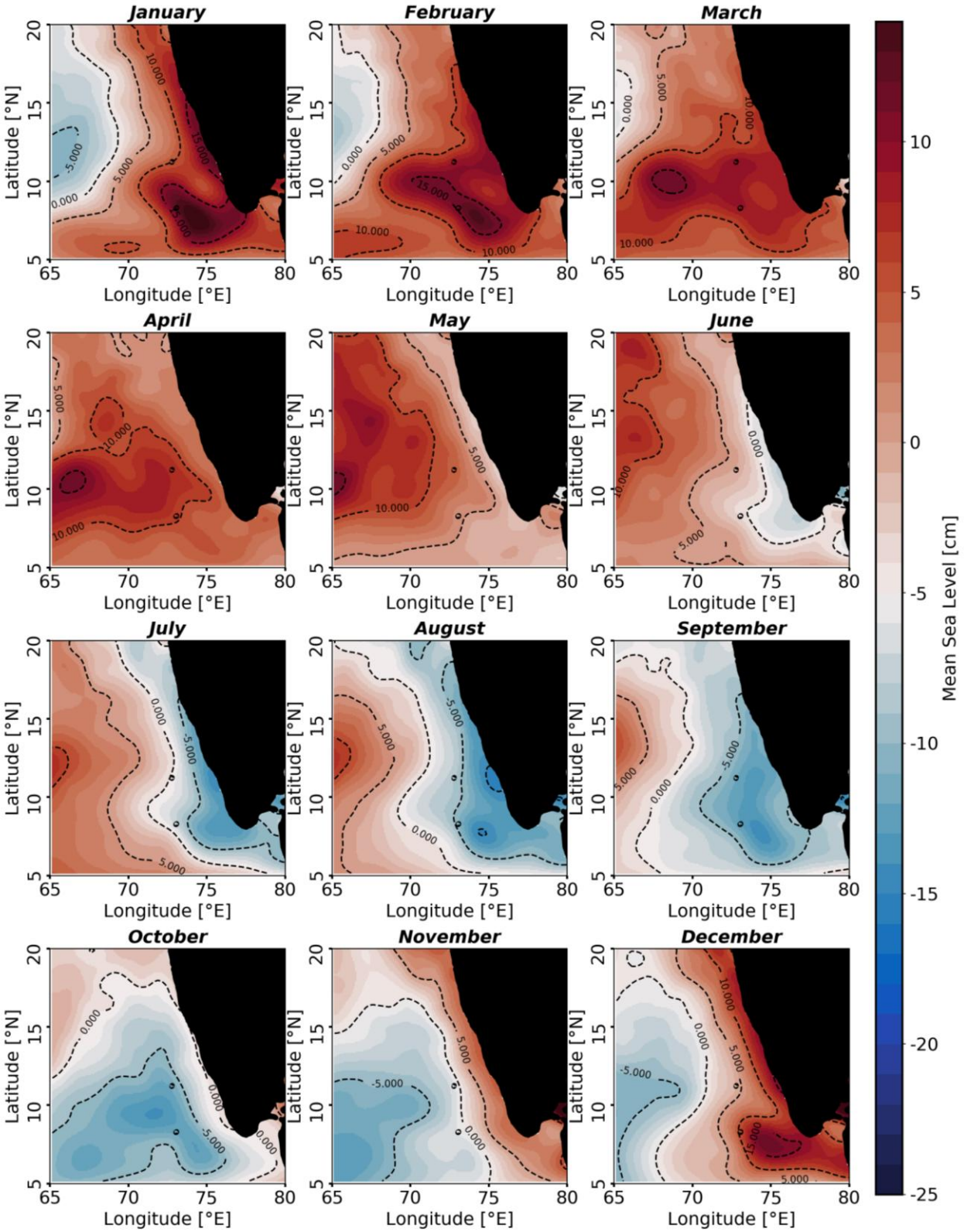

Figure 4.5. Mean Sea Level Climatology during January to December

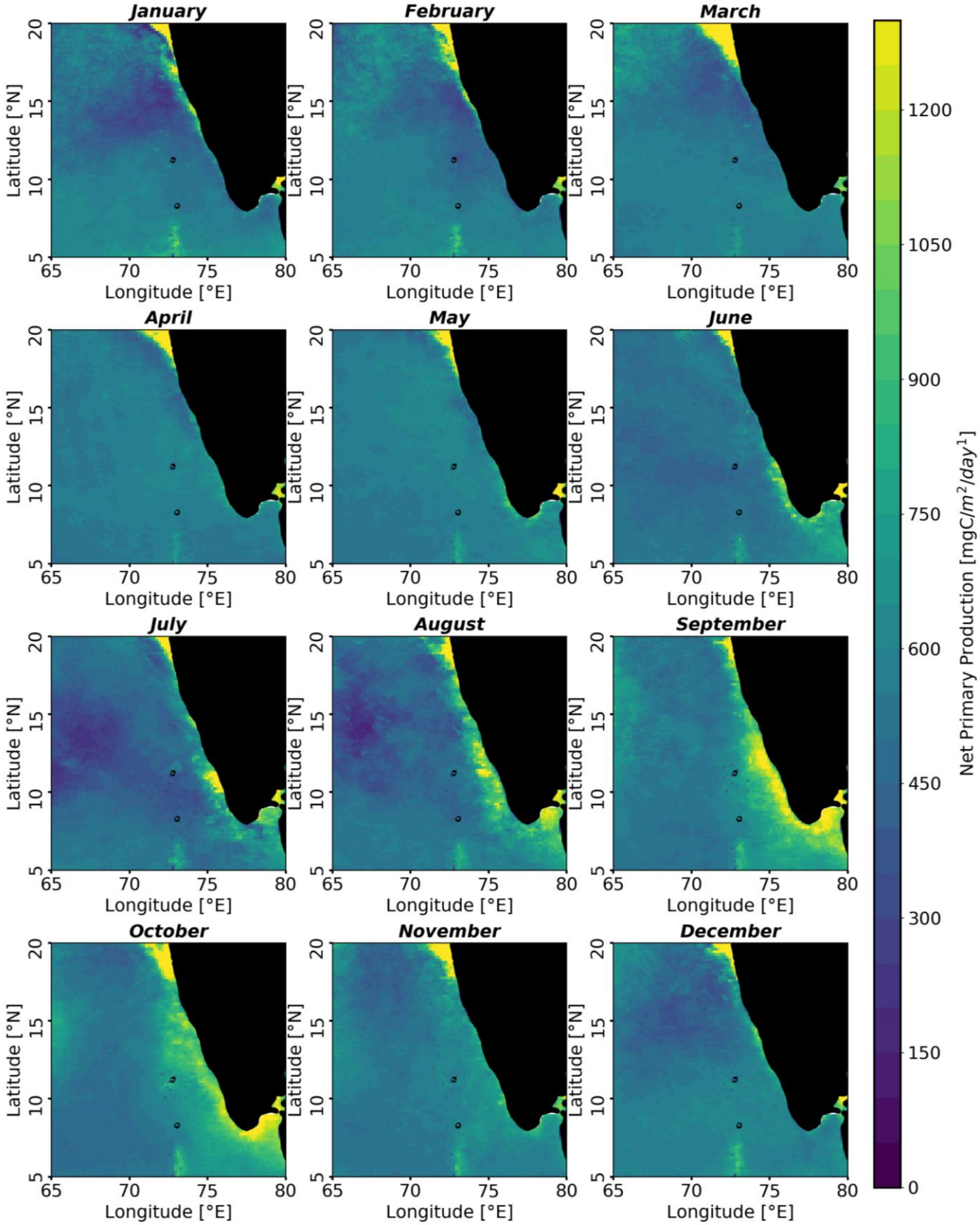

Figure 4.6. Climatology of Net Primary Production during January to December

4.2 VARIATIONS IN UPWELLING INDICES AT DIFFERENT SITES

To understand the variations in upwelling intensity along the southeast Arabian Sea coast, the upwelling indices during the southwest monsoon season from 2000 to 2018 at the 10 different sites are studied. The results showed variations in the values of indices at different sites. Table 4.1 and 4.2 showed the years of ENSO and IOD events from 1979 to 2018. Wind, Ekman transport, SST, MSL, LTA and NPP for different sites were analyzed. The wind speed and Ekman transport varied for different sites but the pattern was almost similar throughout the entire coast. The MSL anomaly was almost similar throughout the coast. The SST and LTA showed high inter-annual as well as spatial variations.

4.2.1. Site 1

Figure 4.7 shows that the wind speed along Site 1 during the southwest monsoon for the study period ranges between 4-7 ms^{-1} with the wind blowing from west-southwest for most of the time. The southerly component of wind is observed to be more prominent at this site which is parallel to the coast and favour upwelling. From figure 4.9, it can be seen that the Ekman Transport ranged between 1750-2000 $kgm^{-1}s^{-1}$ and was almost steady throughout the years. No significant changes can be observed in the wind speed and Ekman transport during the ENSO and IOD years. The D26 showed a deepening trend. The SST at the region showed a continuous increase during 2001-2003. The highest SST is observed during 2015 which was a very strong El Nino year. The MSL anomaly showed negative values during June-September. A slight decrease was noted in the anomaly from 2000-2015, attained positive values in 2015-2016, then again the anomaly started decreasing. The MSL anomaly was found to be increasing during El Nino and positive IOD years. From figure 4.7, the LTA values at summer monsoon period were negative during most of the years. But in 2006, it is observed to reach close to zero. Figure 4.10 showed that the NPP did not show significant variations and ranged between 1000-1500 $mgCm^{-2}day^{-1}$.

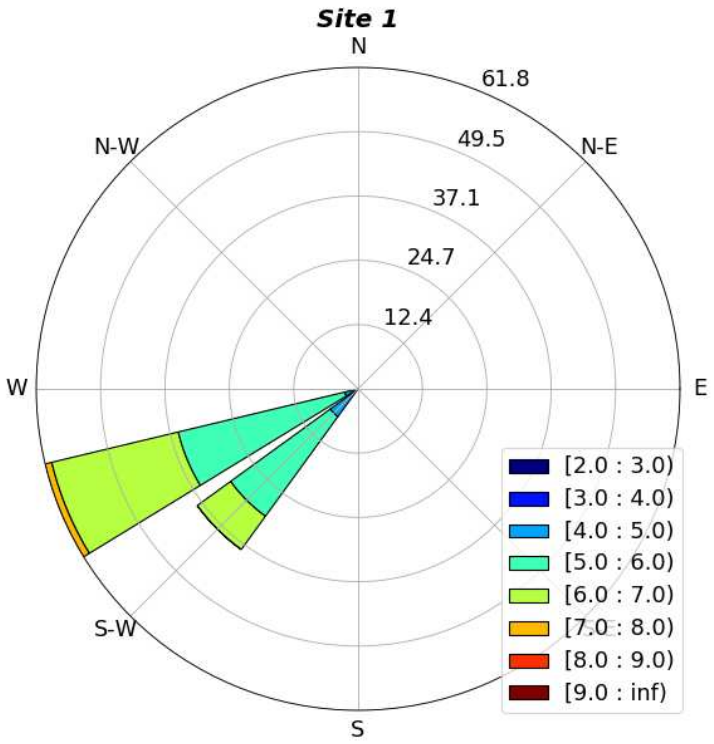

Figure 4.7. Windrose chart for Site 1 during 2000-2018 June-September

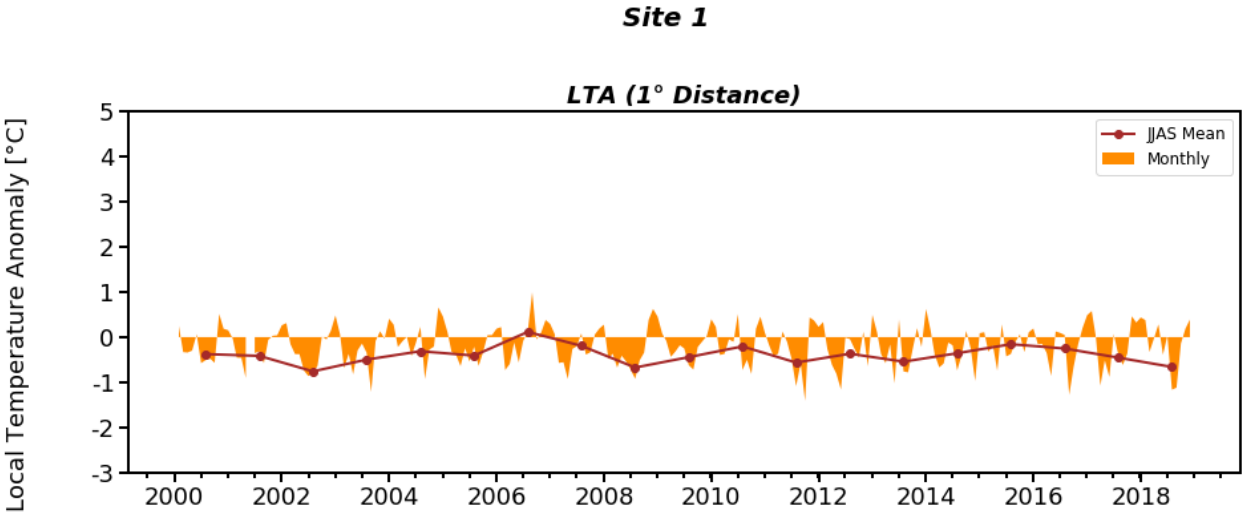

Figure 4.8. LTA for Site 1 during 2000-2018

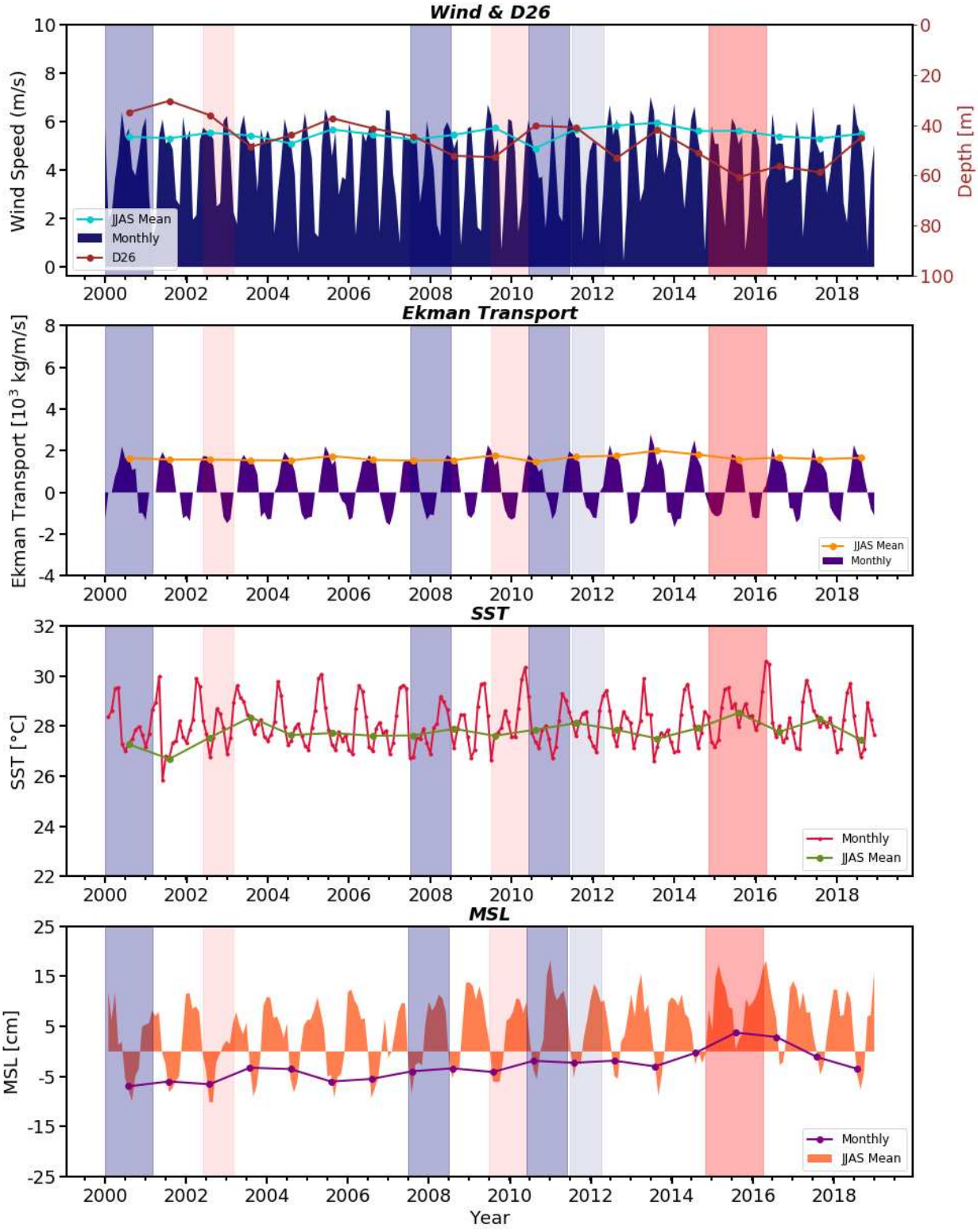

Figure 4.9. Graph showing the wind speed, D26, offshore Ekman Transport, SST and MSL at Site 1 during 2000-2018 with years of moderate El Nino, very strong El Nino, moderate La Nina and strong La Nina shaded by pale brown, darker brown, pale blue and darker blue respectively

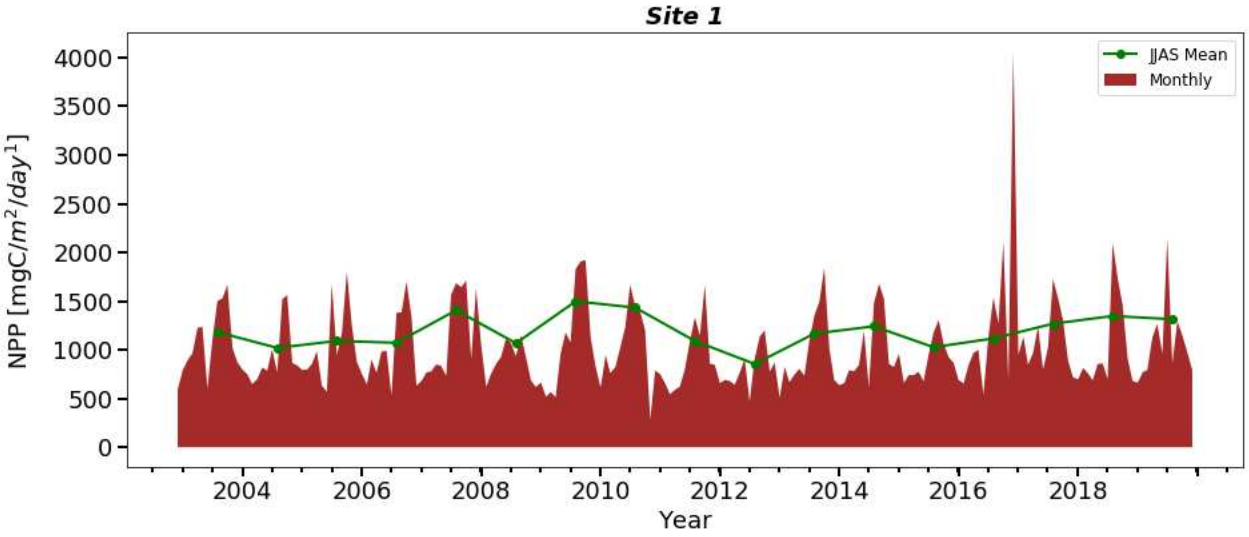

Figure 4.10. NPP for Site 1 during 2003-2019

4.2.2. Site 2

The wind speed at Site 2 ranged between 6-9 ms^{-1} during the southwest monsoon of the study period. The wind was mostly westerly throughout the period. The Ekman transport due to these westerly winds were between 3500-4000 $kgm^{-1}s^{-1}$ and did not show significant variations but a reduction was observed during 2015 and 2017. During the La Nina and IOD years, no particular changes are noted in the wind speed and Ekman transport. The SST showed higher values in 2003, 2015 and 2017. June-September MSL mean showed negative values throughout the study period and a slightly increasing trend can be noted till 2015. In 2015-2016, MSL anomaly showed positive values. During the El Nino and positive IOD years, a rise in MSL anomaly is noted. The LTA at this site was mostly negative at 1° distance from the coast but positive values are observed during 2005-2008. At 2° distance, the LTA was more prominent than that at 1° distance. D26 showed a deepening trend. The NPP ranged between 500-1000 $mgCm^{-2}day^{-1}$ and exceeded 1500 $mgCm^{-2}day^{-1}$ in 2007 and 2015.

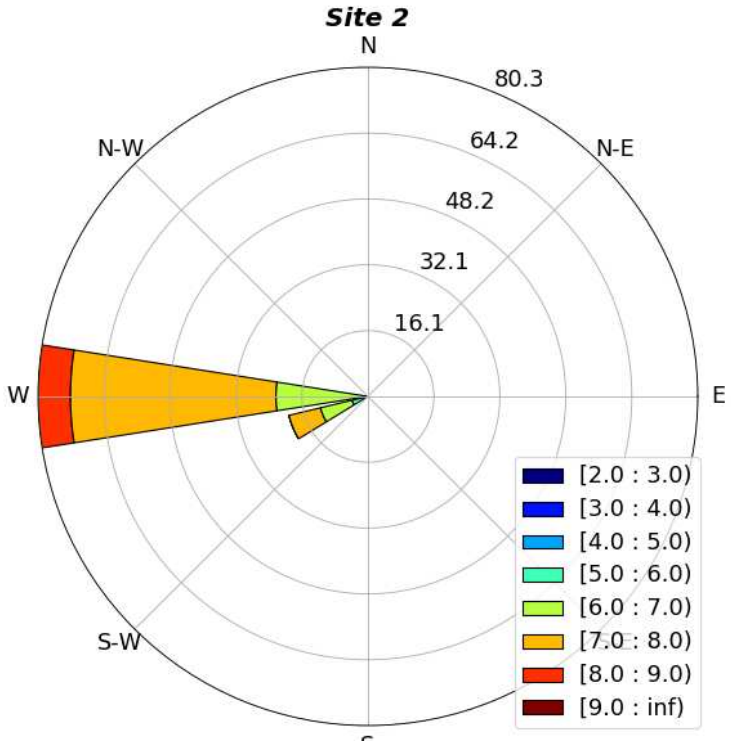

Figure 4.11. Windrose chart for Site 2 during 2000-2018 June-September

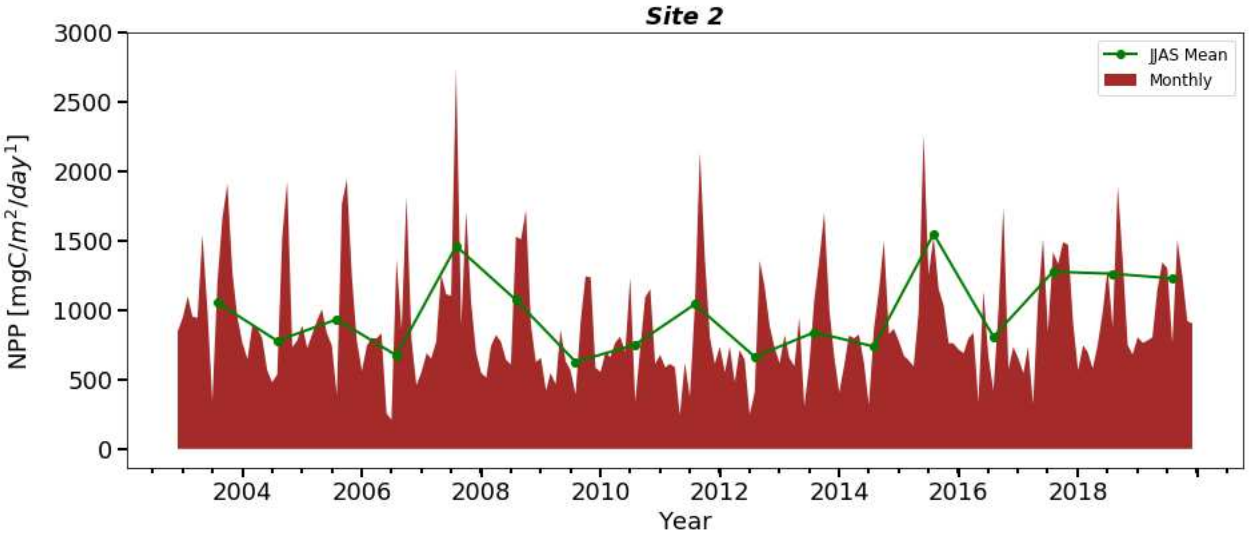

Figure 4.12. NPP for Site 2 during 2003-2019

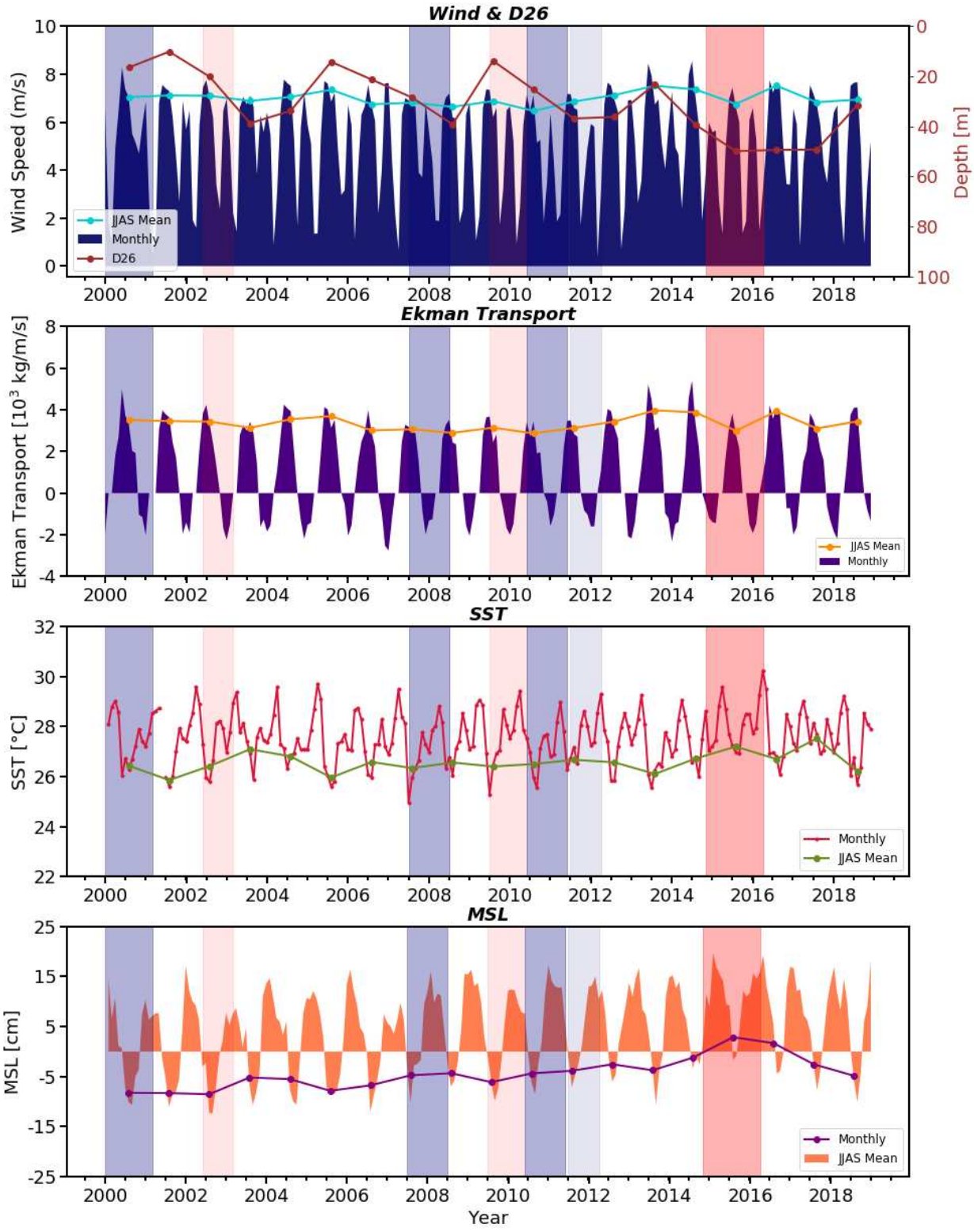

Figure 4.13. Graph showing the wind speed, D26, offshore Ekman Transport, SST and MSL at Site 2 during 2000-2018 with years of moderate El Nino, very strong El Nino, moderate La Nina and strong La Nina shaded by pale brown, darker brown, pale blue and darker blue respectively.

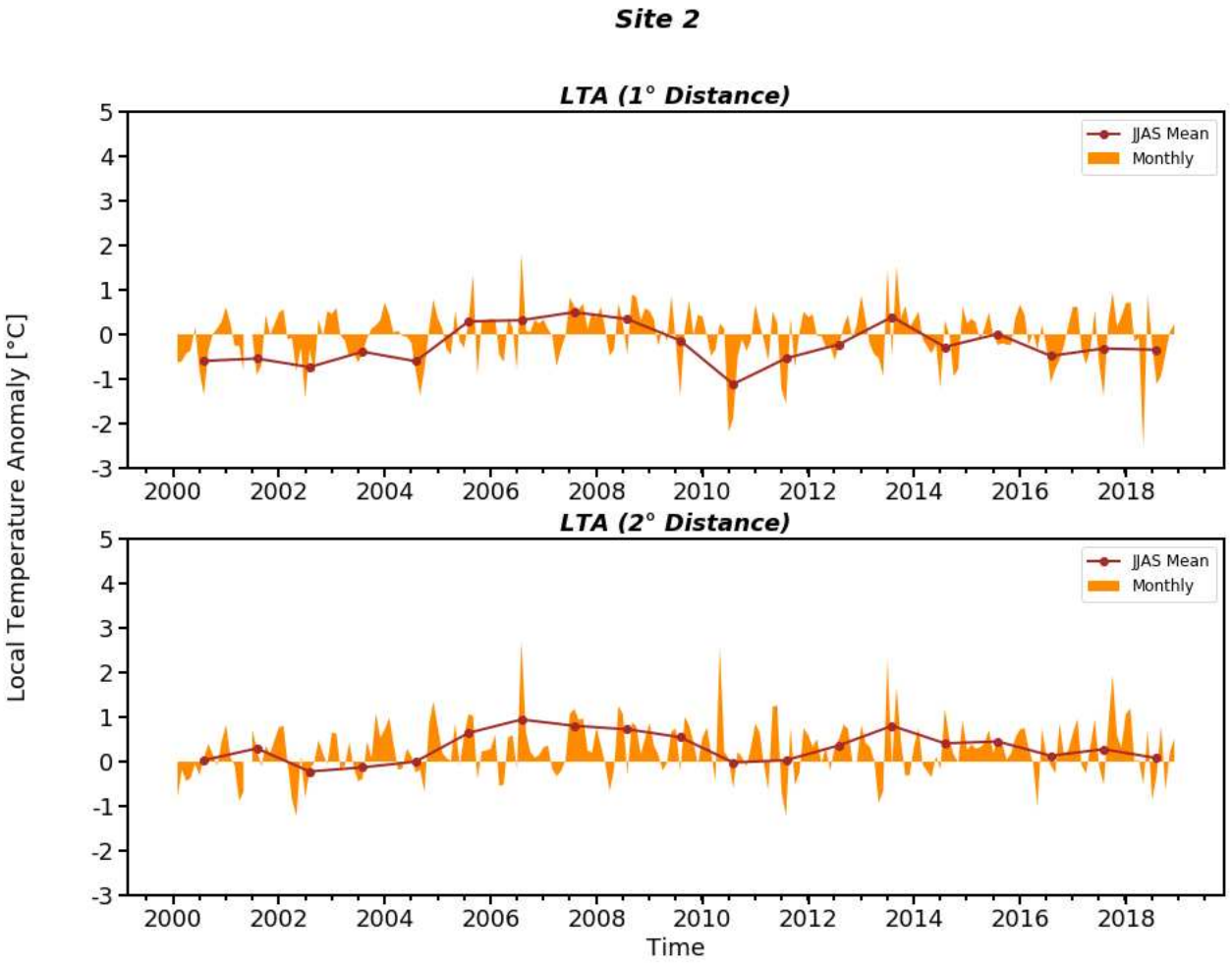

Figure 4.14. LTA for Site 2 during 2000-2018

4.2.3. Site 3

Figure 4.15 showed that the wind speed varied between 6-10 ms^{-1} during June-September of the study period with wind blowing from the west for almost 53% of the time and for the remaining period wind was found to be west-northwesterly. The westerly component of wind was found to be dominant at the site. The highest wind speed as well as offshore Ekman transport is usually observed at Site 3 where the Ekman transport during June-September for the study period ranged between 5000-6000 $kgm^{-1}s^{-1}$ and the maximum was observed during 2014 and 2016. A continuous rise in Ekman transport was observed during 2011-2014. In 2015 and 2017, a sudden decline was observed from the previous year. During the La Nina and IOD events, no significant changes are noted in wind speed and Ekman transport. The June-September SST mean showed inter-annual variations and the highest value of about 27°C occurred in 2015 and the lowest of about 24.5°C in 2001 and 2018. During 2008-2010, a

continuous reduction was noted and during 2010-2012, a continuous rise was noted. A deepening trend is observed in D26. MSL anomaly showed the same pattern as that of Site 1 and Site 2. LTA showed higher values between 1-3°C. From 2001-2004, a continuous decrease is observed and during 2008-2012, a continuous rise is noted. A reduction in LTA is noted during the very strong El Nino year. There is no significant difference between the SST of the two offshore stations. But significant differences in SST between the two offshore stations are observed in 2009, 2016 and 2018. The NPP ranged between 500-1500 $mgCm^{-2}day^{-1}$.

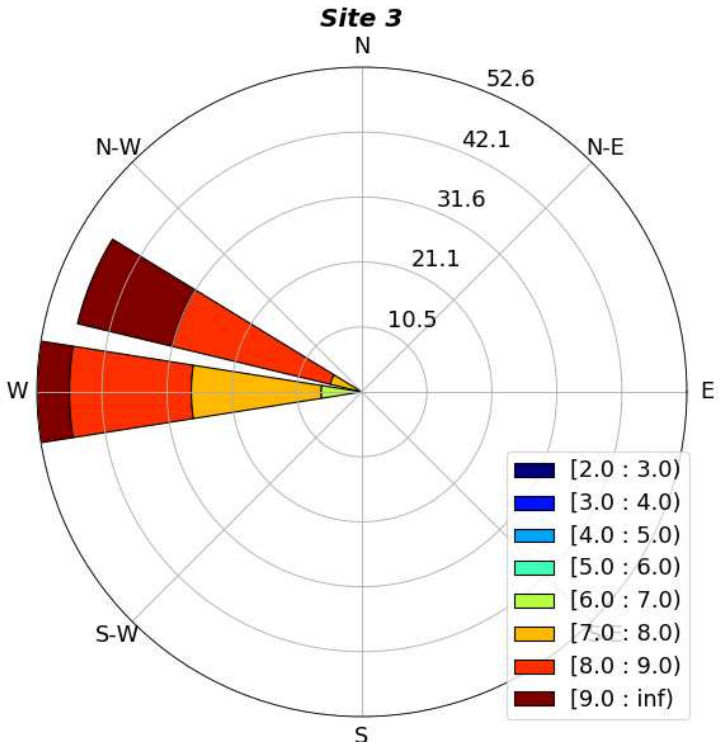

Figure 4.15. Windrose chart for Site 3 during 2000-2018 June-September

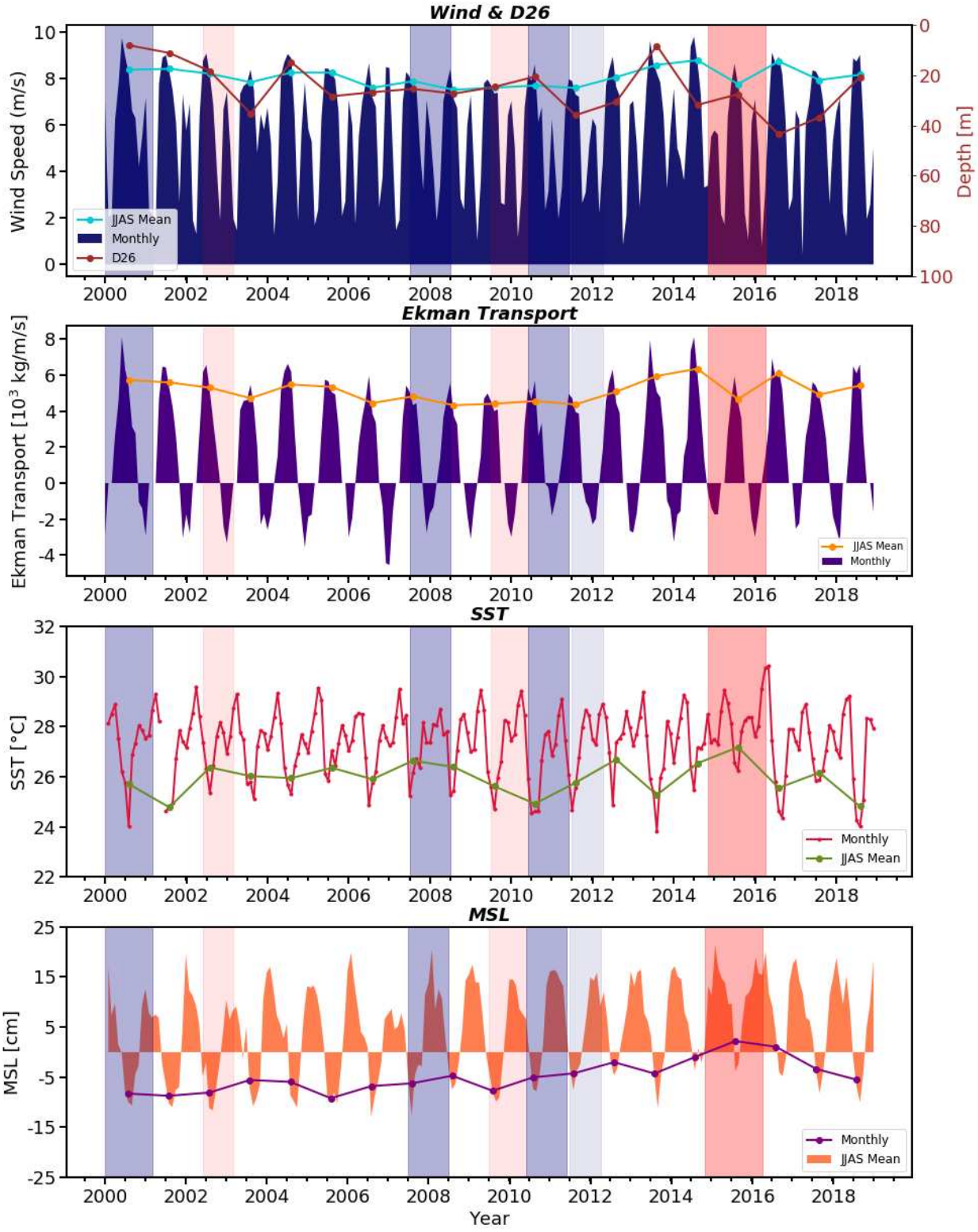

Figure 4.16. Graph showing the wind speed, D26, offshore Ekman Transport, SST and MSL at Site 3 during 2000-2018 with years of moderate El Nino, very strong El Nino, moderate La Nina and strong La Nina shaded by pale brown, darker brown, pale blue and darker blue respectivel

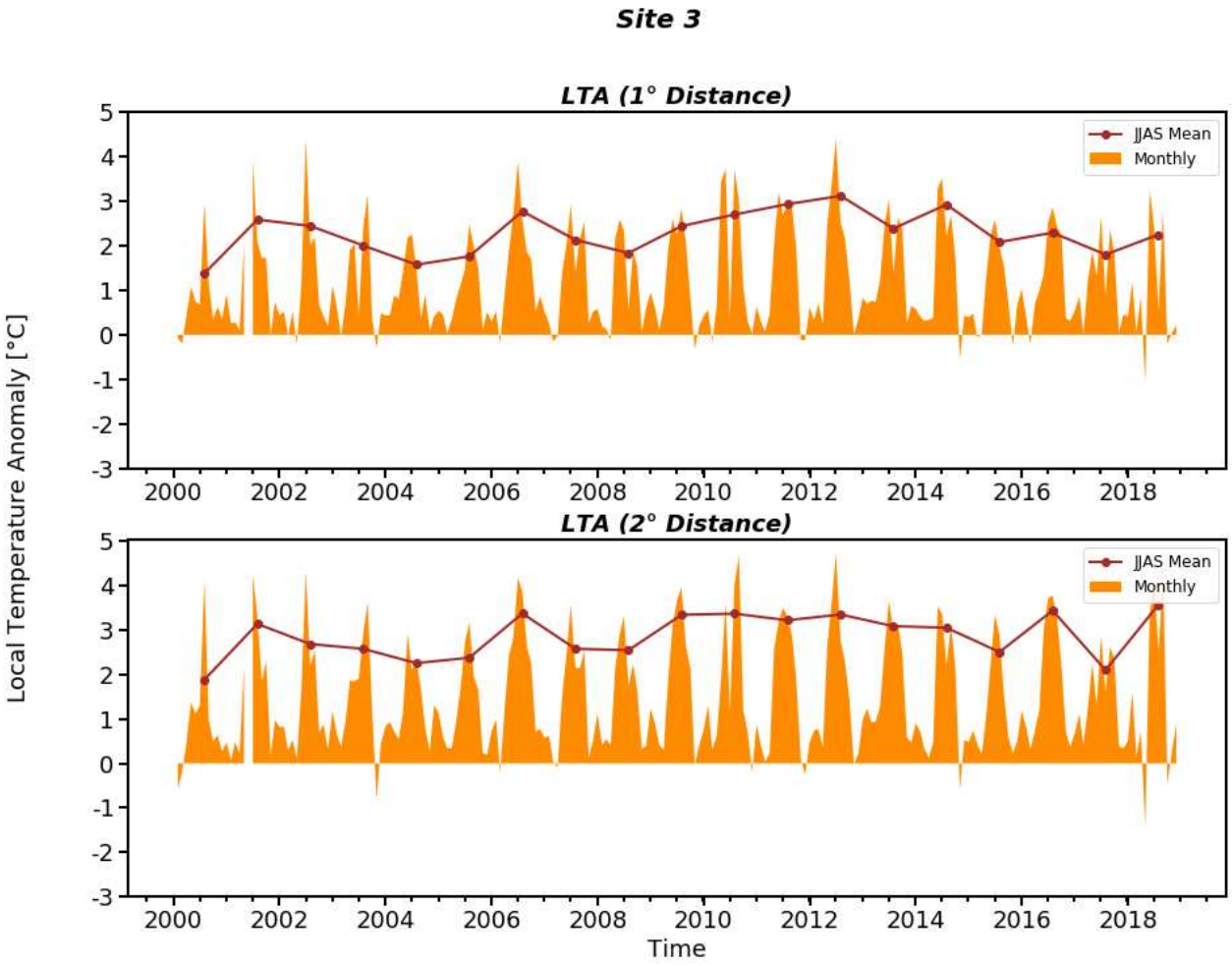

Figure 4.17. LTA for Site 3 during 2000-2018

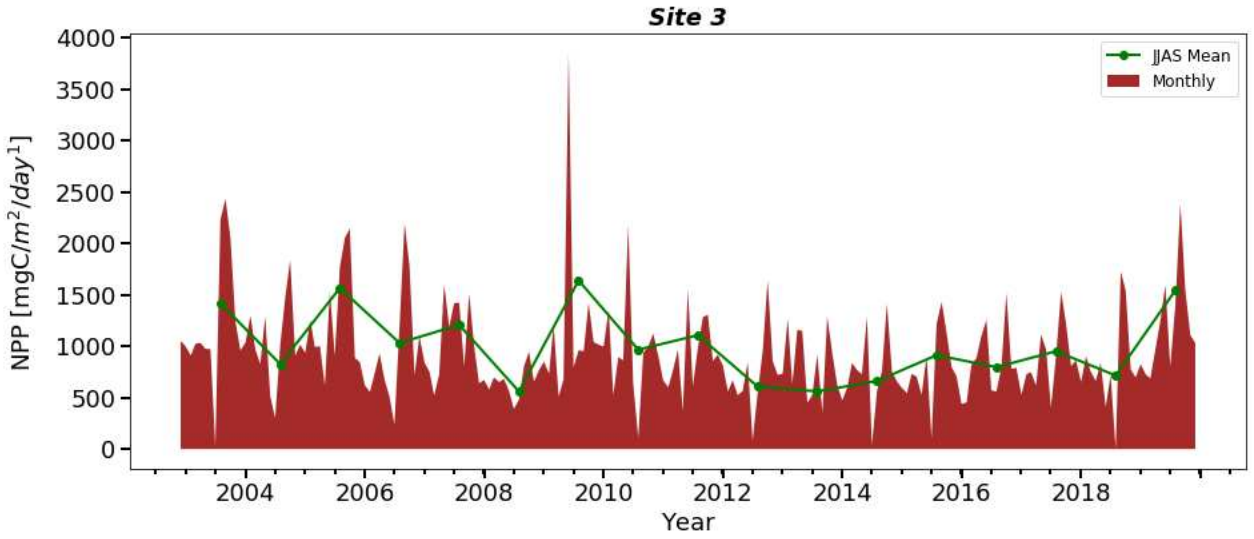

Figure 4.18. NPP for Site 3 during 2003-2019

4.2.4. Site 4

From figure 4.19, it can be seen that the wind speed during the summer monsoon for the study period at Site 4 is ranged between 6-9 ms^{-1} with the direction west-northwesterly for most of the period. This was parallel to the coast. Figure 4.20 showed that the wind speed did not show significant variations inter-annually but was observed to show a sudden decrease during 2015 and 2017. A slight increase in wind speed is observed during 2010-2014. Corresponding changes are observed in Ekman transport. The offshore Ekman transport was negative as the upwelling favorable wind blowing towards the equator and the value ranges between 1000-2000 $kgm^{-1}s^{-1}$. The highest value of about 2000 $kgm^{-1}s^{-1}$ was found during 2016. A continuous reduction was observed during 2004-2009 and from 2011 to 2014, a continuous increase is noted. During the La Nina and IOD years, no significant changes are observed. The SST remained almost steady from 2000 till 2011. In 2015, highest SST close to 28°C was observed and the minimum value of about 25°C was observed in 2018. A slightly deepening trend is observed in D26. The MSL anomaly showed same pattern as that of the previous sites. The LTA ranged between 1-3°C with insignificant variation between the two offshore stations. LTA showed a reduction during the year 2015. D26 was between 20-40 m during most of the period, with the depth reaching close to 10 m below the surface in 2013. The NPP usually varied between 750-1500 $mgCm^{-2}day^{-1}$ but exceeded 2000 $mgCm^{-2}day^{-1}$ during 2009 summer monsoon period.

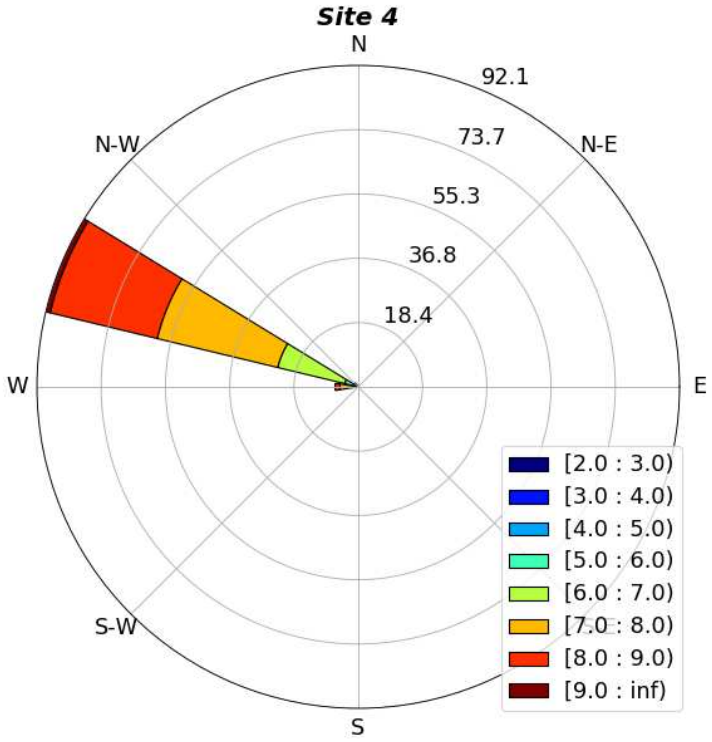

Figure 4.19. Windrose chart for Site 4 during 2000-2018 June-September

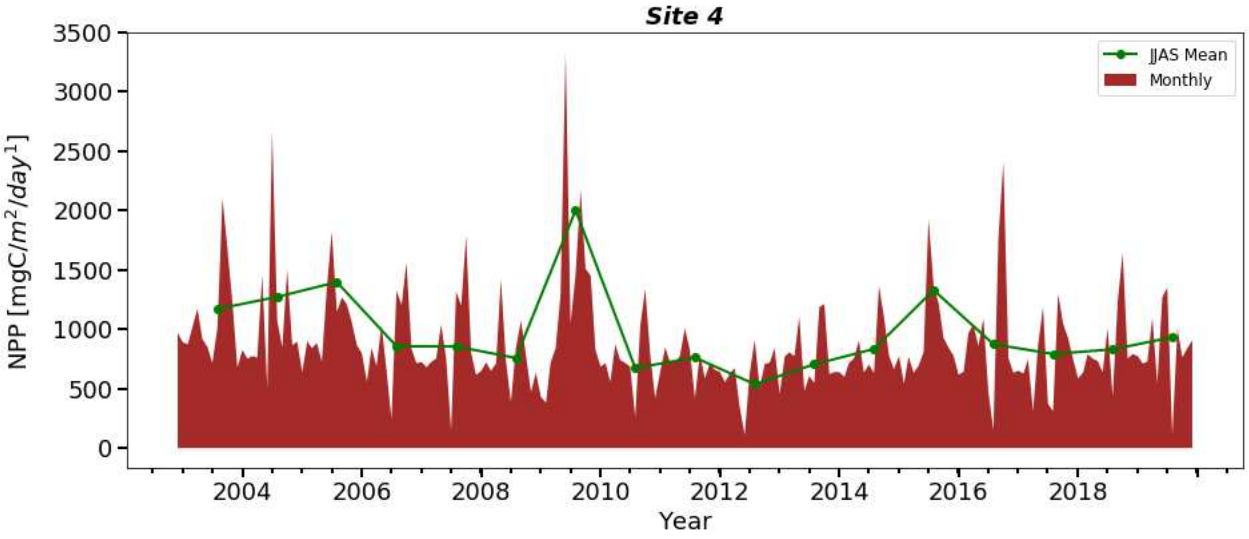

Figure 4.20. NPP for Site 4 during 2003-2019

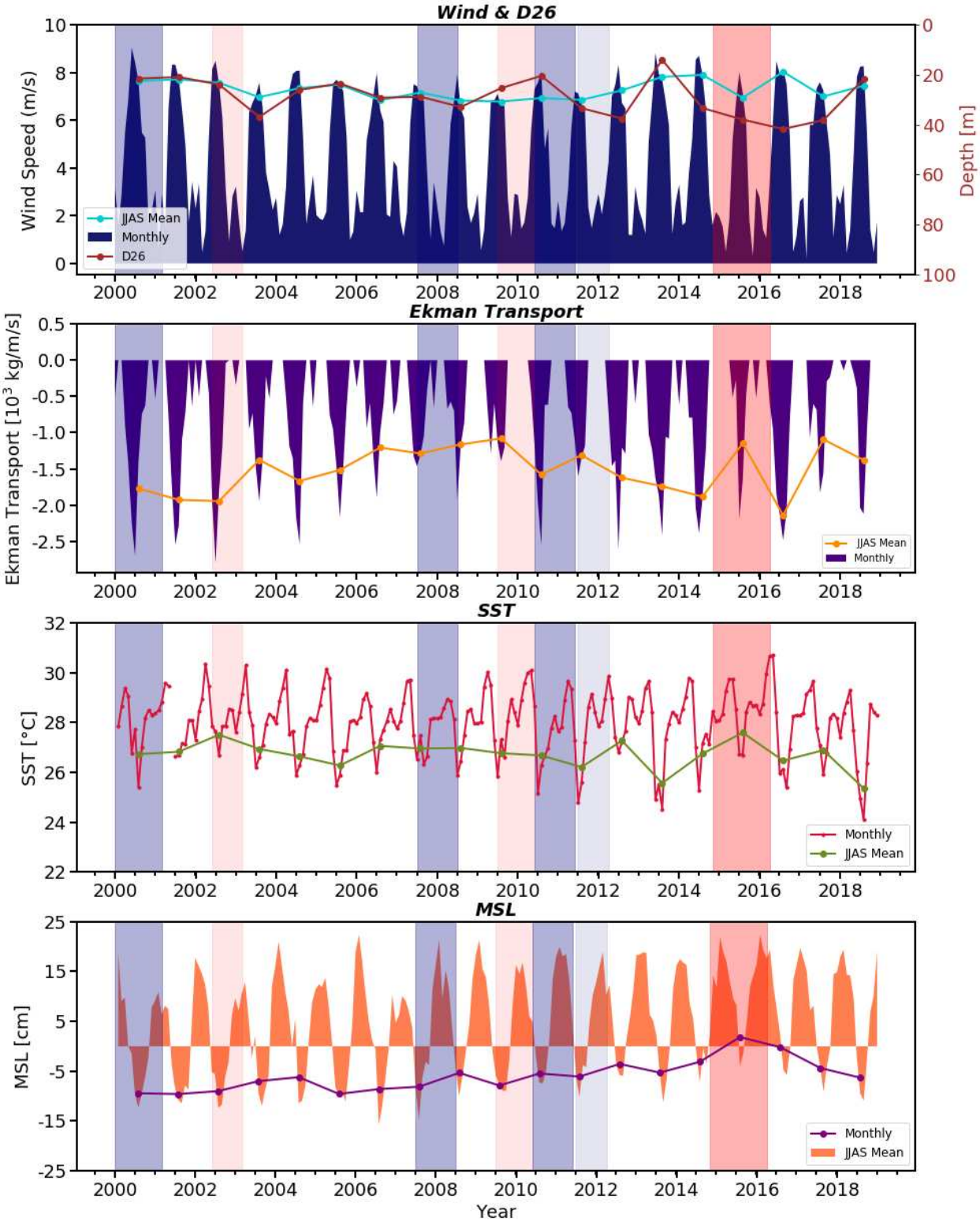

Figure 4.21. Graph showing the wind speed, D26, offshore Ekman Transport, SST and MSL at Site 4 during 2000-2018 with years of moderate El Nino, very strong El Nino, moderate La Nina and strong La Nina shaded by pale brown, darker brown, pale blue and darker blue respectively

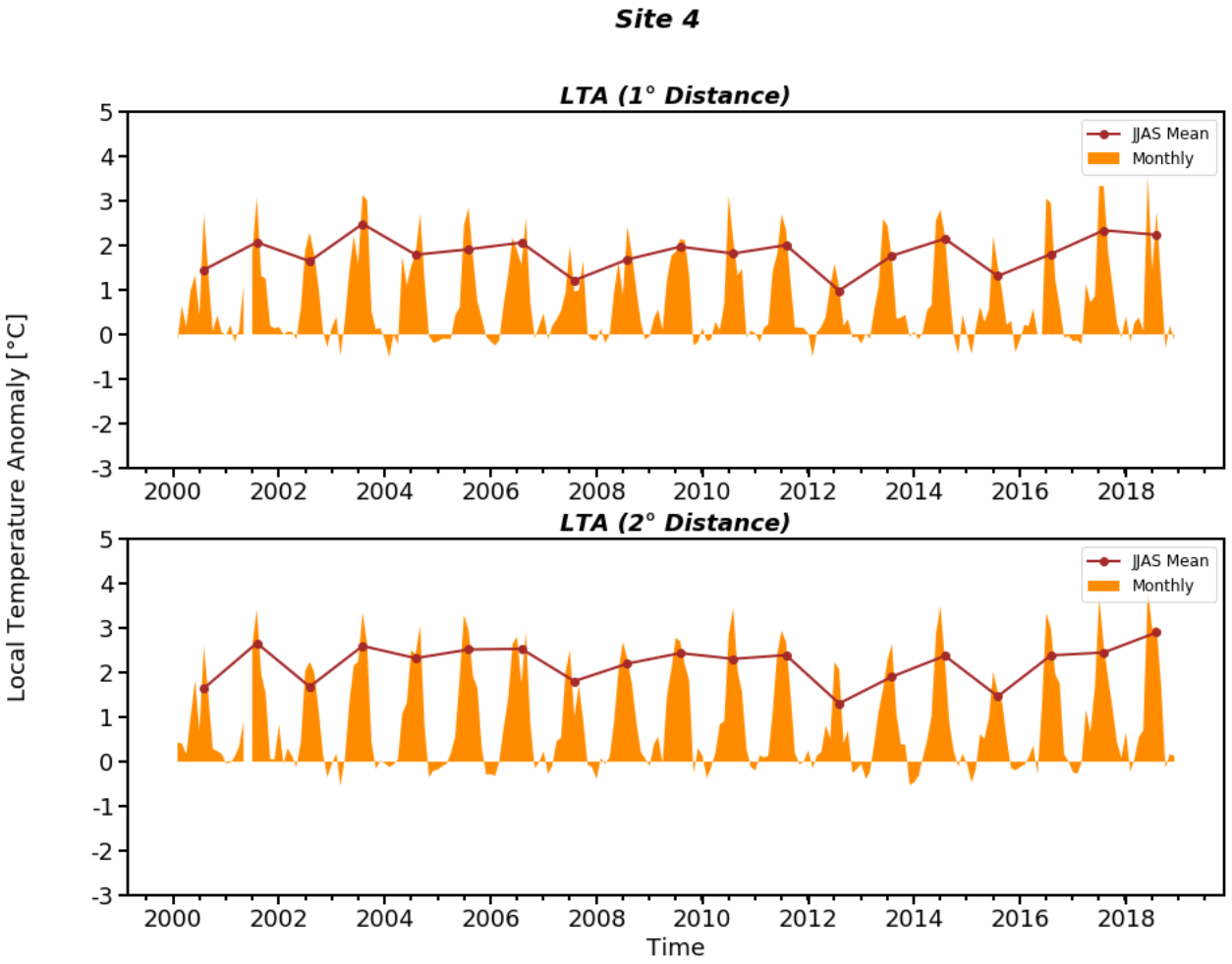

Figure 4.22. LTA for Site 4 during 2000-2018

4.2.5. Site 5

The wind speed during June-September of the study period varied between 5-8 ms^{-1}. The direction was mostly west-southwesterly during the period which is almost parallel to the coast. The wind was nearly steady throughout the period. the Ekman transport was lower than that of Site 4 which varied between 500-1500 $kgm^{-1}s^{-1}$ with highest value greater than 1500 $kgm^{-1}s^{-1}$ observed during 2016. The wind speed and Ekman transport showed reduction in 2003, 2015 and 2017 but was strong in 2016. A sudden increase was also noted in 2010. During the La Nina and IOD events, no particular changes are observed in the wind speed and Ekman transport. The SST was almost steady with the highest SST observed in 2015 which was nearly 28°C. D26 showed a slightly deepening trend. The MSL anomaly showed same range and pattern as that of the previous sites. The LTA values were found to be between 1-2°C. The SSTs at the two offshore stations were nearly similar. A reduction in LTA values was observed in 2015. The NPP usually

varied between 1000-1500 $mgCm^{-2}day^{-1}$ but the value exceeded 1500 $mgCm^{-2}day^{-1}$ during 2009-2010.

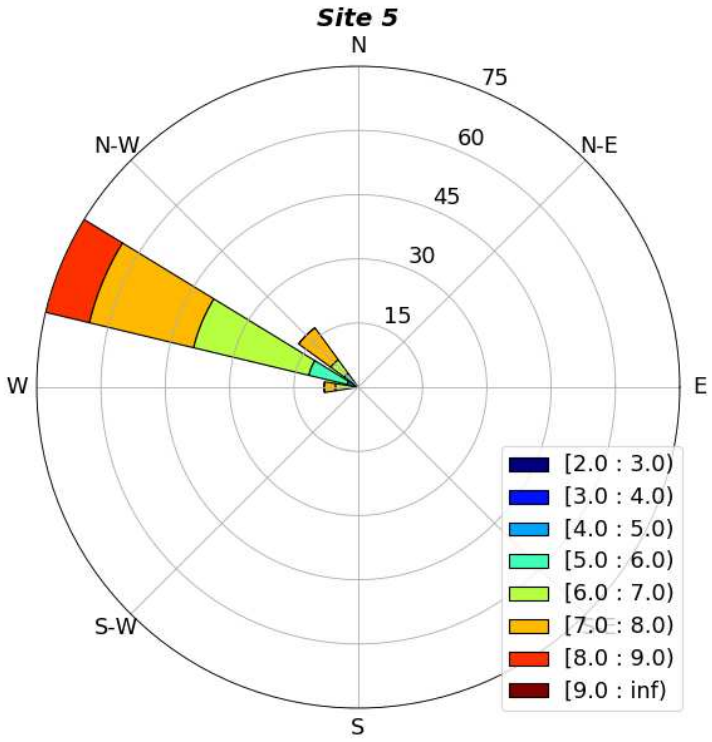

Figure 4.23. Windrose chart for Site 5 during 2000-2018 June-September

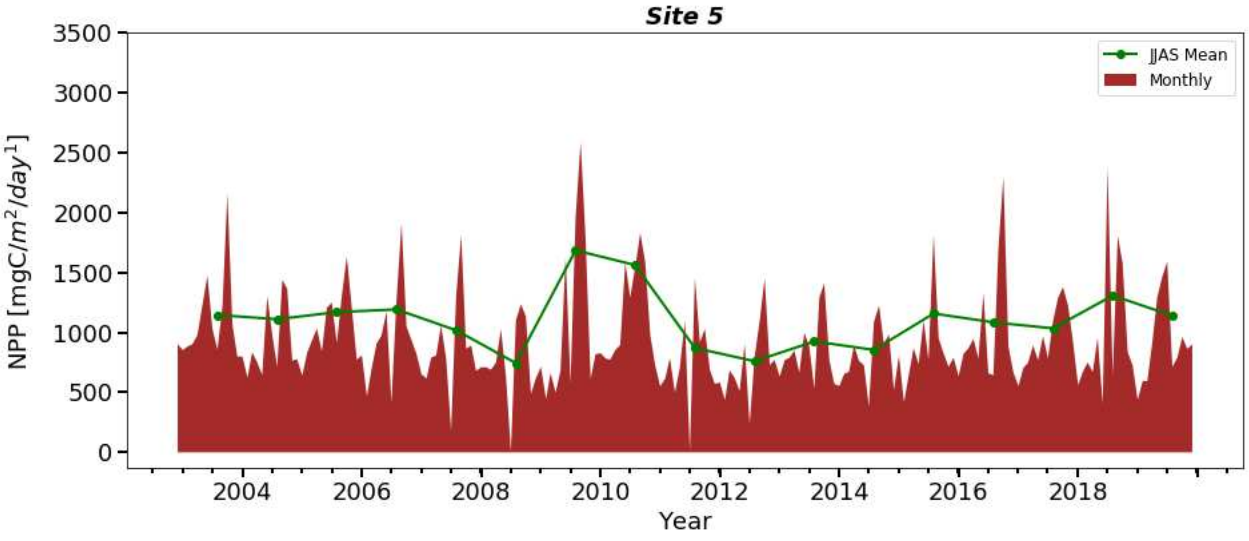

Figure 4.24. NPP for Site 5 during 2003-2019

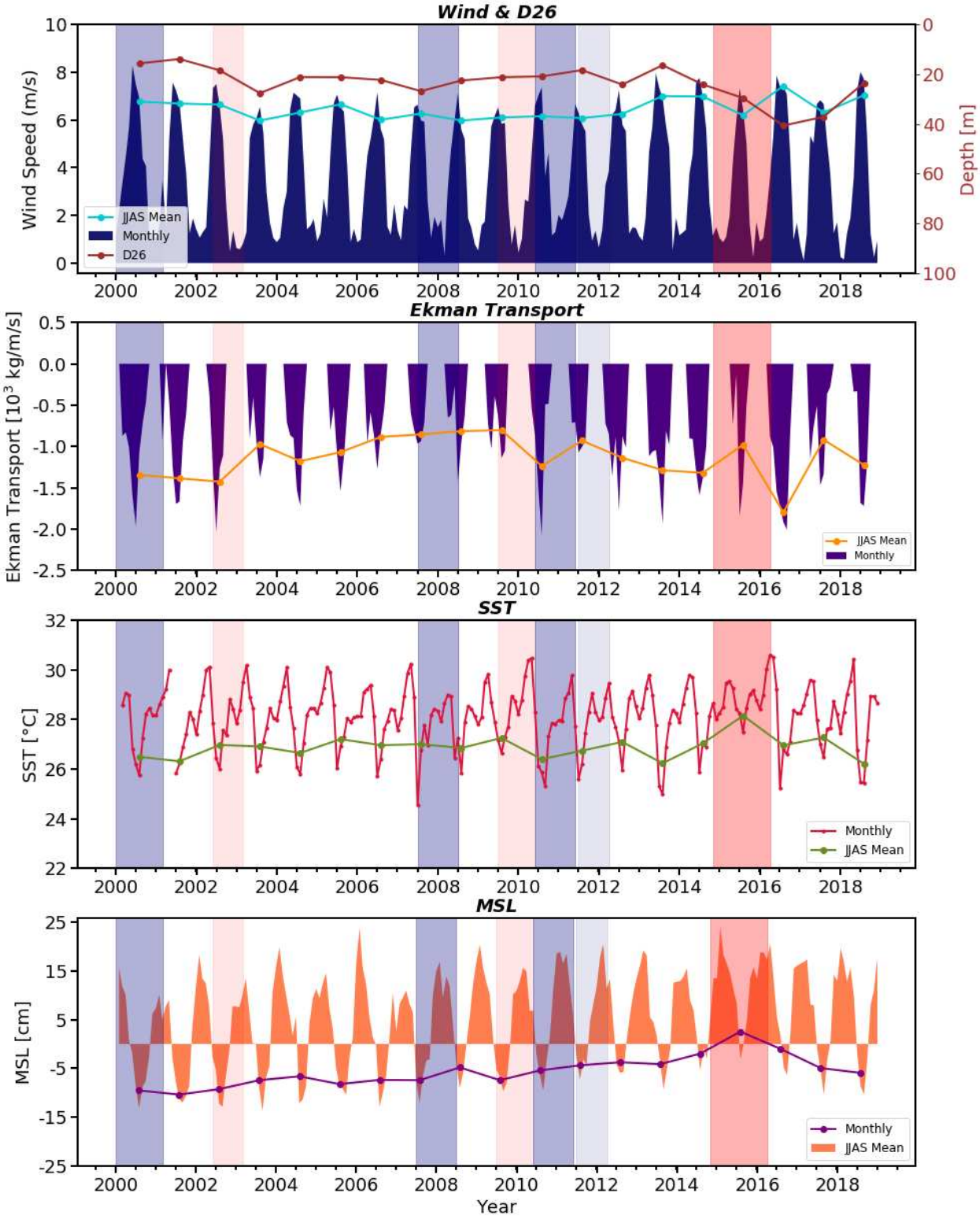

Figure 4.25. Graph showing the wind speed, D26, offshore Ekman Transport, SST and MSL at Site 5 during 2000-2018 with years of moderate El Nino, very strong El Nino, moderate La Nina and strong La Nina shaded by pale brown, darker brown, pale blue and darker blue respectively

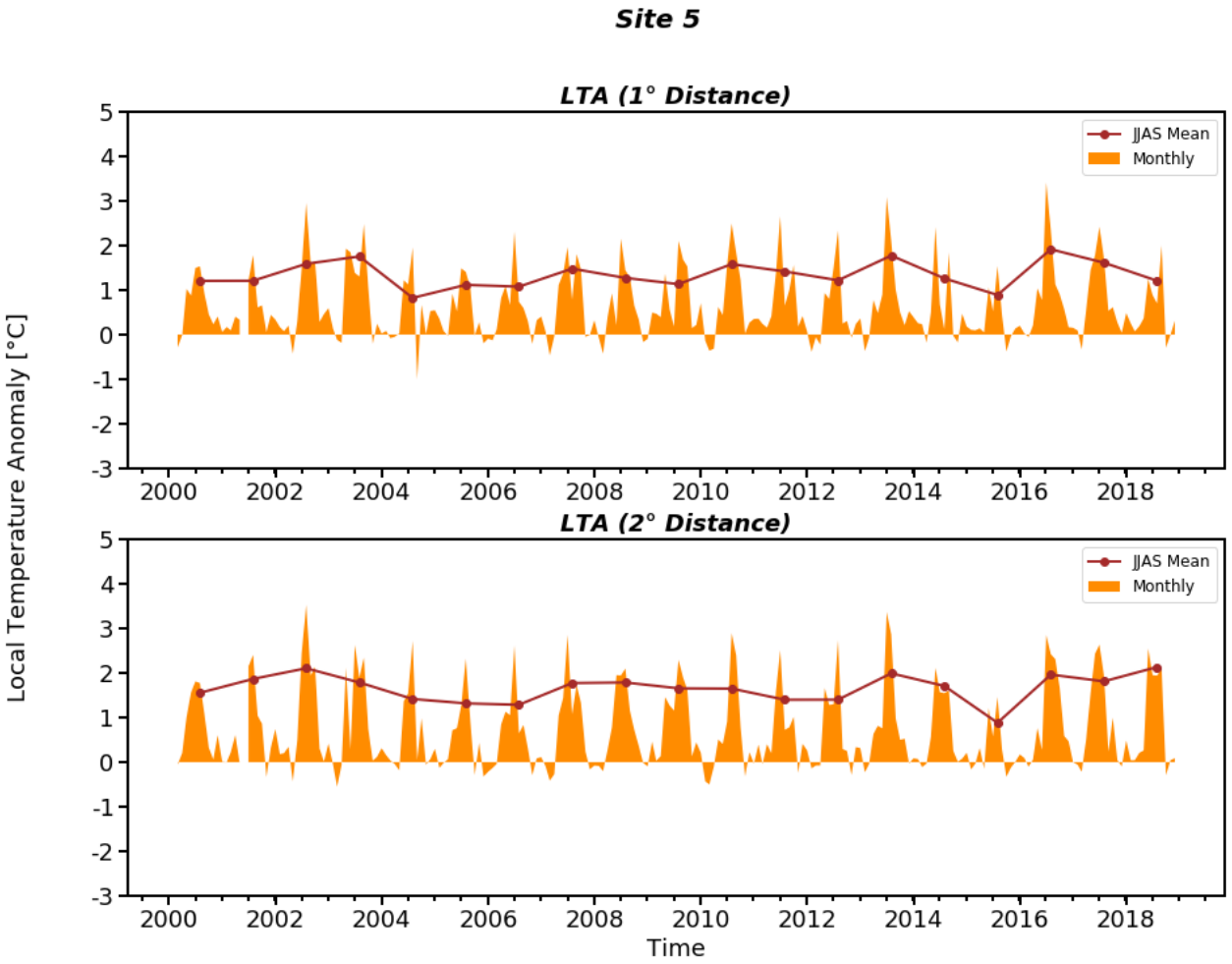

Figure 4.26. LTA for Site 5 during 2000-2018

4.2.6. Site 6

Windrose chart showed that the wind speed varied between 4.5-7.5 ms^{-1} during June-September of the study period and the wind was west-northwesterly for almost 74% of the period. The wind speed throughout the period was almost steady. The offshore Ekman transport was almost steady during the entire study period with values ranging between 500-1000 $kgm^{-1}s^{-1}$ and the highest value was observed during 2016. Both the wind speed and Ekman transport showed a reduction in 2015 and 2017 but showed an increase in 2016. No particular changes were noted during the La Nina and IOD events in wind speed and Ekman transport. The SST varied between 26-27°C and was nearly steady throughout the years but a reduction is noted in 2004. A rise is observed during 2013-2015 with highest SST of about 28°C occurring in 2015. MSL anomaly showed similar pattern as that of the previous sites. A slight, continuous

deepening trend was noted in D26. LTA at a distance of 2° was more prominent at this site and the value was observed to be between 1-2°C. LTA was lowest during 2015. The NPP showed considerable variations inter-annually with the values between 500-2000 $mgCm^{-2}day^{-1}$. The highest NPP values were observed during 2007 and 2014.

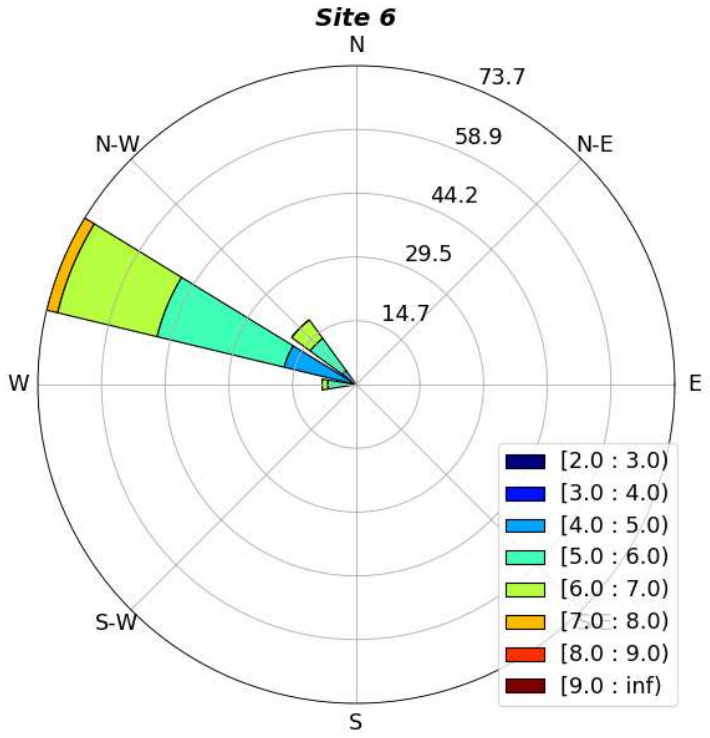

Figure 4.27. Windrose chart for Site 6 during 2000-2018 June-September

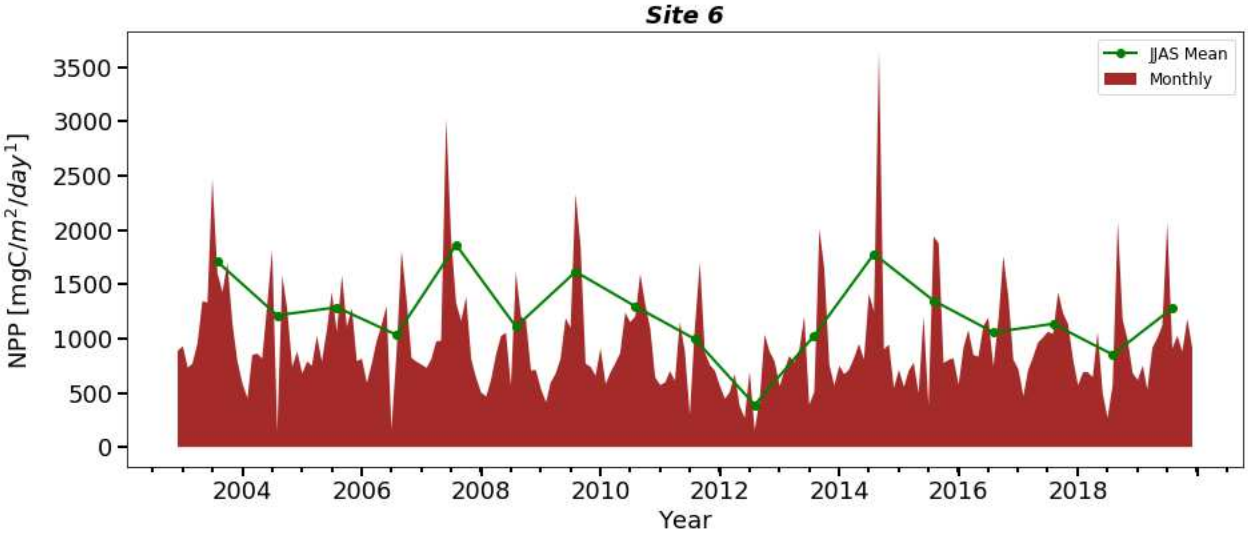

Figure 4.28. NPP for Site 6 during 2003-2019

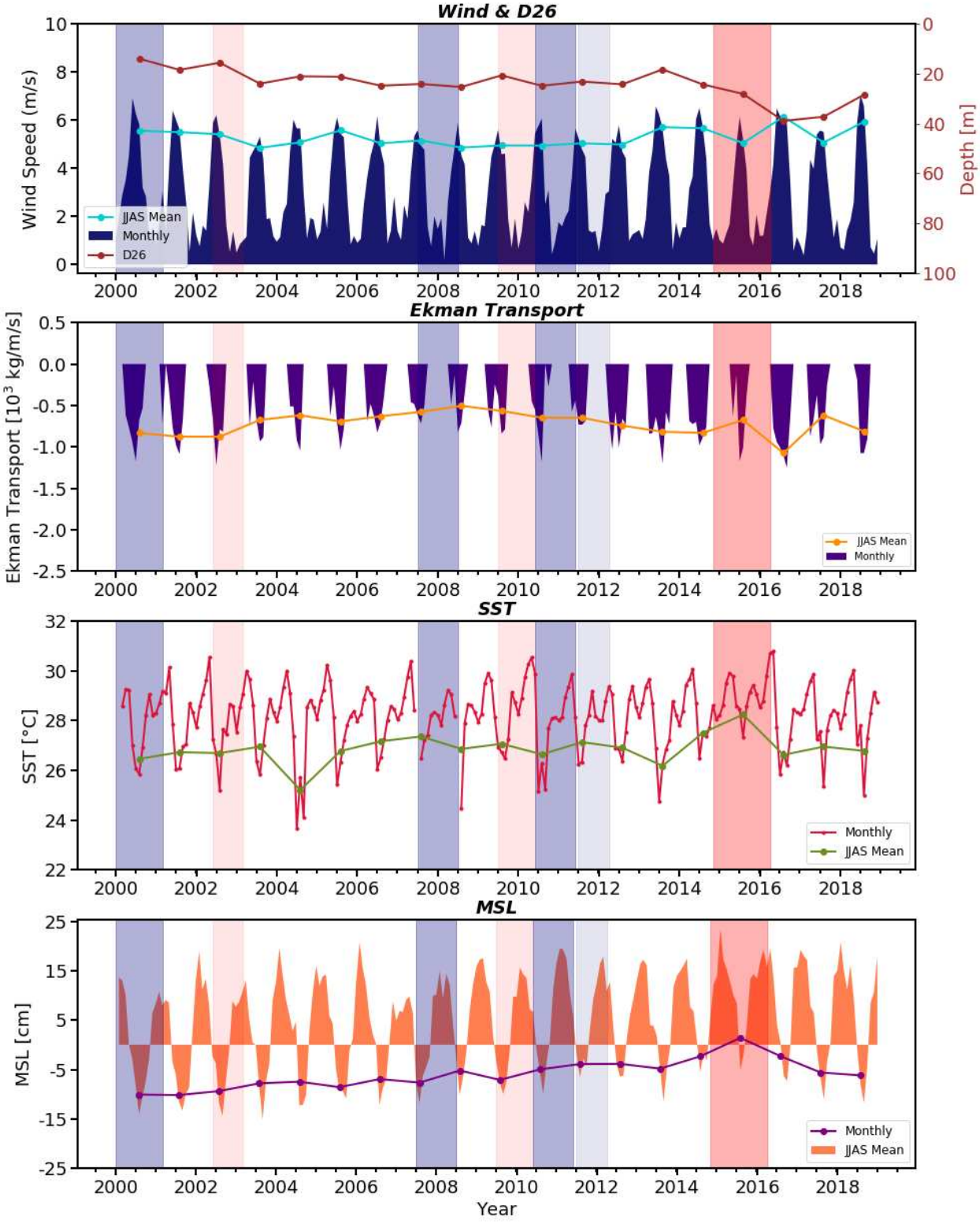

Figure 4.29. Graph showing the wind speed, D26, offshore Ekman Transport, SST and MSL at Site 6 during 2000-2018 with years of moderate El Nino, very strong El Nino, moderate La Nina and strong La Nina shaded by pale brown, darker brown, pale blue and darker blue respectively

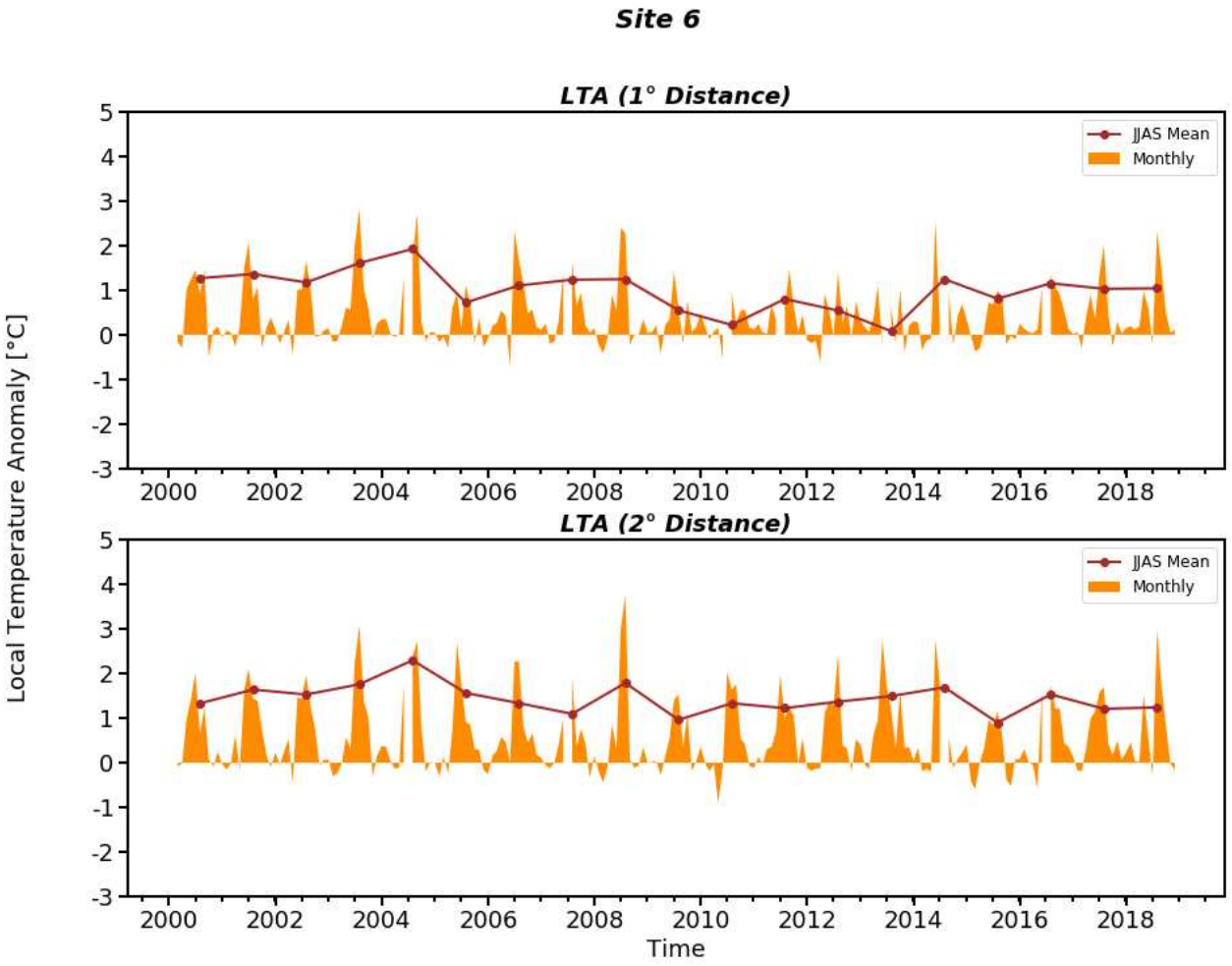

Figure 4.30. LTA for Site 6 during 2000-2018

4.2.7. Site 7

The wind speed during the summer monsoon months of the study period ranged between 2-5 ms^{-1} and the direction was mostly west-northwesterly. The wind speed was almost steady for the period. the Ekman transport was lower than that of Site 6 and occurred to be below 500 $kgm^{-1}s^{-1}$. The value showed continuous reduction during 2005-2009 and was almost absent in 2009. Strongest Ekman transport was observed in 2016. SST varied between 25-27°C and the lowest was in 2013. The MSL anomaly showed similar pattern as that of the previous sites. The LTA values were more prominent than that of Site 6. Continuous reduction is observed during 2003 to 2008. In 2013, 2014 and 2016, highest values are observed. The SSTs between the two offshore stations were almost similar but showed significant variations in 2013 and 2014. D26 showed a deepening trend, with the maximum depth observed during 2017. The NPP ranged between 1000-1500 $mgCm^{-2}day^{-1}$.

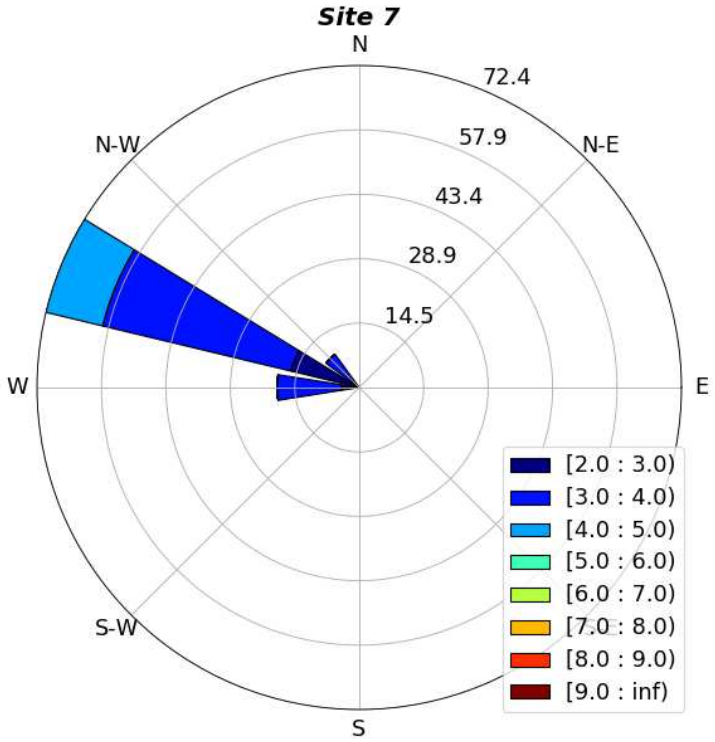

Figure 4.31. Windrose chart for Site 7 during 2000-2019

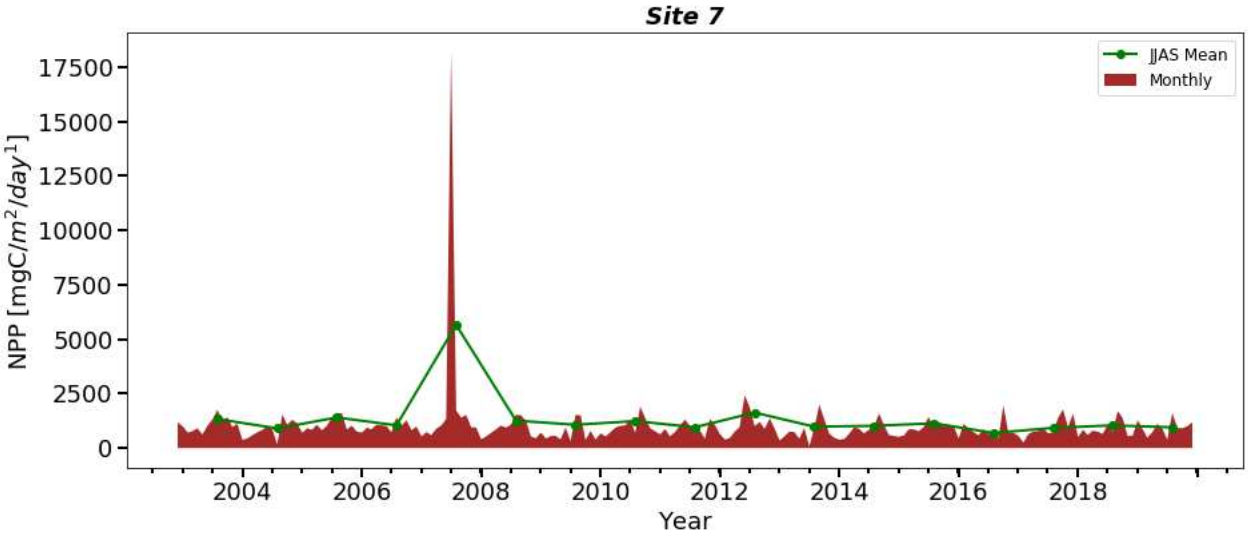

Figure 4.32. NPP for Site 7 during 2003-2019

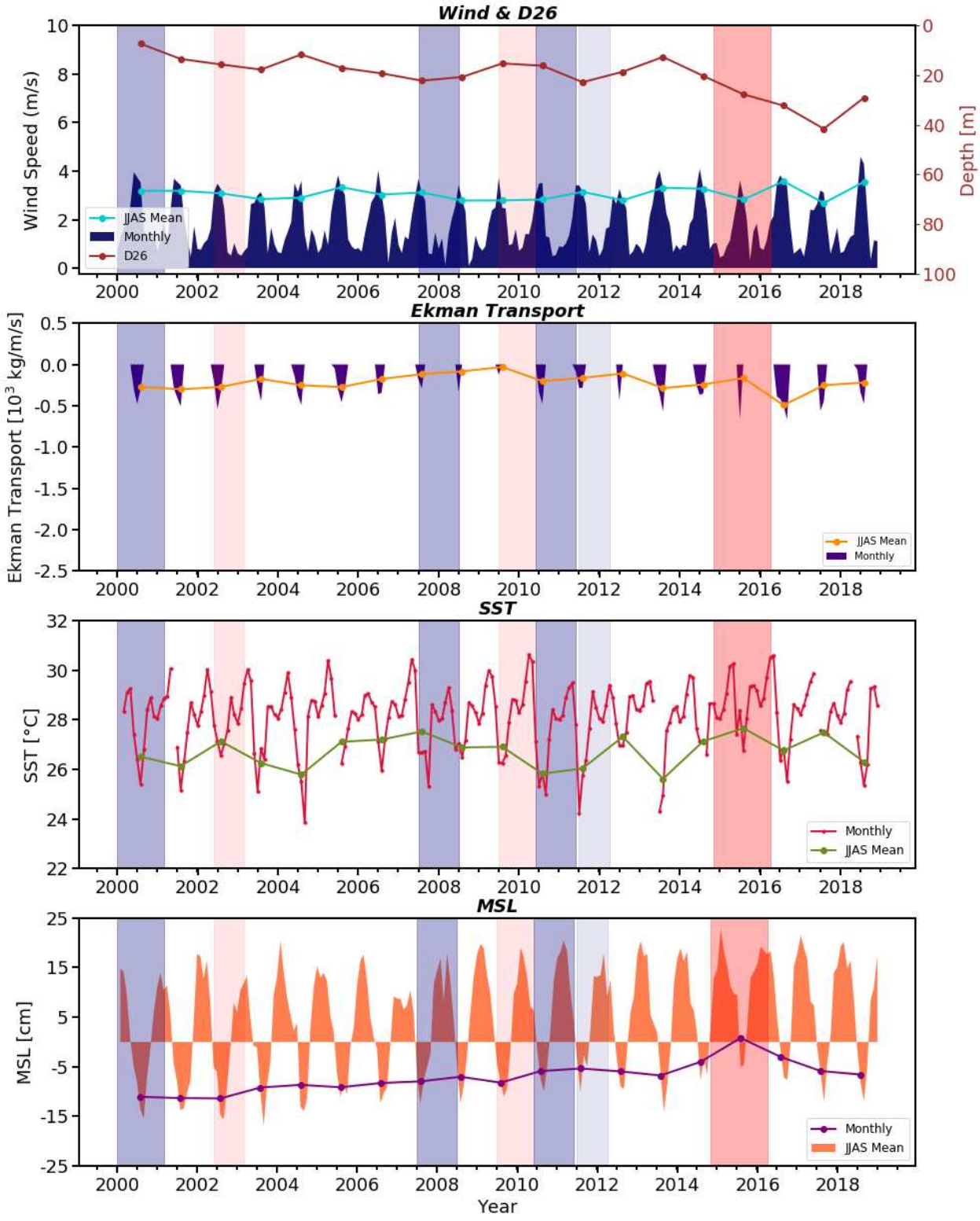

Figure 4.33. Graph showing the wind speed, D26, offshore Ekman Transport, SST and MSL at Site 7 during 2000-2018 with years of moderate El Nino, very strong El Nino, moderate La Nina and strong La Nina shaded by pale brown, darker brown, pale blue and darker blue respectively

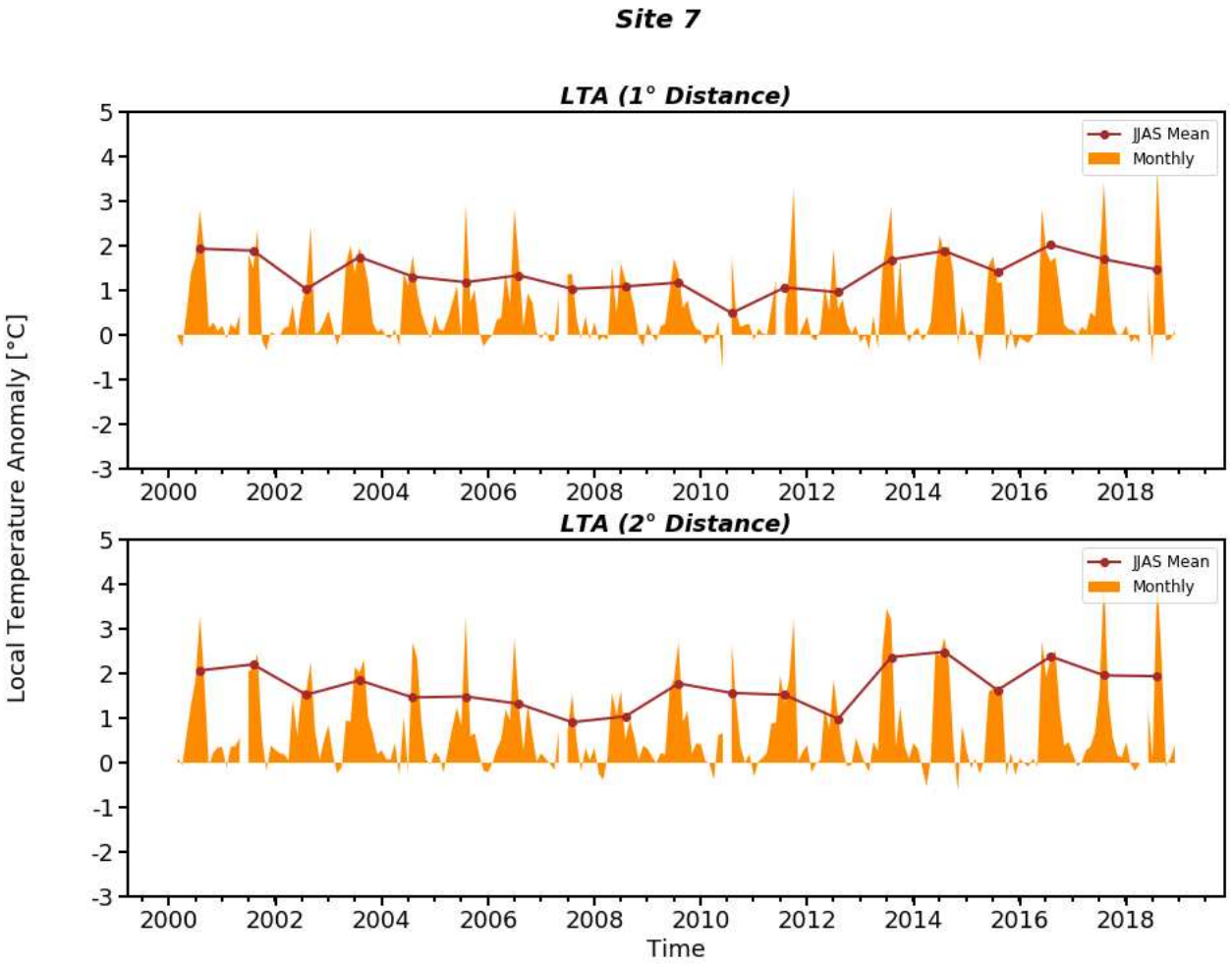

Figure 4.34. LTA for Site 7 during 2000-2018

4.2.8. Site 8

The wind was mostly west-northwesterly during the monsoon season of the study period and was stronger than that of Site 7. For about 20% of the time, the direction was observed to be westerly and for about 10% of the time, the wind was northwesterly. The wind during most of the period was not clearly parallel to the coast. This can be understood from the figure 4.36 which showed low Ekman transport which was below 500 $kgm^{-1}s^{-1}$. In 2015 and 2017, a reduction in wind speed and Ekman transport is observed. But no significant changes are noted during the La Nina and IOD years. The June-September SST mean was almost steady from 2000 to 2012 and in 2013, a sudden reduction of SST is observed. The lowest summer monsoon SST of about 25°C was observed in that particular year. The SST then rose and reached highest value of about 28°C in 2014 and 2015. D26 was observed to be deepening. MSL showed similar pattern as that of the other sites. The LTA showed almost similar values as that of Site 7 and

varied between 1-2°C. The NPP values ranged between 750-2000 $mgCm^{-2}day^{-1}$ with the highest value observed during 2014.

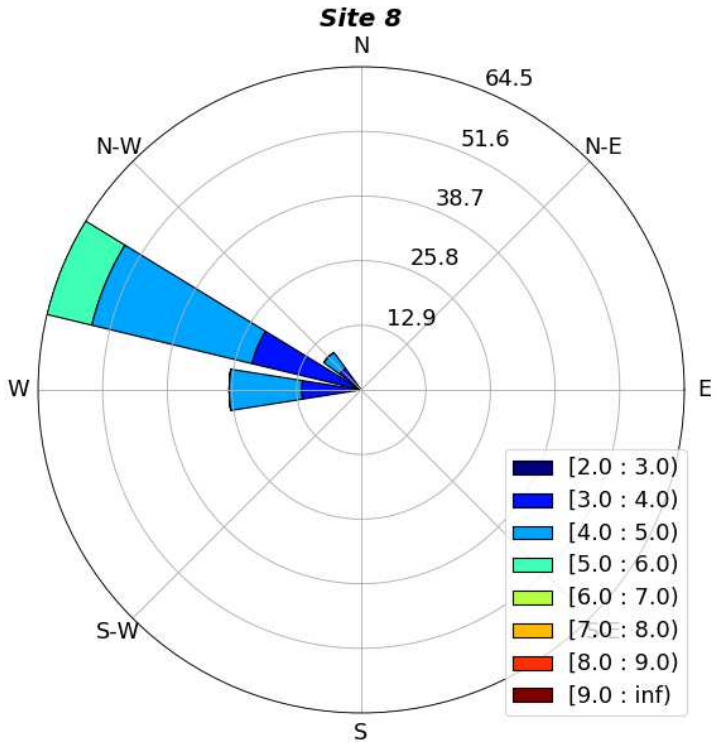

Figure 4.35. Windrose chart for Site 8 during 2000-2018 June-September

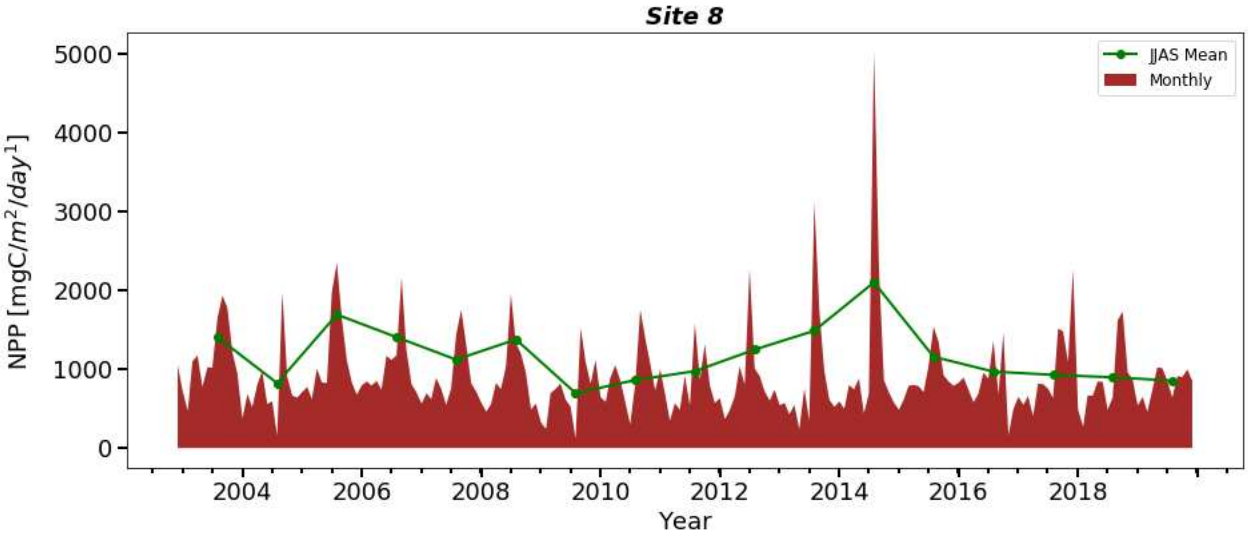

Figure 4.36. NPP for Site 8 during 2003-2019

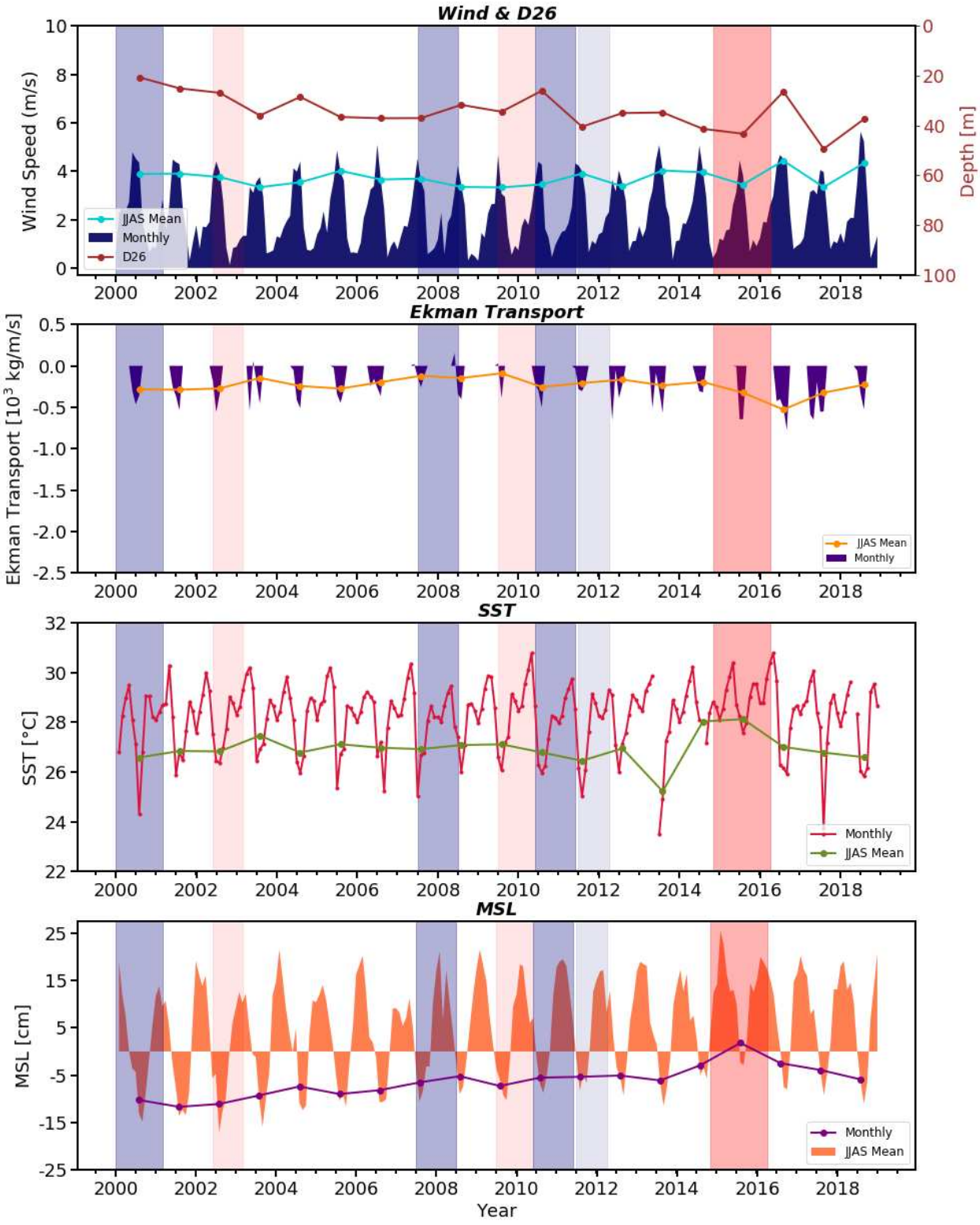

Figure 4.37. Graph showing the wind speed, D26, offshore Ekman Transport, SST and MSL at Site 8 during 2000-2018 with years of moderate El Nino, very strong El Nino, moderate La Nina and strong La Nina shaded by pale brown, darker brown, pale blue and darker blue respectively

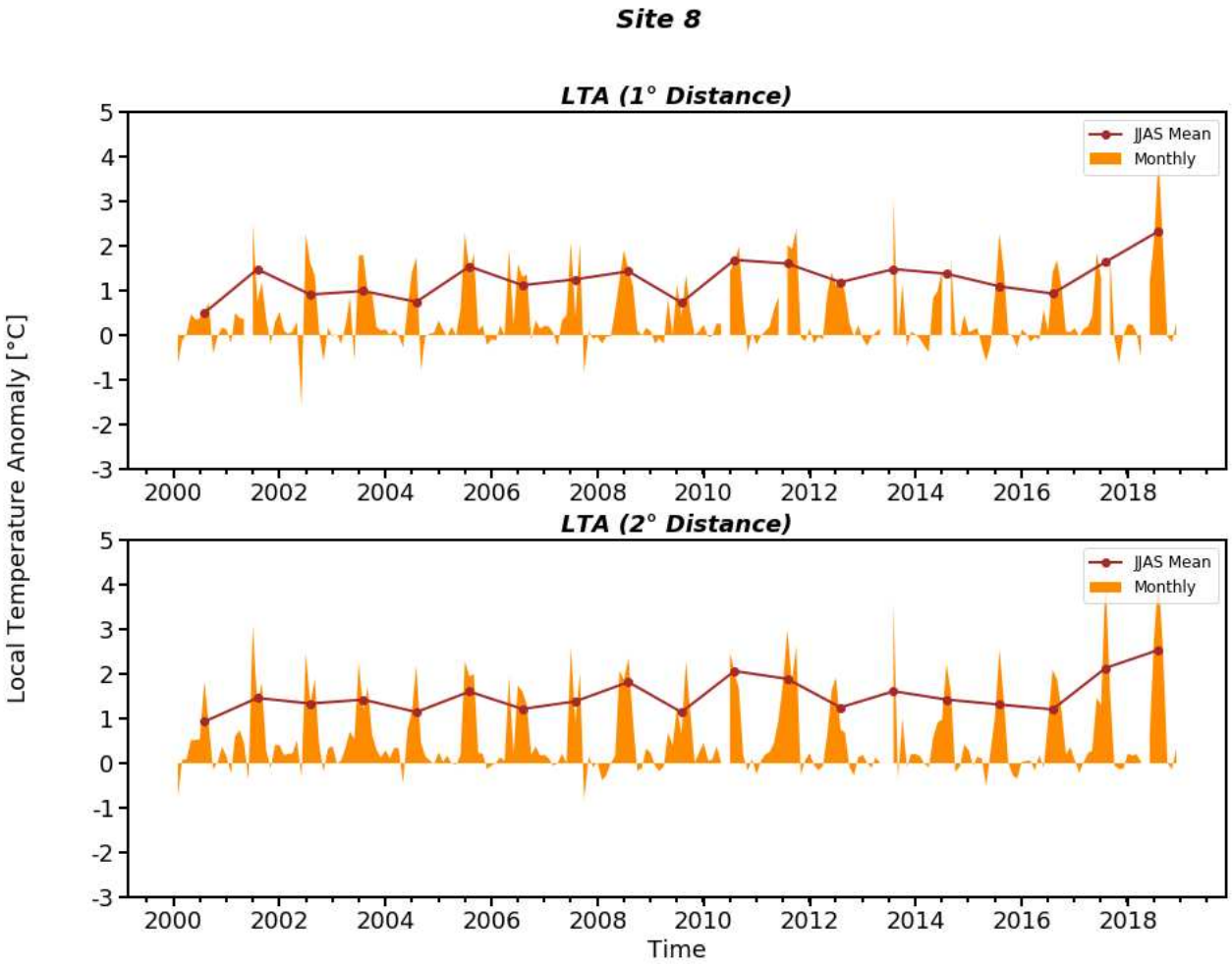

Figure 4.38. LTA for Site 8 during 2000-2018

4.2.9. Site 9

At this site, the wind direction varied between west-northwesterly and westerly and the wind speed ranged between 4-8 ms^{-1}. The wind speed was higher than that of Site 8. The wind throughout the period was nearly perpendicular to the coast. Even though the wind speed during the study period was higher than that of Site 8, the Ekman transport was negligible. The SST was almost steady showing lowest value of about 26°C in 2013 and highest of about 28°C in 2015. MSL anomaly showed similar pattern as that of other sites. LTA values were positive but most of the years, it showed values less than 1°C and appeared to be close to zero during 2009. The SST at both offshore stations were almost similar. The D26 showed a continuous deepening trend. The NPP was slightly lesser than that of Site 8 with values ranging within 500-1000 $mgCm^{-2}day^{-1}$ during most of the years but the value reached up to 2000 $mgCm^{-2}day^{-1}$ during 2004.

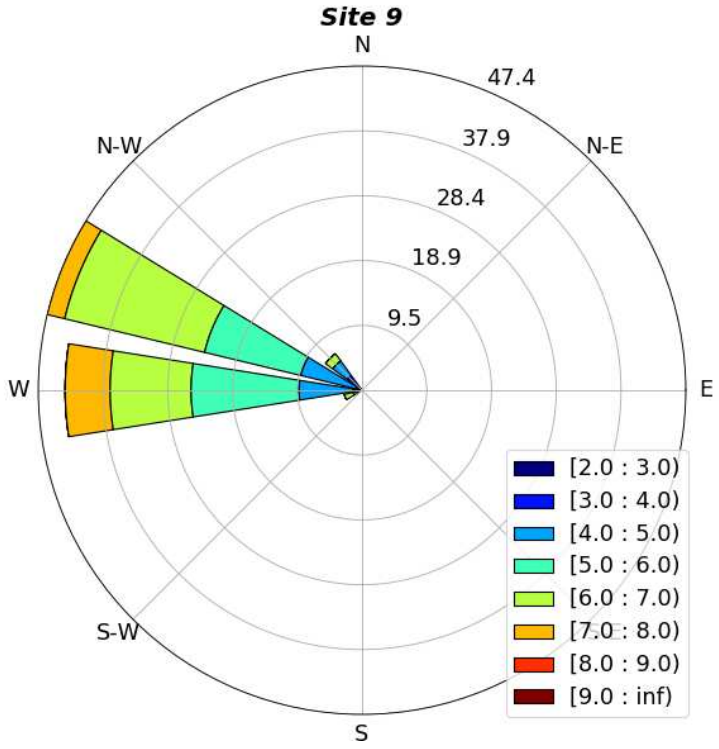

Figure 4.39. Windrose chart for Site 9 during 2000-2018 June-September

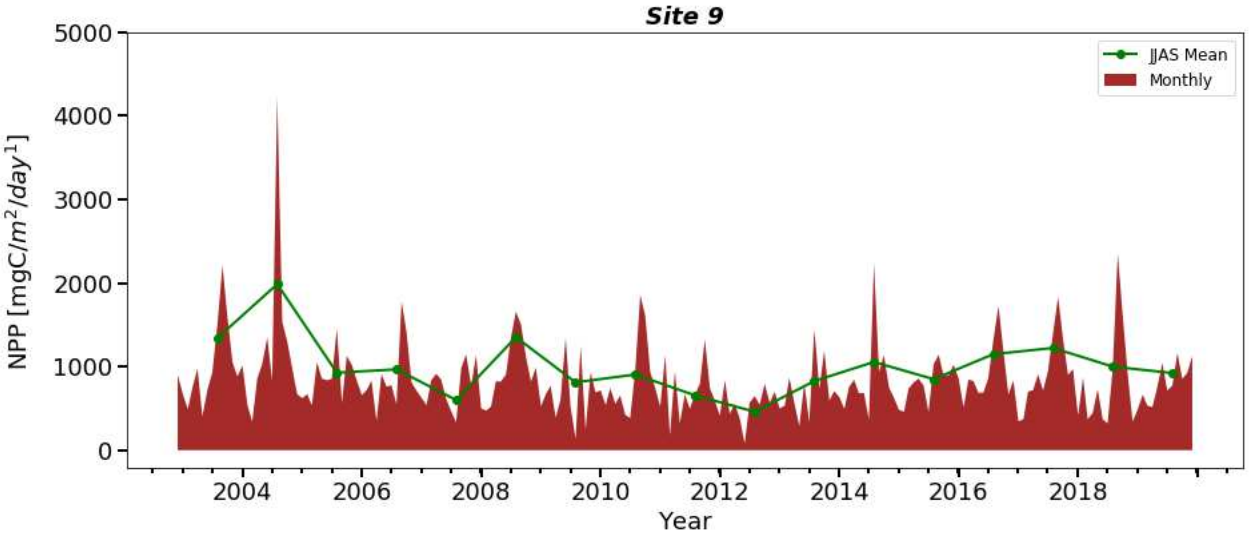

Figure 4.40. NPP for Site 9 during 2003-2019

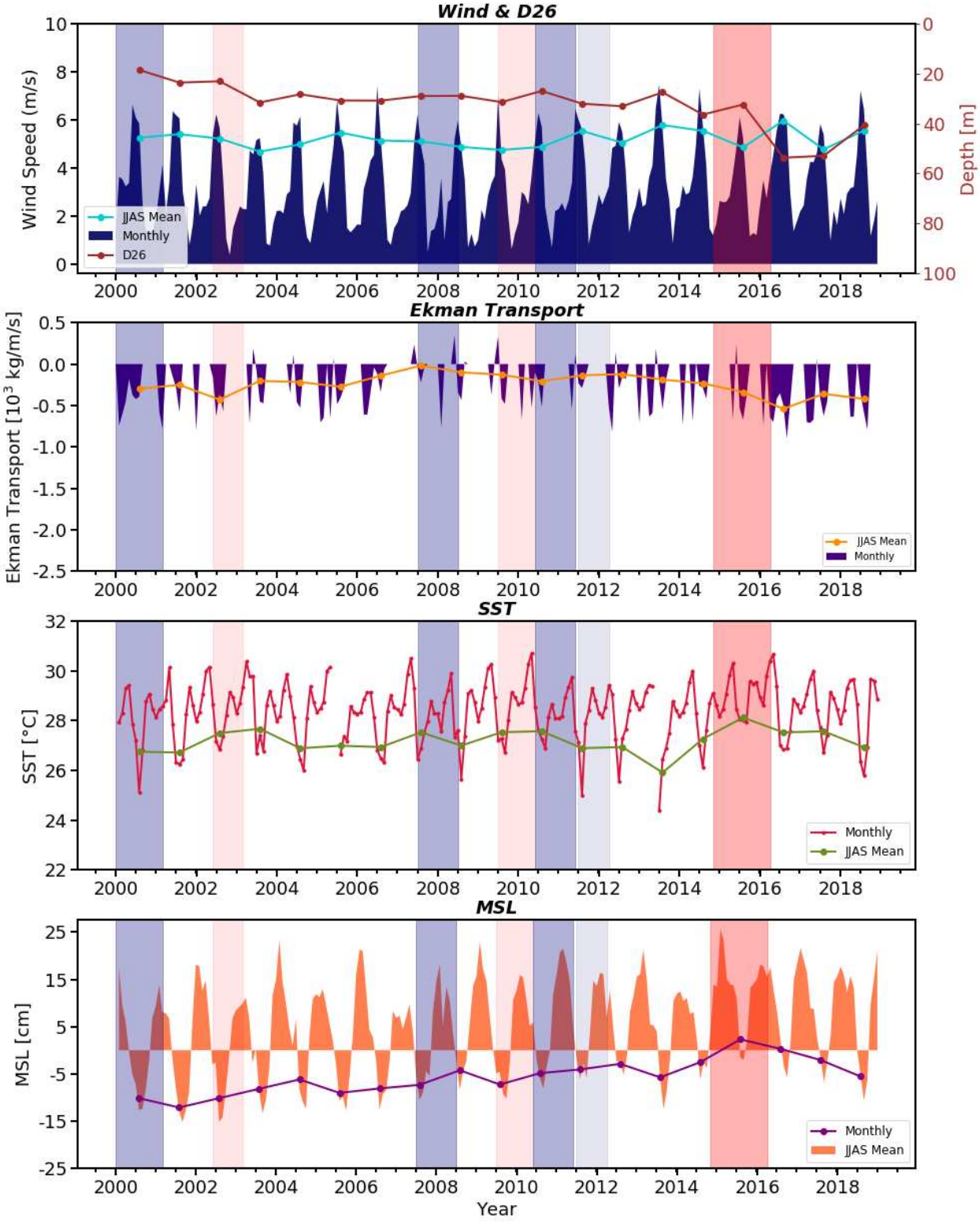

Figure 4.41. Graph showing the wind speed, D26, offshore Ekman Transport, SST and MSL at Site 9 during 2000-2018 with years of moderate El Nino, very strong El Nino, moderate La Nina and strong La Nina shaded by pale brown, darker brown, pale blue and darker blue respectively

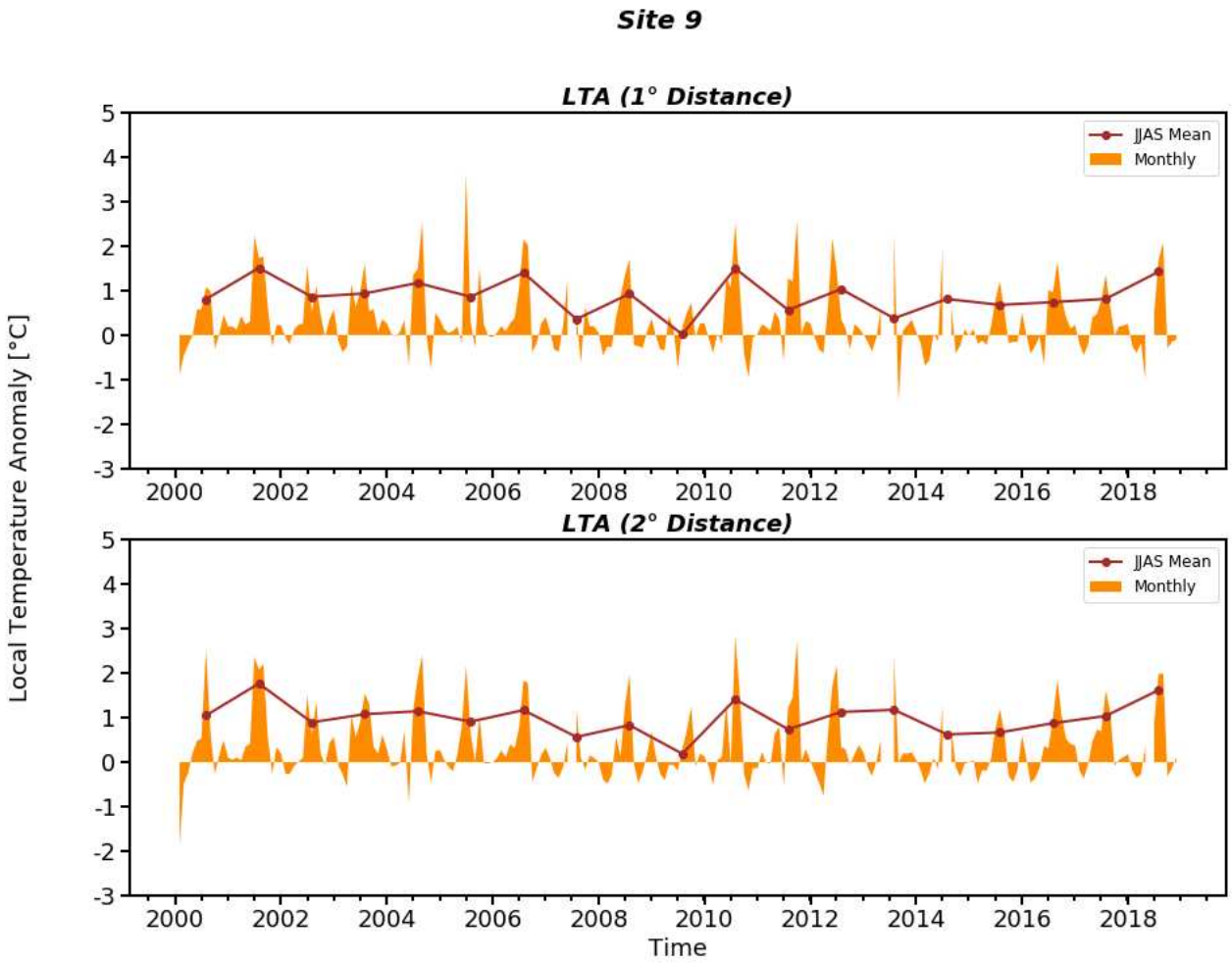

Figure 4.42. LTA for Site 9 during 2000-2018

4.2.10. Site10

The wind speed was between 3-6 ms^{-1} and the wind was mostly westerly during the monsoon season of the study period. The wind was weaker than that of Site 9. This wind being mostly westerly was nearly perpendicular to the coast. The Ekman transport was observed to be nearly absent at this site. The June-September SST mean was almost steady throughout the years fluctuating between 26-27°C. the highest SST was bout 28°C and was observed in 2015. D26 was observed to show a deepening trend. MSL anomaly had similar pattern as that of other sites. LTA values was less than 1°C but reached up to 2°C in 2004. The SSTs at two offshore stations were almost similar. NPP varied between 500-1250 $mgCm^{-2}day^{-1}$ during most of the time and occurred to be lowest during 2012.

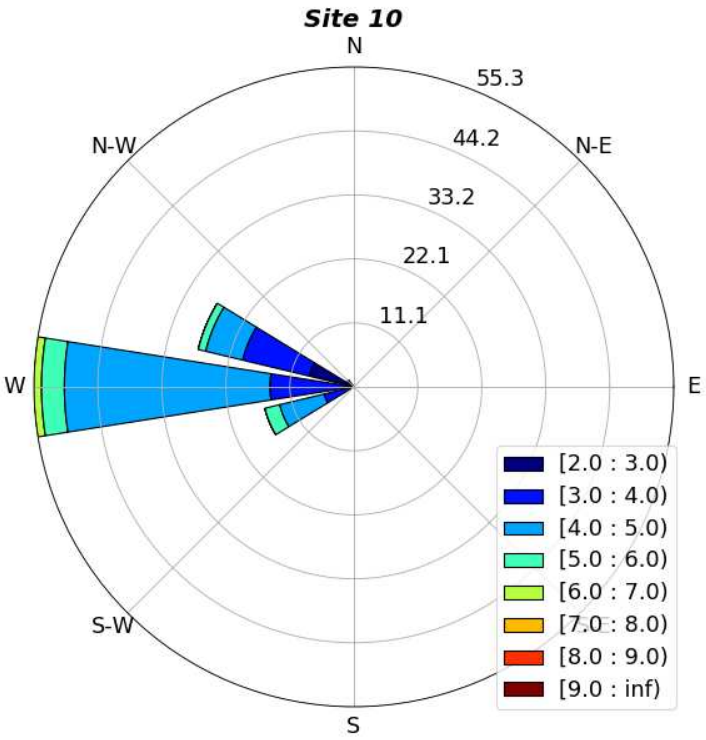

Figure 4.43. Windrose chart for Site 10 during 2000-2018 June-September

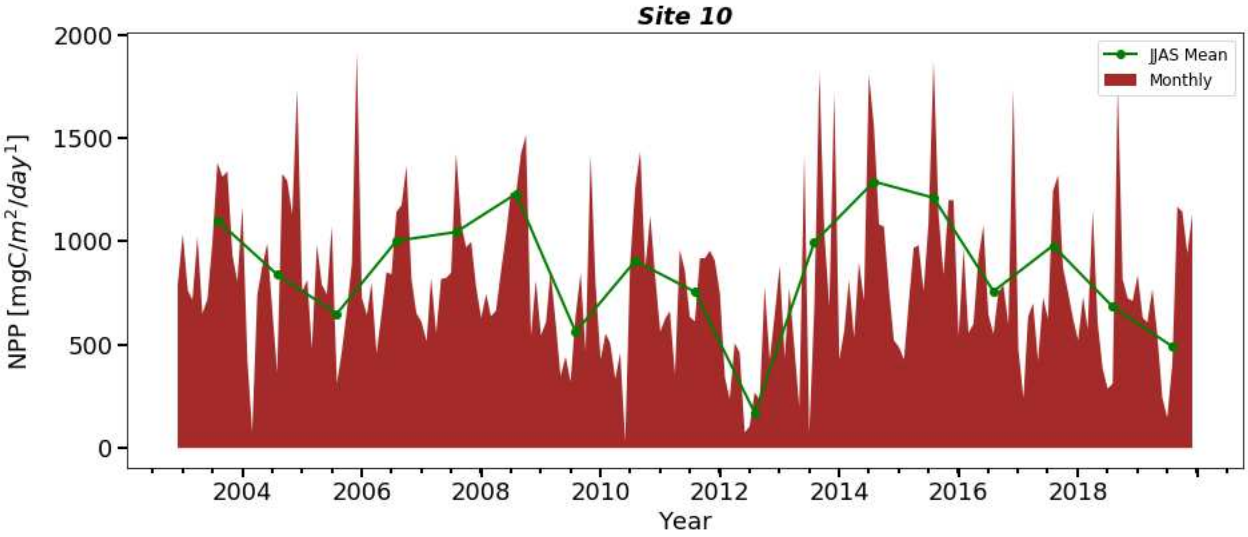

Figure 4.44. NPP for Site 10 during 2003-2019

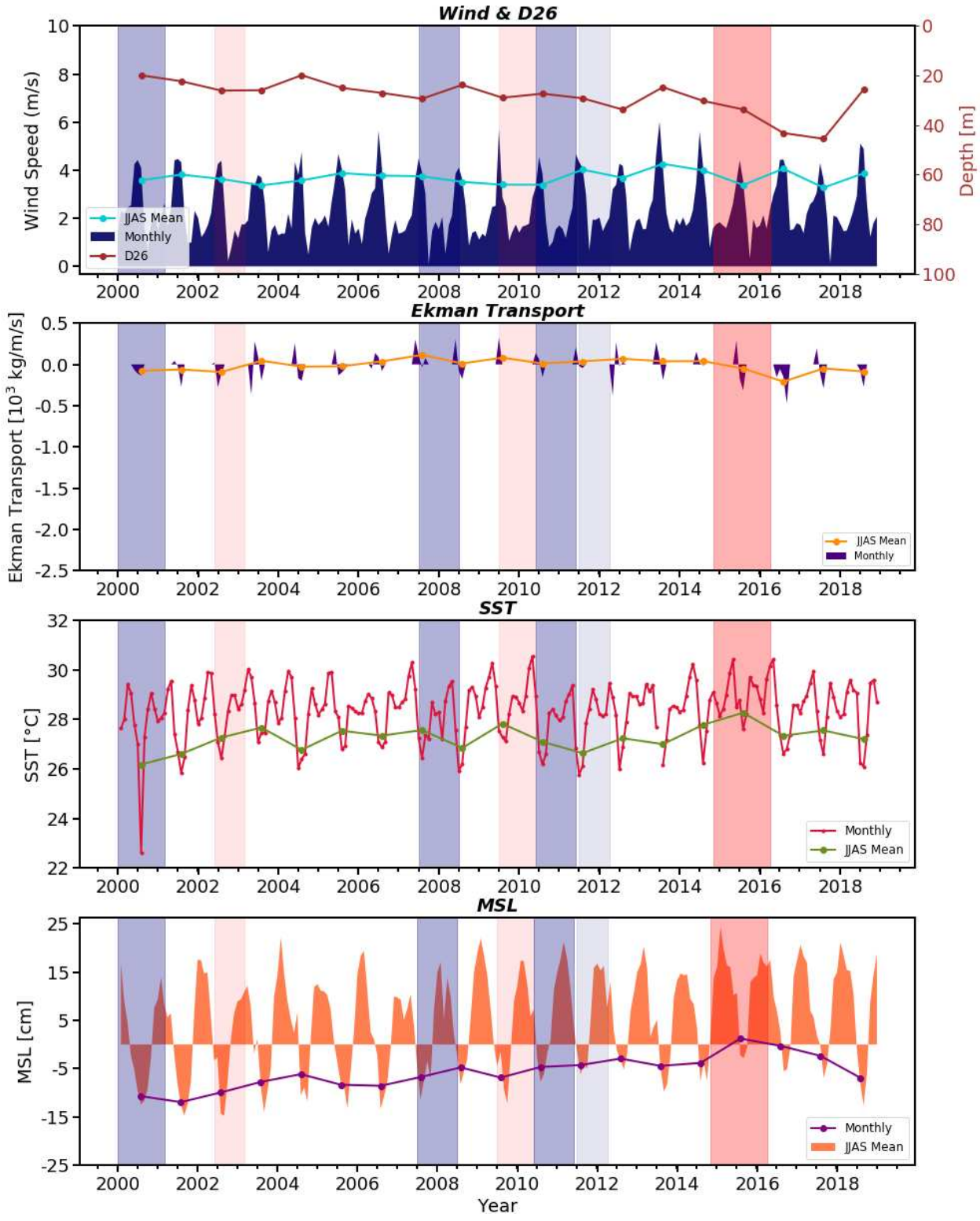

Figure 4.45. Graph showing the wind speed, D26, offshore Ekman Transport, SST and MSL at Site 10 during 2000-2018 with years of moderate El Nino, very strong El Nino, moderate La Nina and strong La Nina shaded by pale brown, darker brown, pale blue and darker blue respectively

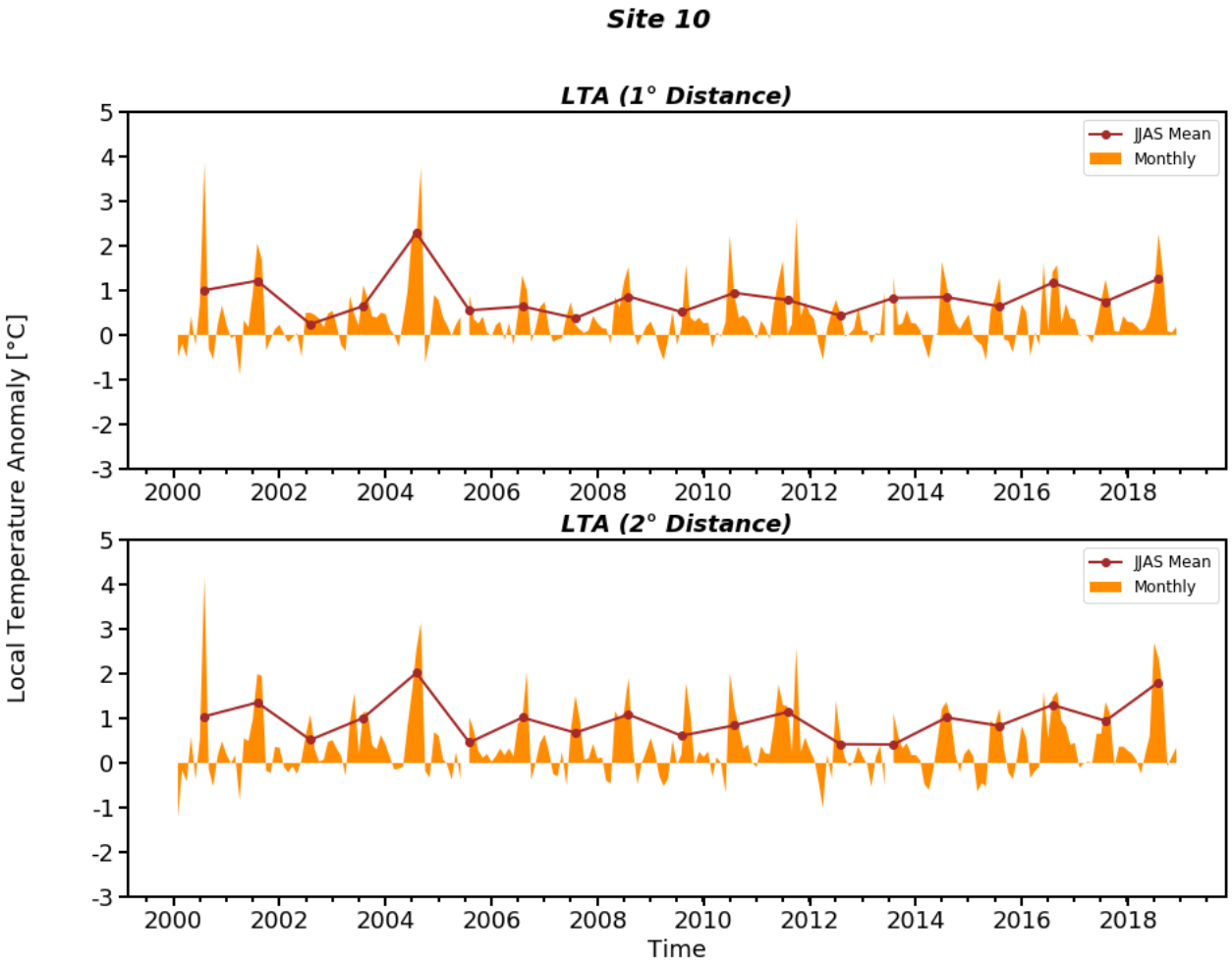

Figure 4.46. LTA for Site 10 during 2000-2018

4.3. MARINE FISH LANDINGS ALONG KERALA COAST

Figure 4.48 shows the district-wise marine fish landings along the Kerala coast during 2007-2018. The fish landing was found to be the highest along Ernakulam, Kollam and Kozhikode coast which ranged between 50 to 150 lakh kg. The fish landings were found to be the highest during the summer monsoon period of the year which happens to coincide with the upwelling indices. The lowest fish landings are found along Kasargode coast which were reported to be less than 50 lakh kg. However, the data was found unavailable during certain months between June-September.

Figure 4.48(a) showed that the June-September mean landing during 2007-2018 was between 25-100 lakh kg. The landing showed a reduction from 2008 to 2010 along the coast and

the highest landings were recorded in the years 2007, 2011 and 2018. An increasing trend was observed from 2014 onwards.

Along the coast of Kollam, the June-September mean landing ranged between 50-150 lakh kg. A continuous decrease was observed from 2008 to 2010 and afterwards, an increasing trend is noted. The landing during the monsoon period showed high fluctuations alternatively during 2007-2011. During 2012-2015, the landing was almost steady and an increase was noted in 2016. From 2016 onwards, the landing showed decline.

At Ernakulam district, the landings ranged between 50-150 lakh kg. Generally, an increasing trend is observed along the coast but a reduction is noted during 2015-2016.

At Malappuram coast, the landing was mostly between 50-100 lakh kg during 2007-2013. During the rest of the study period, the landing was observed to be below 50 lakh kg.

At Kozhikode district, the landing during monsoon season was mostly between 50-100 kg. A sudden increase which reached up to 200 lakh kg was observed in 2012.

At Kannur and Kasargode coasts, the landings were lower than that of other districts and were observed to be mostly below 50 lakhs kg. Kannur coast showed landing greater than 50 lakhs kg in 2013 which coincided with the highest landing in Kozhikode and at Kasargode coast, the higher landing was noted in 2009 and 2015.

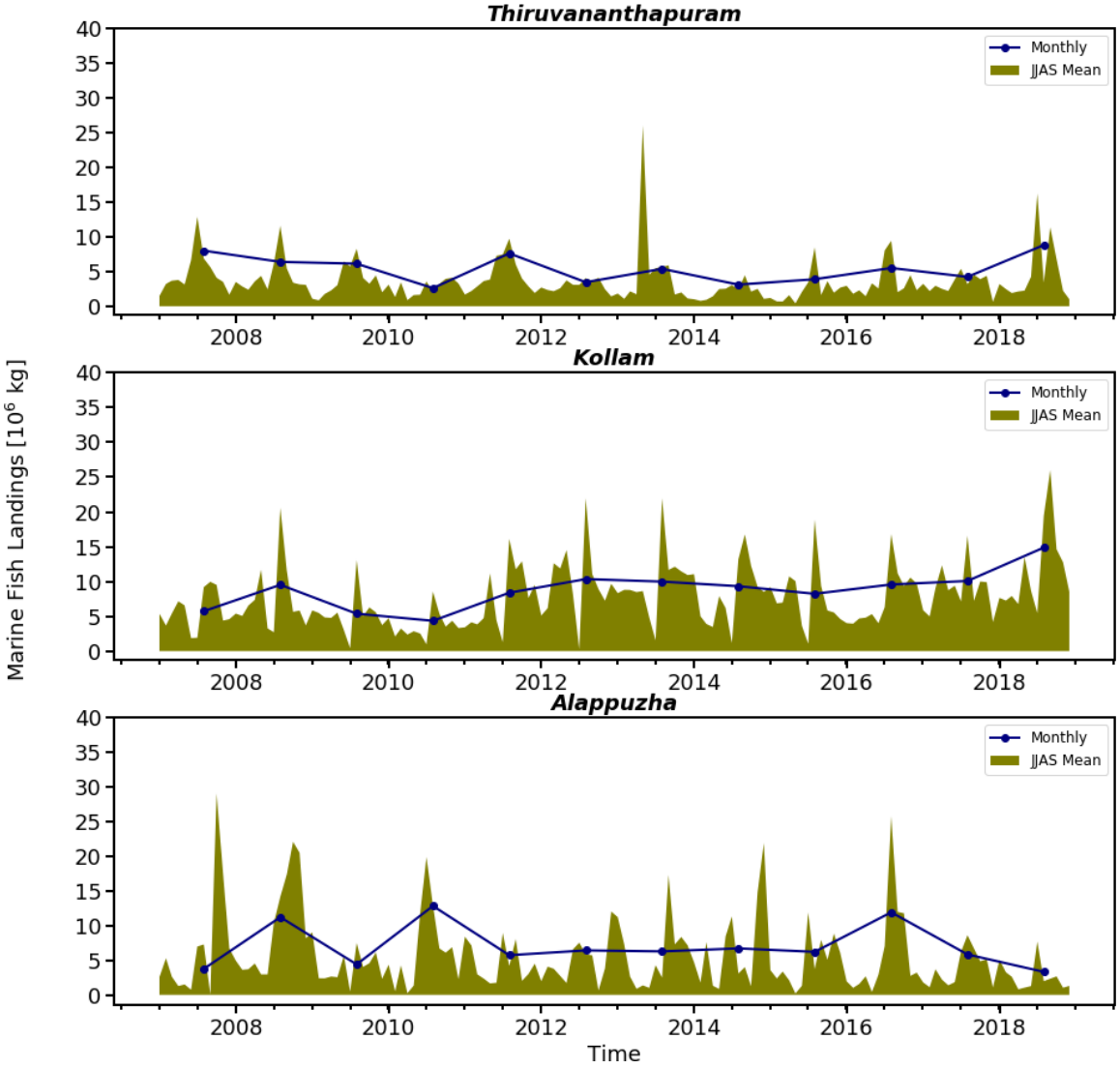

Figure 4.47.A. District-wise annual marine fish landings along the Kerala coast during 2007-2018 for the districts Thiruvananthapuram, Kollam and Alappuzha

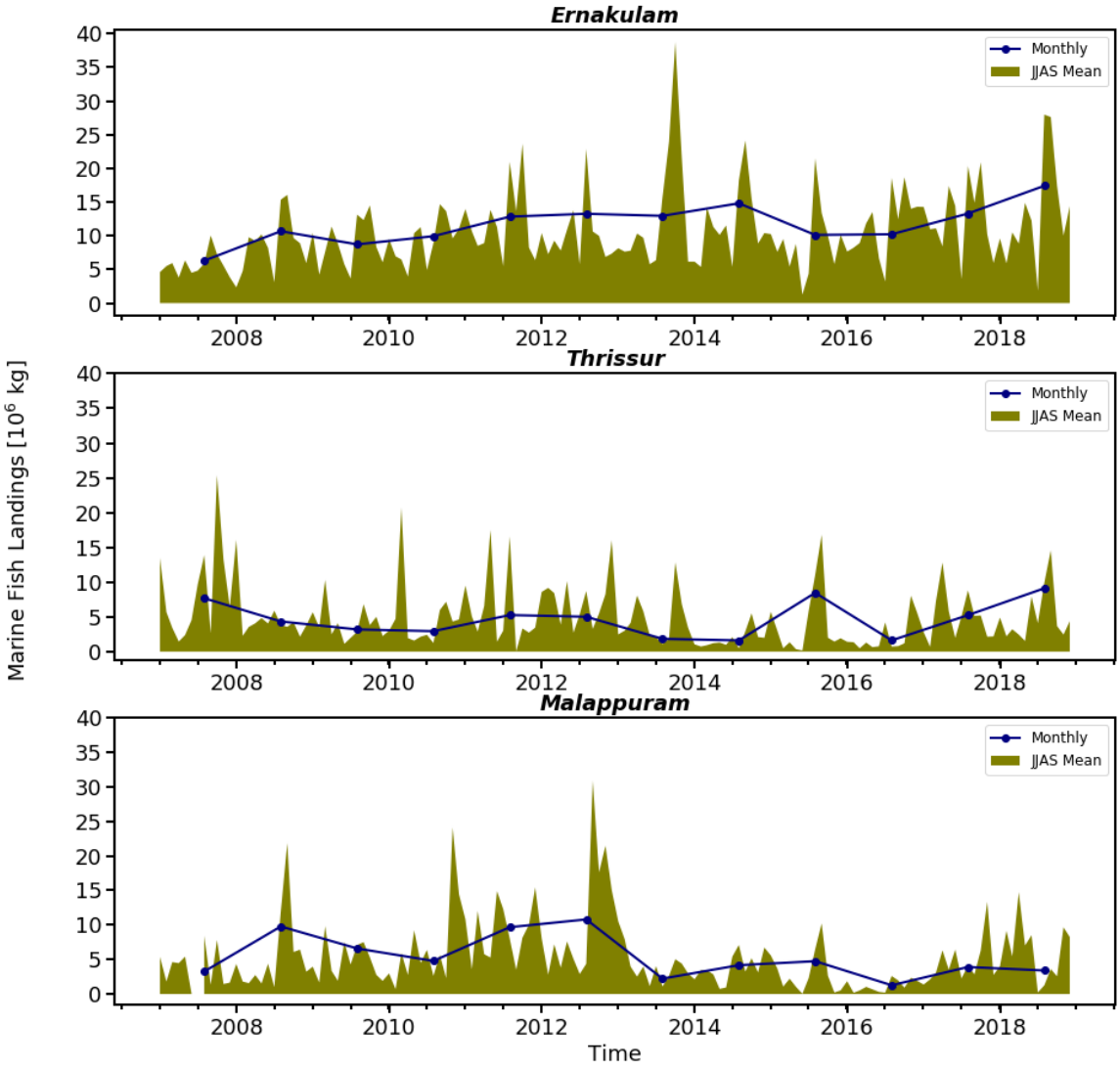

Figure 4.47.B. District-wise annual marine fish landings along the Kerala coast during 2007-2018 for the districts Ernakulam, Thrissur and Malappuram

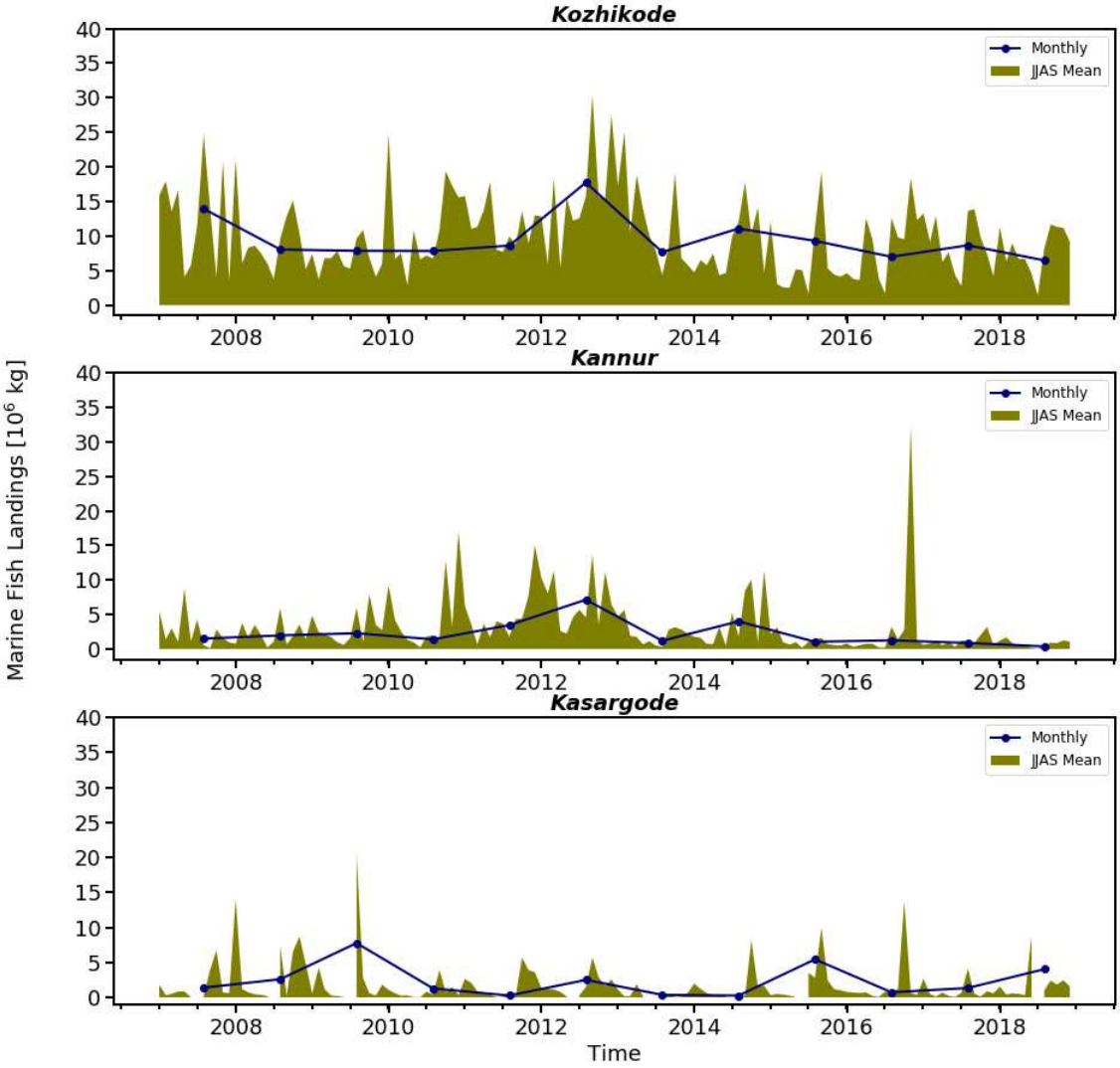

Figure 4.47.C. District-wise annual marine fish landings along the Kerala coast during 2007-2018 for the districts Kozhikode, Kannur and Kasargode

4.4. MODEL RESUTLS

The model was ran for two conditions, 'with wind' and 'without wind'. Figure 4.48 shows the model output of SST along the southwest coast for 'with wind' condition for the year 2014. The result showed a usual pattern as the SST is higher in non-monsoon season and lower during monsoon season. Maximum SST of 30^{o}C is observed during April and it can be seen that coastal SST starts to decrease from May onwards by the influence of monsoonal wind towards the coast. Maximum cooling is attained in July and October onwards the water begins to warm

up again. The lowest SST of 24°C was found between the latitudes 11°N and 12°N along the southwest coast during July which indicates the peak upwelling stage. Figure 4.49 is the transect plot of temperature at Kochi upto 150 m depth from the coast under 'with wind' condition during 2014. The major upwelling indices of 26^{o}C isotherm at Cochin coastal water is usually observed at a depth between 40 to 50m during non-monsoon months. During the southwest monsoon, the rapid uplifting of 26^{o}C isotherm is observed from May onwards and it reaches the surface during July and August. Downwelling process was imitated by October and intensified from November onwards.

Figure 4.50 shows the model output of SST for 'without wind' condition for the same year and it confirms that there is no upwelling without wind. On an average the SST is higher than the real condition (wind on). Maximum SST of 30^{o}C was observed all along the coast during April. The figure shows SST cooling during June-September, the cooling was not found to reach the same extent when the model was ran for 'with wind' condition and the maximum cooling of 27^{o}C was observed during August. Slight uplifting of 26^{o}C isotherm can be observed during June-September but the surface water reaches up to 27°C (Figure 4.51). The isotherm is shifted from 40-50 m to 20-30 m. This indicates that apart from wind there may be other factors favourable for upwelling phenomena. The SST continues to warms up from October onwards similar to 'wind ON' condition.

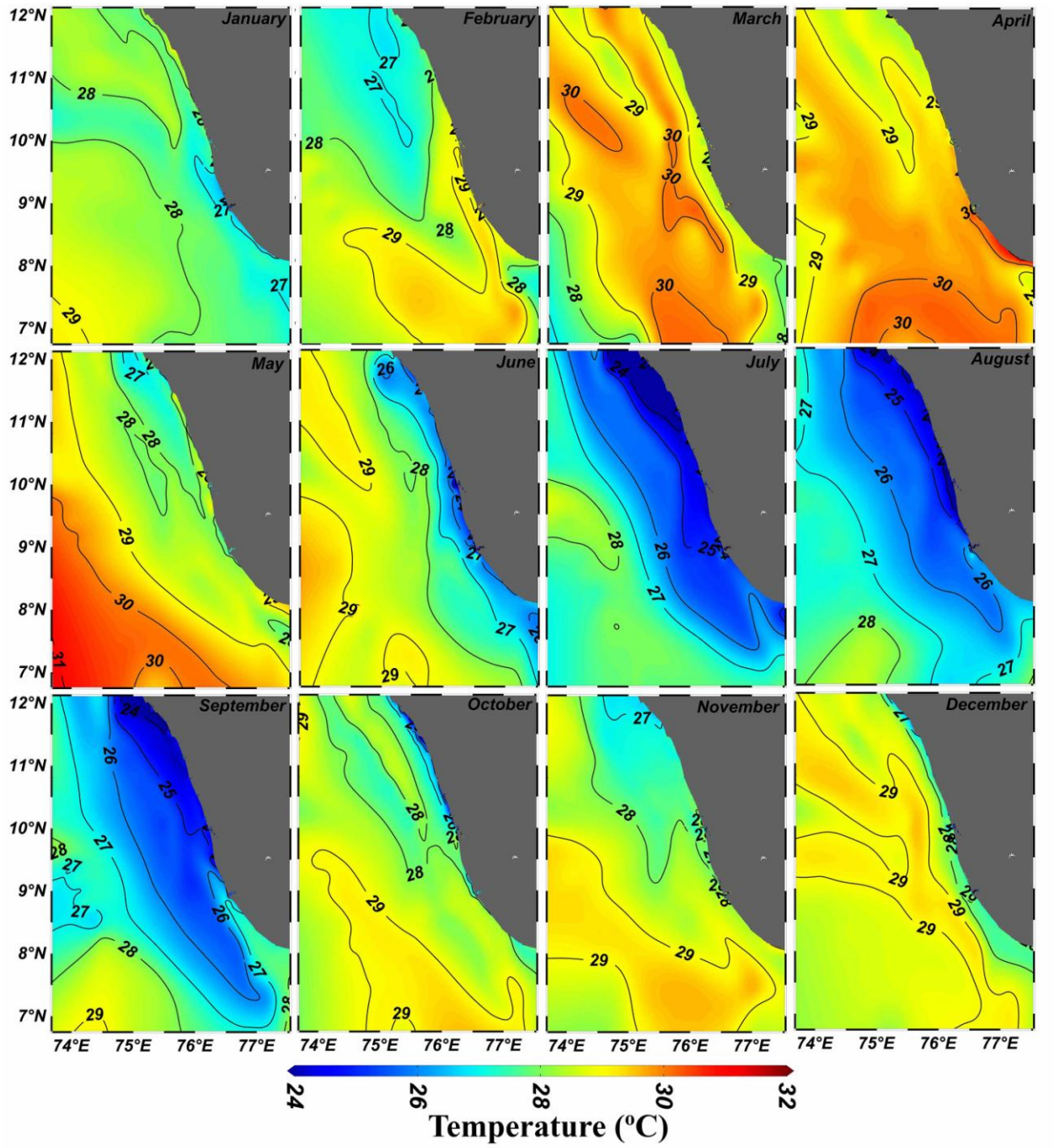

Figure 4.48. SST along the south west coast of India for the year 2014 (wind ON condition)

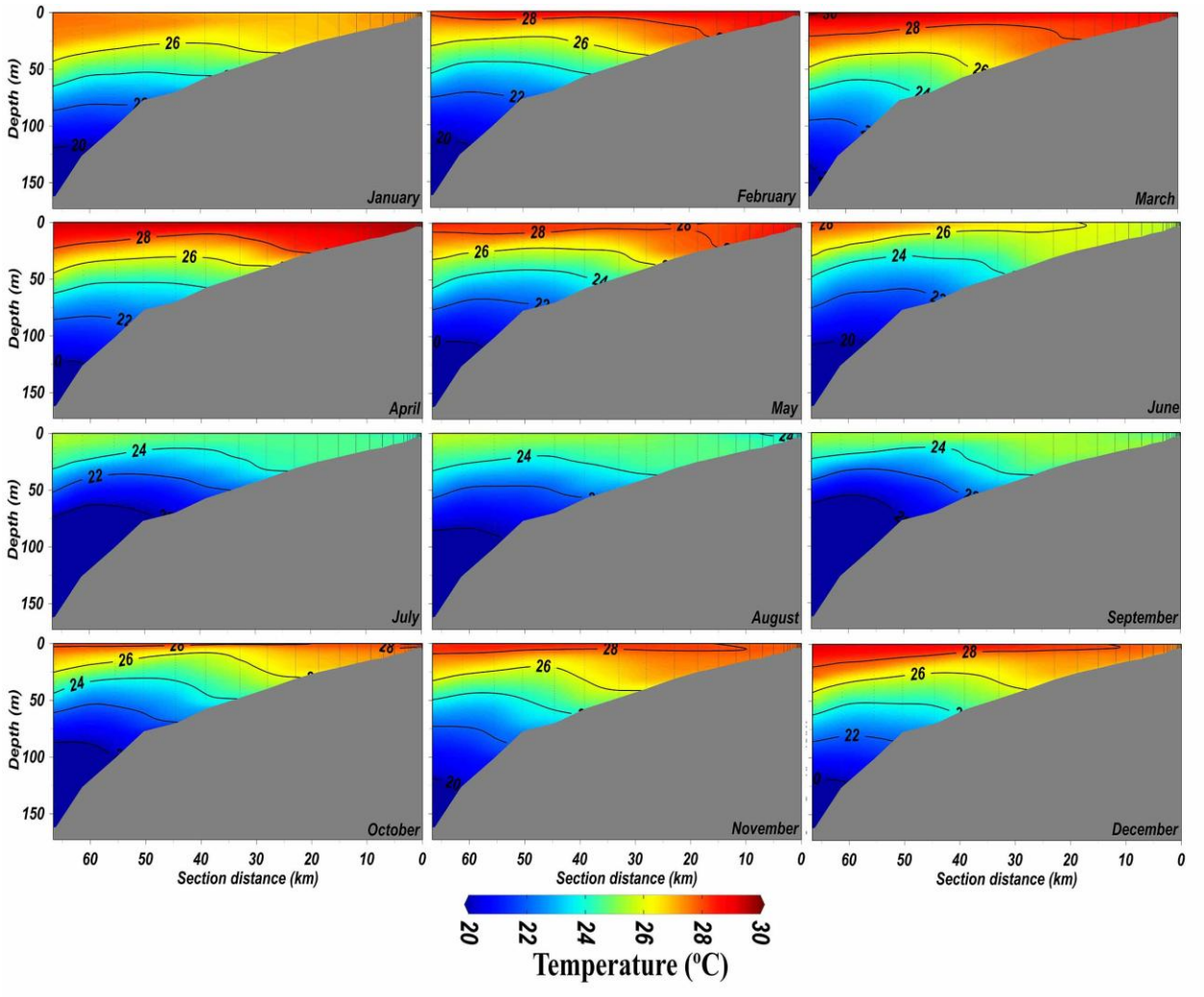

Figure 4.49. Vertical transect of temperature at Kochi up to 150 m depth from coast for the year 2014 (wind ON condition)

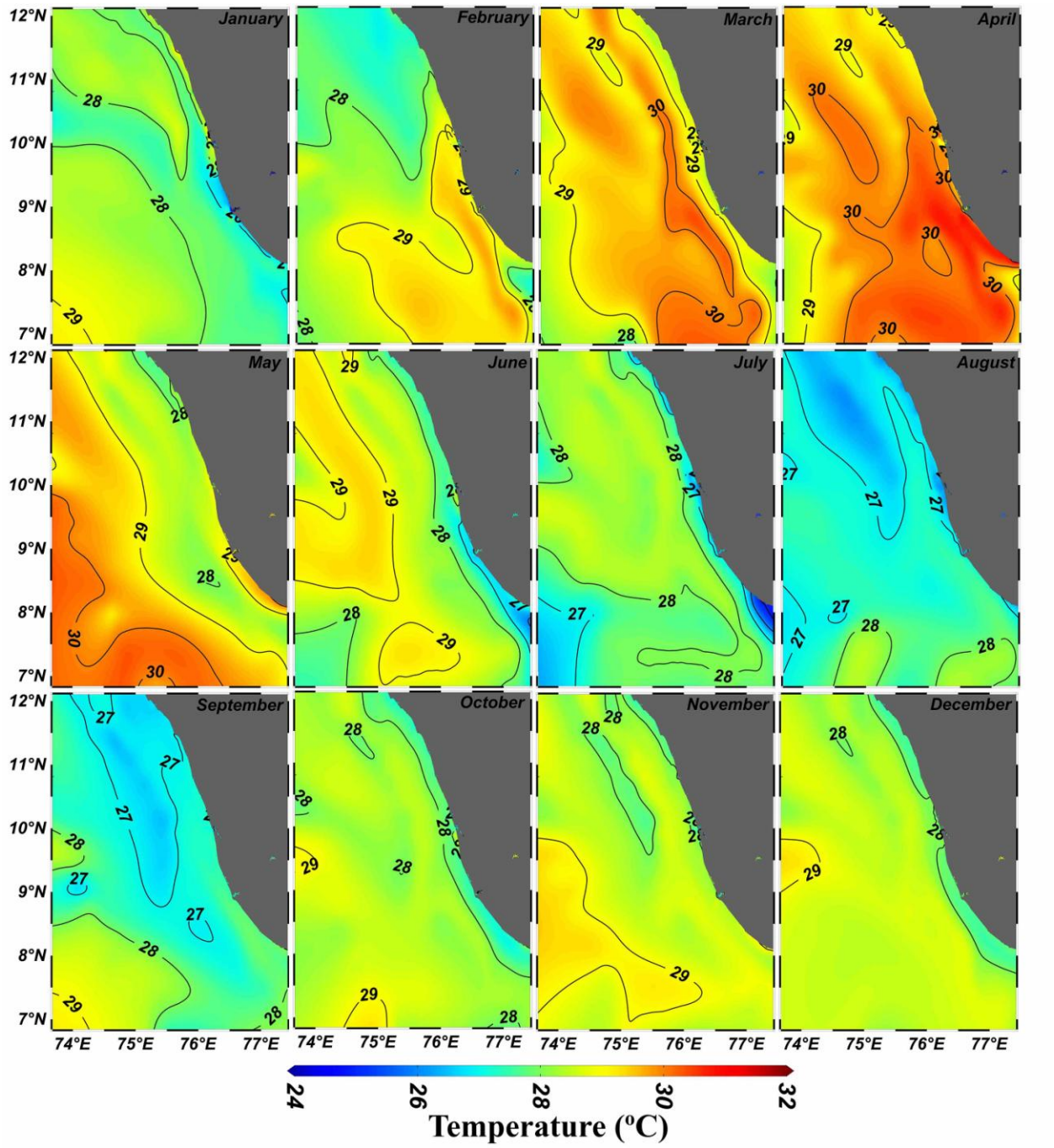

Figure 4.50. SST along the south west coast of India for the year 2014 (wind OFF condition)

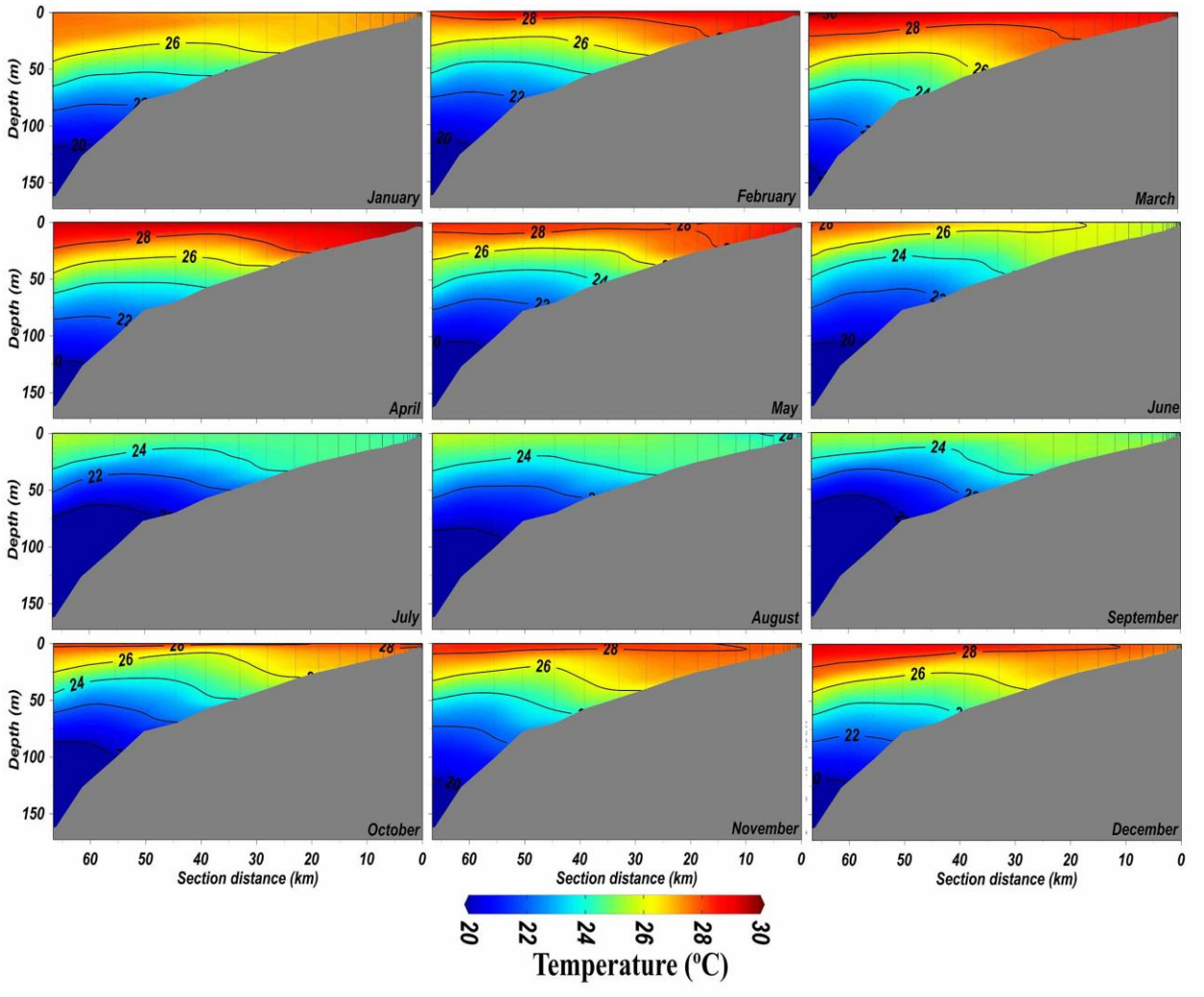

Figure 4.51. Vertical transect of temperature at Kochi up to 150 m depth from coast for the year 2014 (wind OFF condition)

4.5. SST, WIND SPEED AND MSL ANOMAY ANALYSIS

Figure 4.52, 4.53 and 2.54 show the variation of wind speed, SST and MSL with latitude respectively in the study region. The wind speed is observed to increase from April onwards with the maximum speed attained within the months of May-July. The wind speed during this time is found to increase northward. The strongest wind during the study period was observed during the years 2013 and 2018. The SST is found to be low at the beginning of the year as well as during the summer monsoon period with the value showing a decrease to the north. The occurrence of maximum wind speed and lowest SST coincide with each other. The MSL begin to decrease

from April onwards and the lowest value was observed during June-October of the year at the southern latitudes and the value seemed to increase to the north.

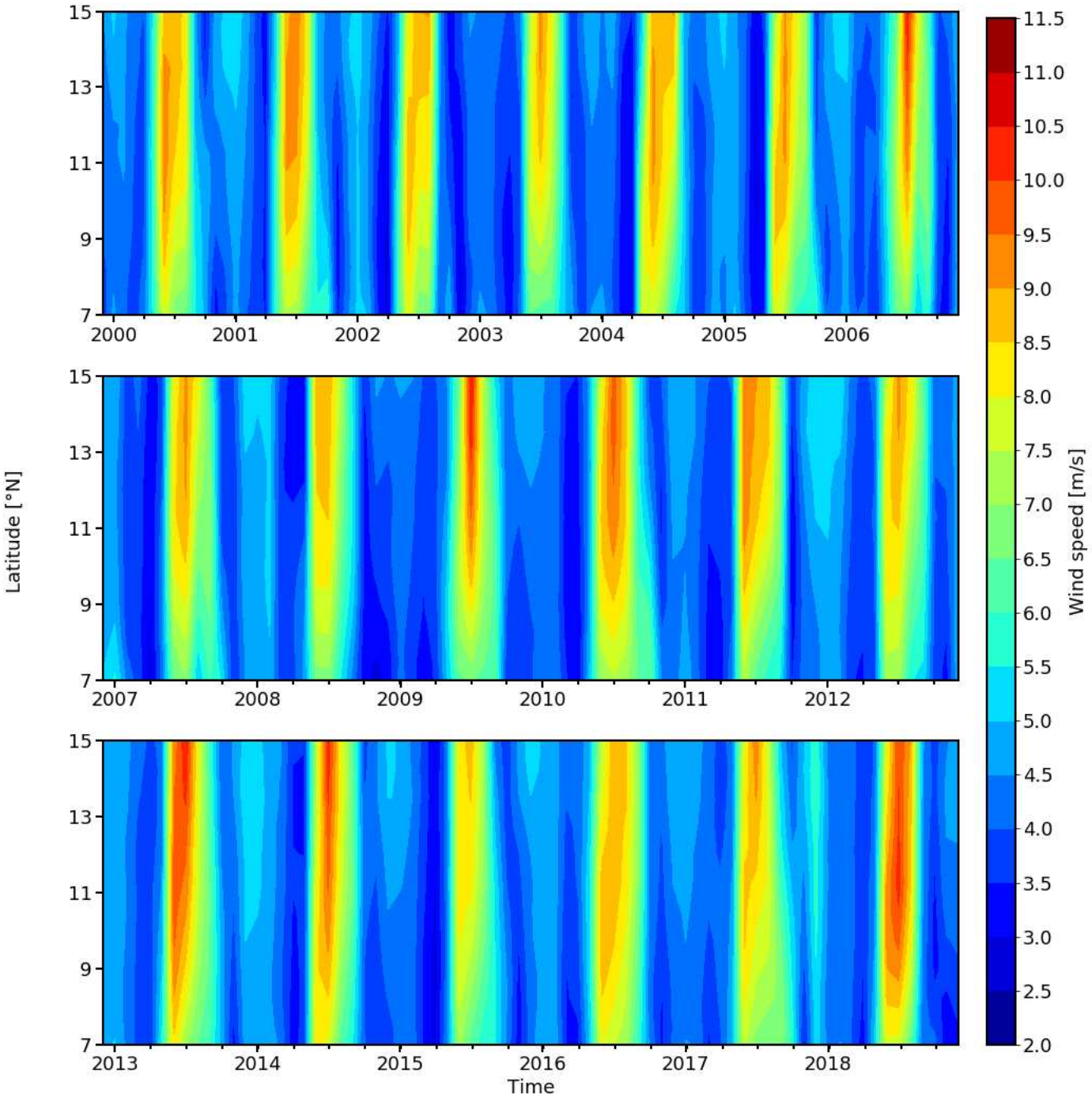

Figure 4.52. Variation in wind speed with latitude during 2000 to 2018

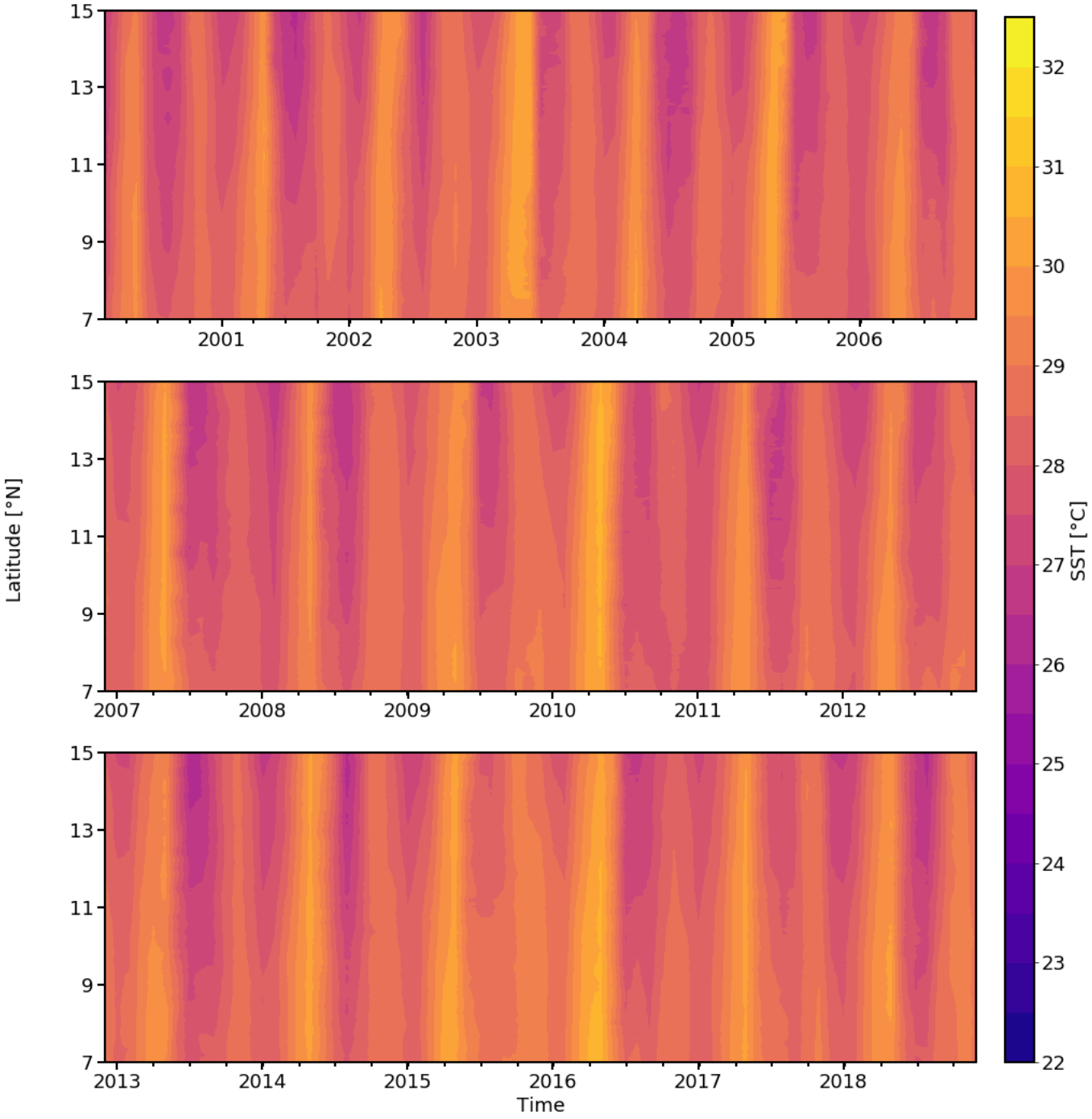

Figure 4.53. Variation in SST with latitude during 2000 February to 2018 December

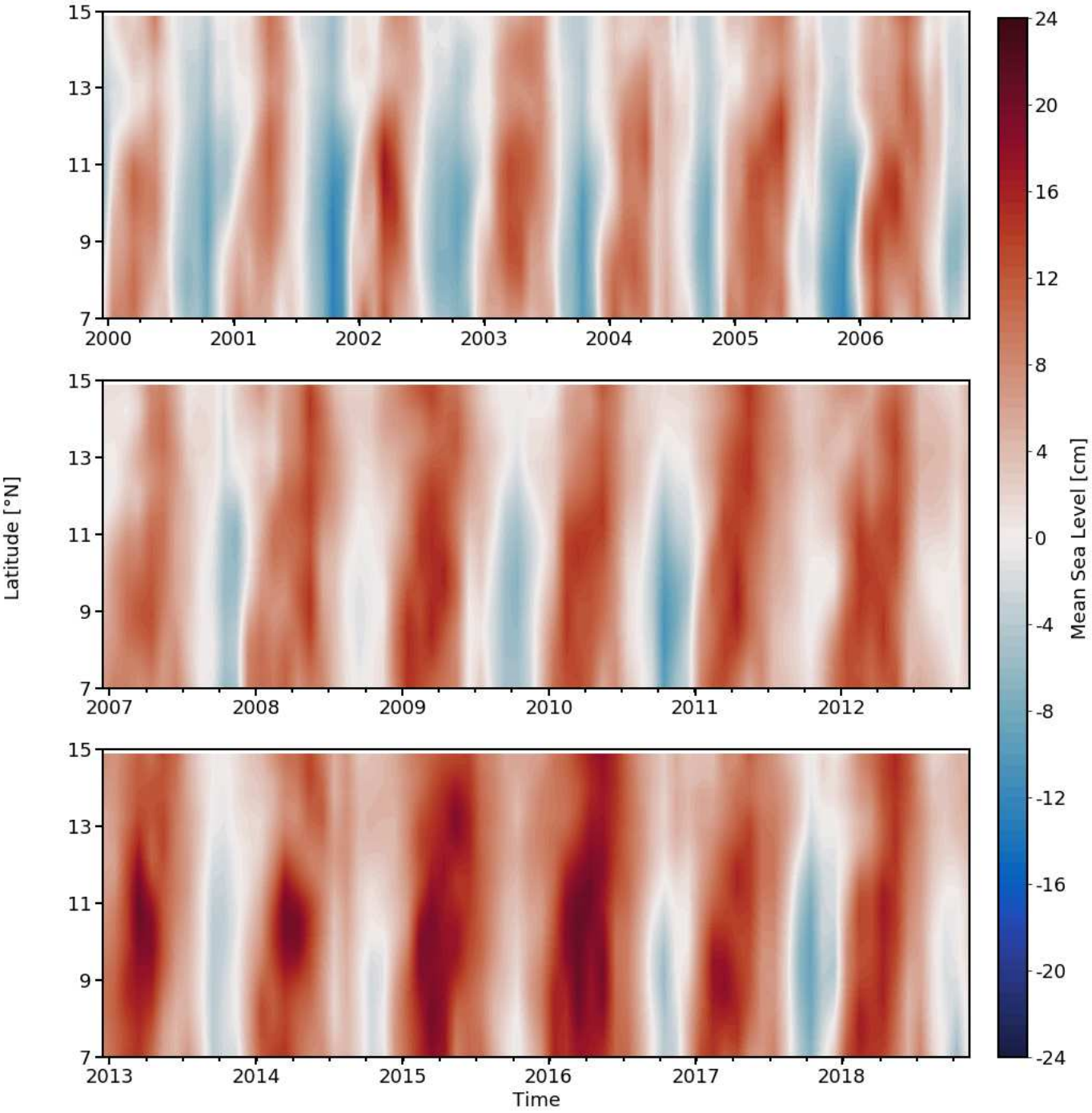

Figure 4.54. Variation in MSL with latitude during 2000-2018

4.6. LONG-TERM ANALYSIS

Table 4.1 shows the ENSO years during 1979 to 2018. Figures 4.55, 4.56 and 4.57 show the monthly and yearly wind speed, SST and MSL respectively at five out of the 10 sites (Sites 2,

3, 4, 6 and 8) which are expected to show considerable variations in the pattern of wind speed and Ekman transport. From figure 4.55, it can be seen that the wind speed did not show any long term trend. That is the wind speed was almost steady for the past 4 decades at almost all of the sites. But during 1997-1998 and 2015-2016 very strong El Nino event, the wind speed at most of the sites showed a reduction. But the following year, the wind is found to retain the strength. During the La Nina and IOD events, no significant changes are found in the wind speed.

From figure 4.56, the SST along the southwest coast of India did not show any long-term trend. The SST was almost steady for the past 3 decades. But during the 1997-1998 and 2015-2016 very strong El Nino years, a drastic increase in the annual SST is observed with the highest SST for the past 3 decades occurring in 1997. Soon after the very strong El Nino years, a continuous reduction in annual SST is noted for the following one or more years. Even though the SST decreased in 2016 after the very strong El Nino event of 2015, a rise is again observed during 2017 at most of the sites. In 2018, again a reduction in annual SST is noted. During the La Nina and IOD events, no significant changes are observed in SST.

From figure 4.57 it is evident that the MSL anomaly showed almost similar pattern throughout the entire coast. An increasing trend is noted from 1993 till 2015. A drastic reduction is visible after 2015 for 3 consecutive years. During the 1997-1998 and 2015-2016 El Nino event, a sudden increase in MSL can be observed corresponding to the increased SST from figure 4.56. But after both the events, a reduction is observed for two or three consecutive years. During the positive IOD events, an increase in MSL is observed. But during the La Nina and negative IOD events, no significant changes are noted.

Table 4.1. The years of weak, moderate, strong and very strong El Nino and La Nina during 1979 to 2018.

Years	**ENSO**	**Strength**
1979-1980	El Nino	Weak
1982-1983	El Nino	Very strong
1983-1984	La Nina	Weak
1984-1985	La Nina	Weak
1986-1987	El Nino	Moderate

1987-1988	El Nino	Strong
1988-1989	La Nina	Strong
1991-1992	El Nino	Strong
1994-1995	El Nino	Moderate
1995-1996	La Nina	Moderate
1997-1998	El Nino	Very strong
1998-1999	La Nina	Strong
1999-2000	La Nina	Strong
2000-2001	La Nina	Weak
2002-2003	El Nino	Moderate
2004-2005	El Nino	Weak
2005-2006	La Nina	Weak
2006-2007	El Nino	Weak
2007-2008	La Nina	Strong
2008-2009	La Nina	Weak
2009-2010	El Nino	Moderate
2010-2011	La Nina	Strong
2011-2012	La Nina	Moderate
2014-2015	El Nino	Weak
2015-2016	El Nino	Very strong
2016-2017	La Nina	Weak
2017-2018	La Nina	Weak

Table 4.2. IOD events from 1979 to 2018

Year	IOD
1981	Negative
1982	Positive
1983	Positive
1989	Negative

1992	Negative
1994	Positive
1996	Negative
1997	Positive
1998	Negative
2006	Positive
2007	Positive
2008	Positive
2010	Negative
2012	Positive
2014	Negative
2015	Positive
2016	Negative

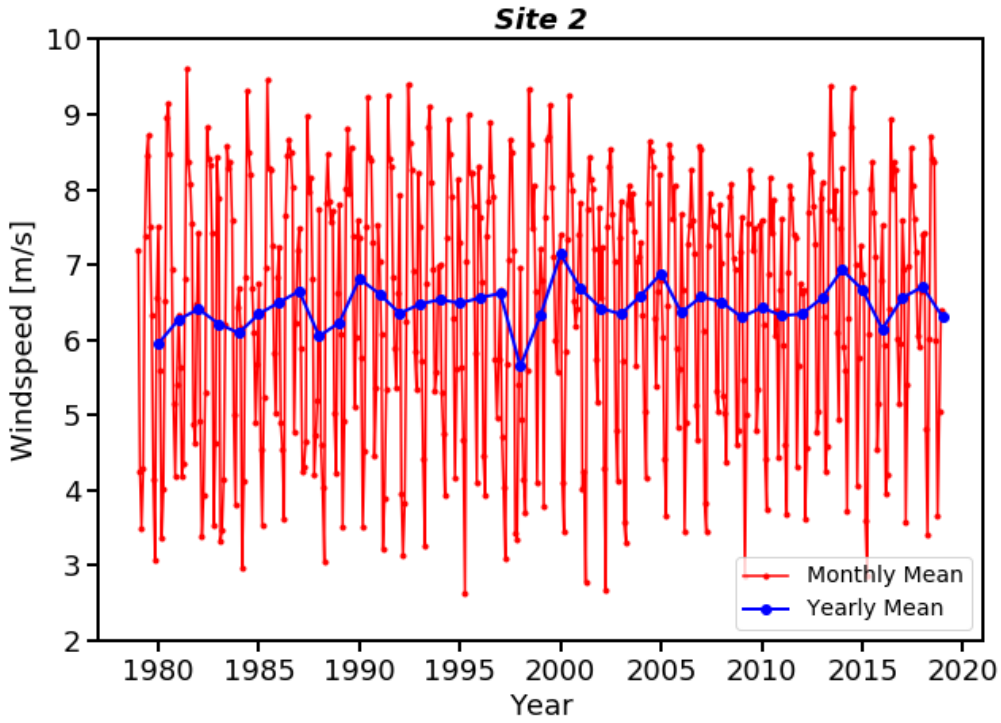

Figure 4.55.A. Monthly mean and yearly mean of wind speed from 1979 to 2018 for Site 2

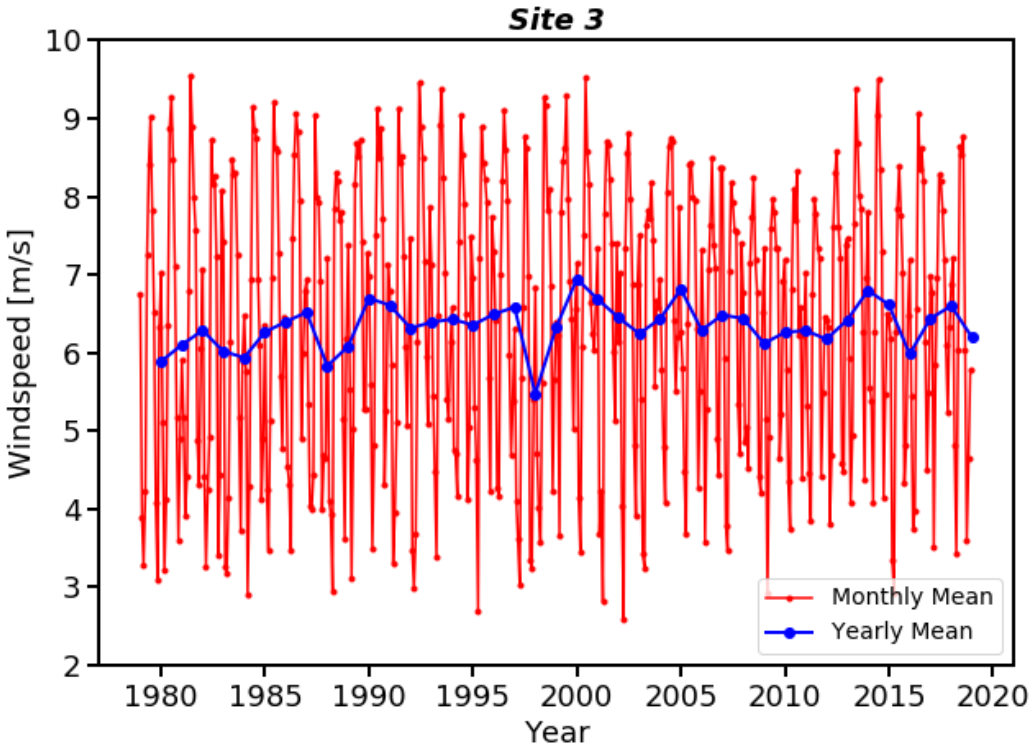

Figure 4.55.B. Monthly mean and yearly mean of wind speed from 1979 to 2018 for Site 3

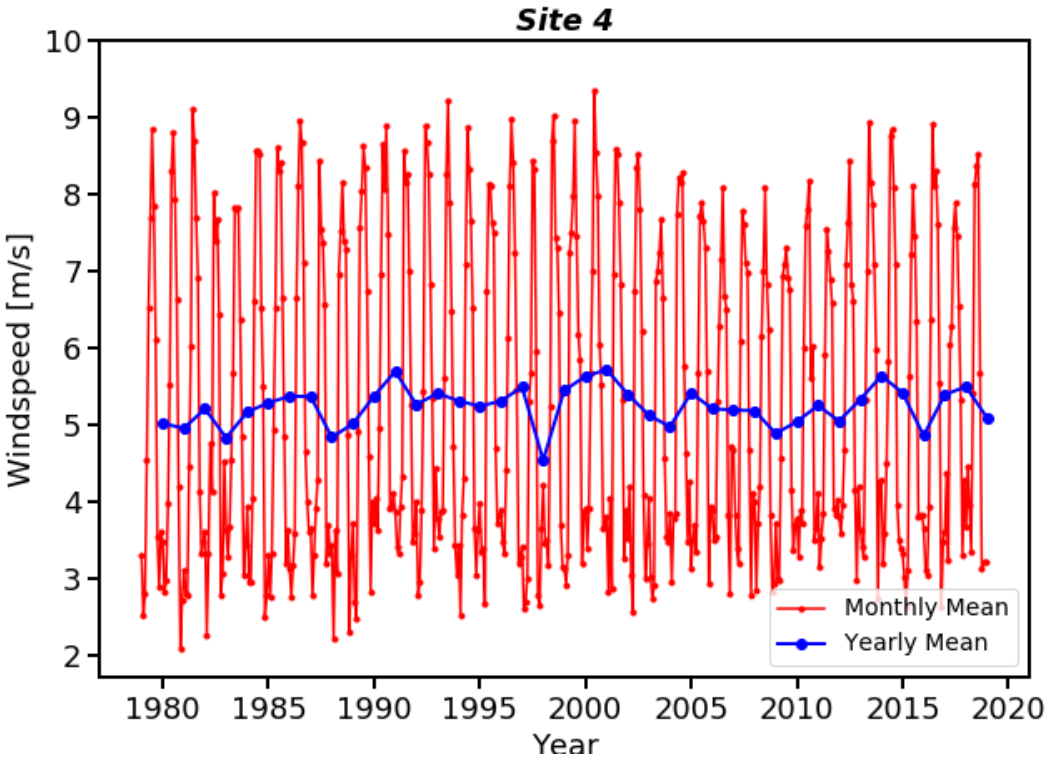

Figure 4.55.C. Monthly mean and yearly mean of wind speed from 1979 to 2018 for Site 4

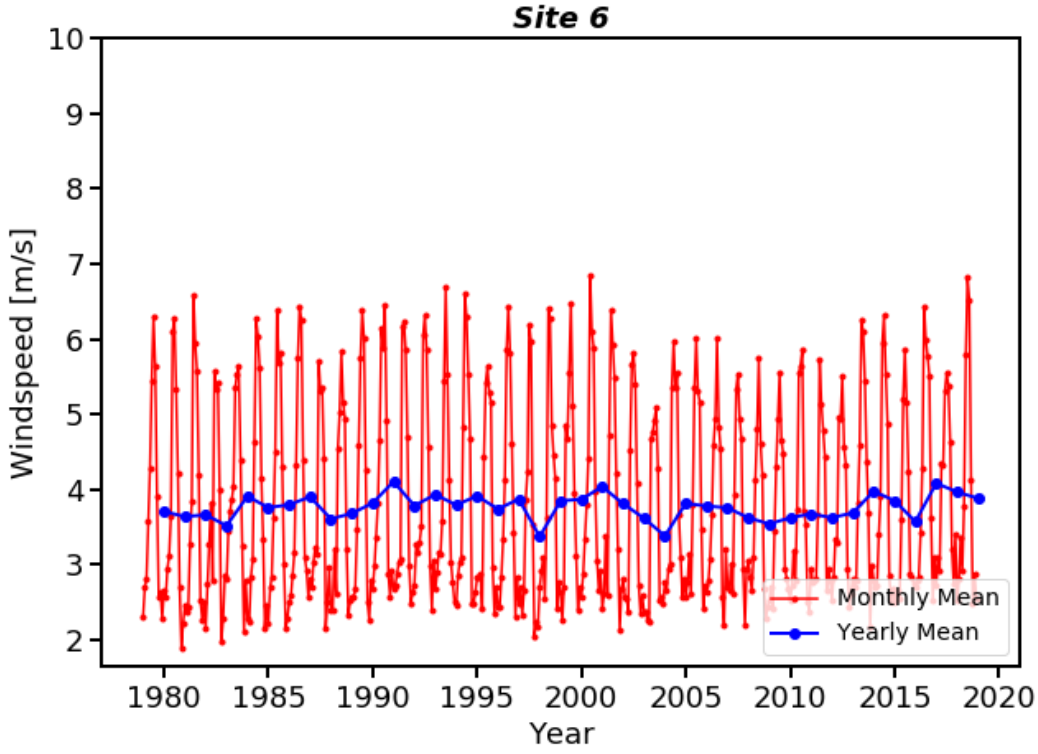

Figure 4.55.D. Monthly mean and yearly mean of wind speed from 1979 to 2018 for Site 6

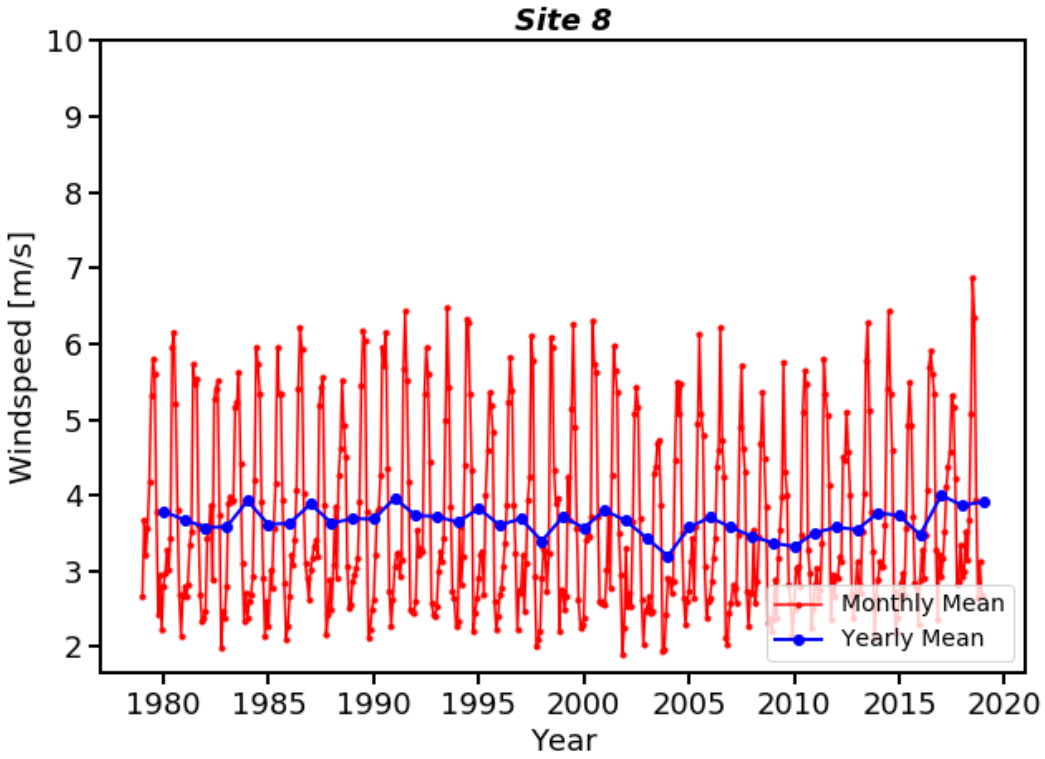

Figure 4.55.E. Monthly mean and yearly mean of wind speed from 1979 to 2018 for Site 8

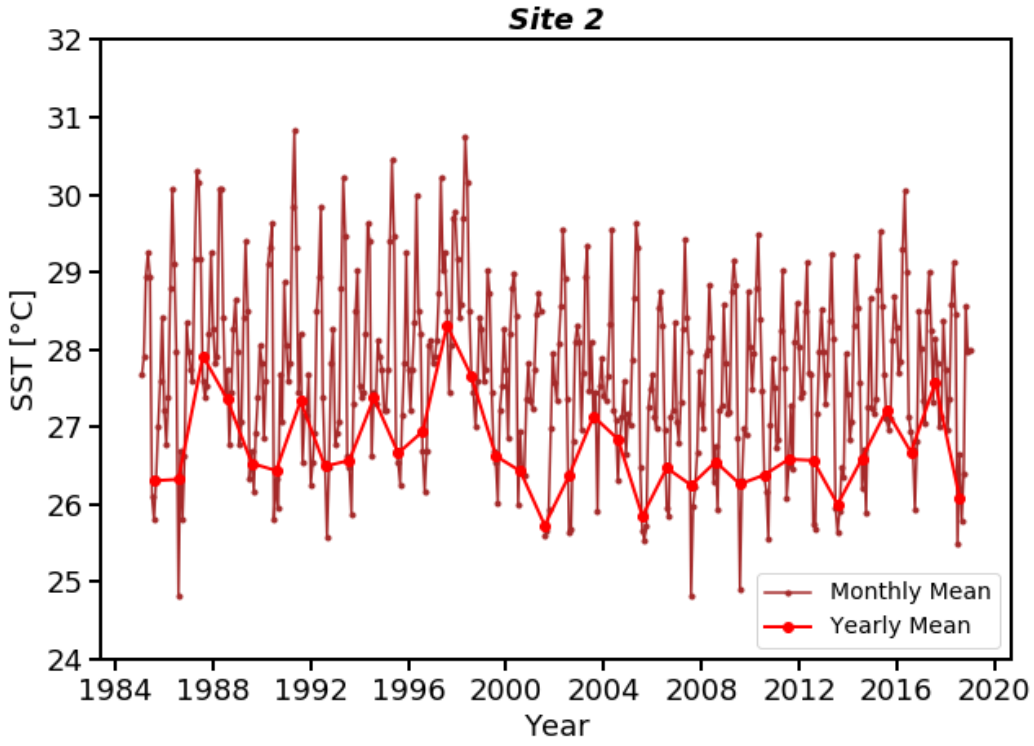

Figure 4.56.A. Monthly and yearly mean SST from 1985 to 2018 at Site 2

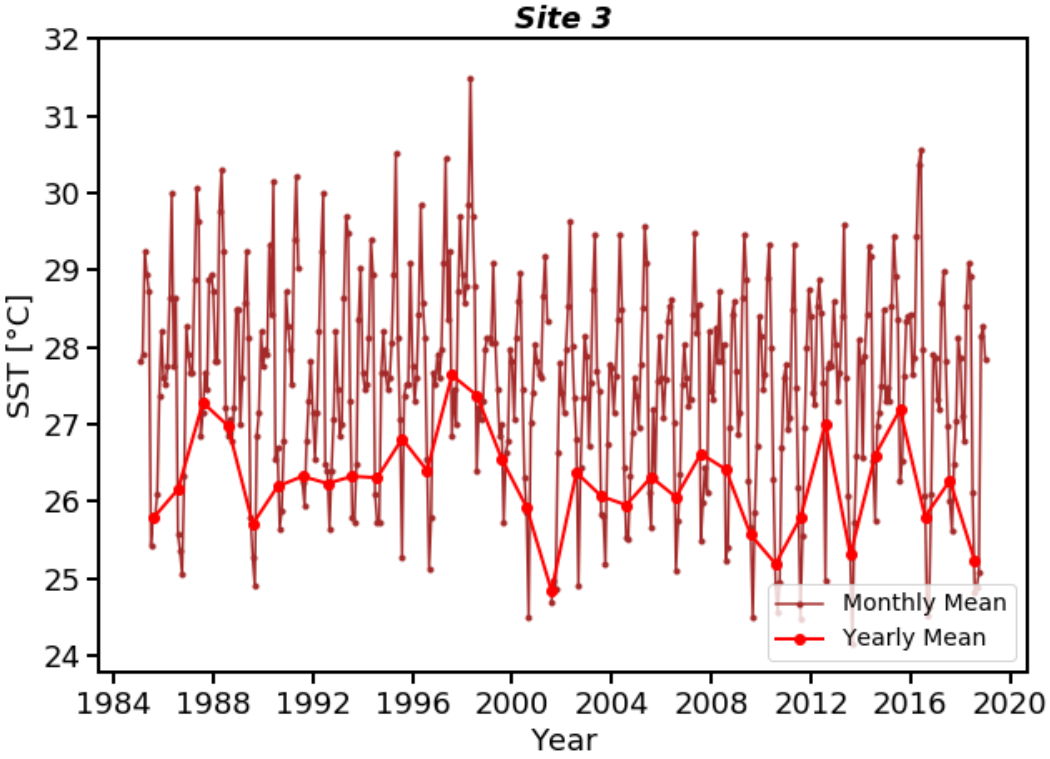

Figure 4.56.B. Monthly and yearly mean SST from 1985 to 2018 at Site 3

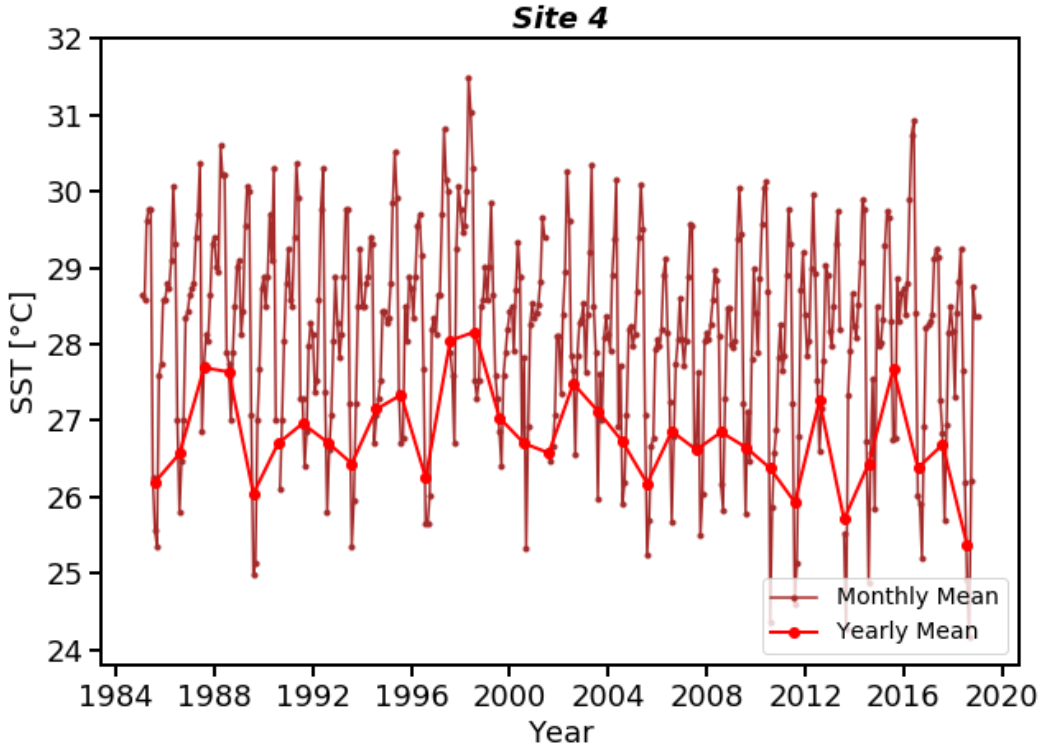

Figure 4.56.C. Monthly and yearly mean SST from 1985 to 2018 at Site 4

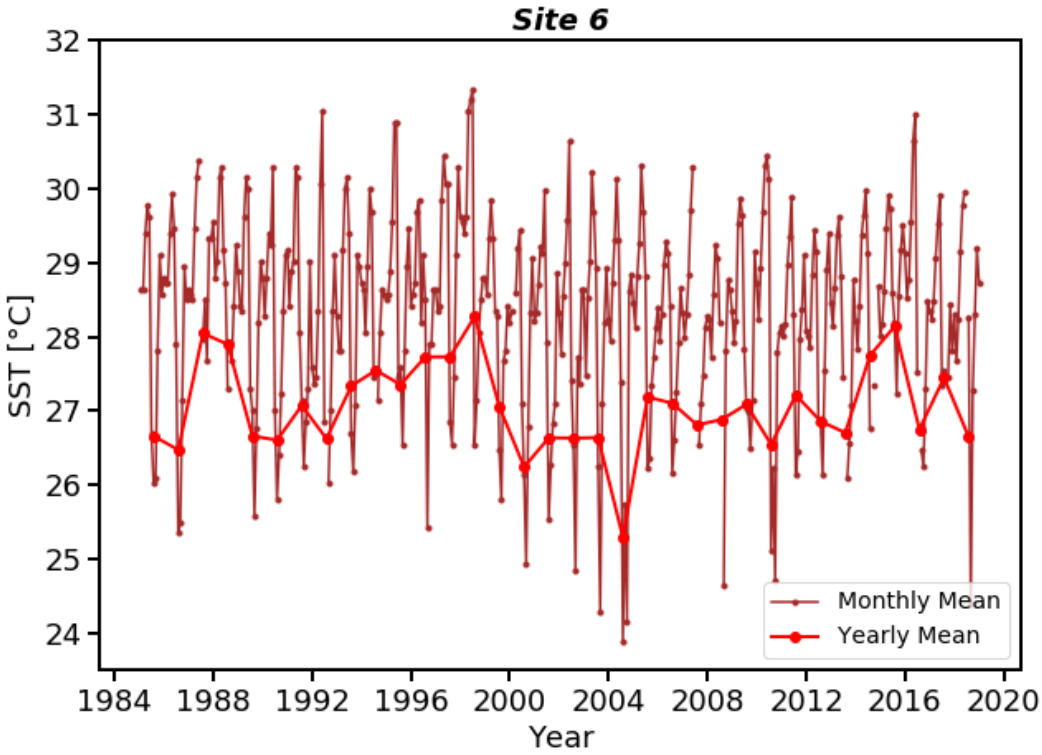

Figure 4.56.D. Monthly and yearly mean SST from 1985 to 2018 at Site 6

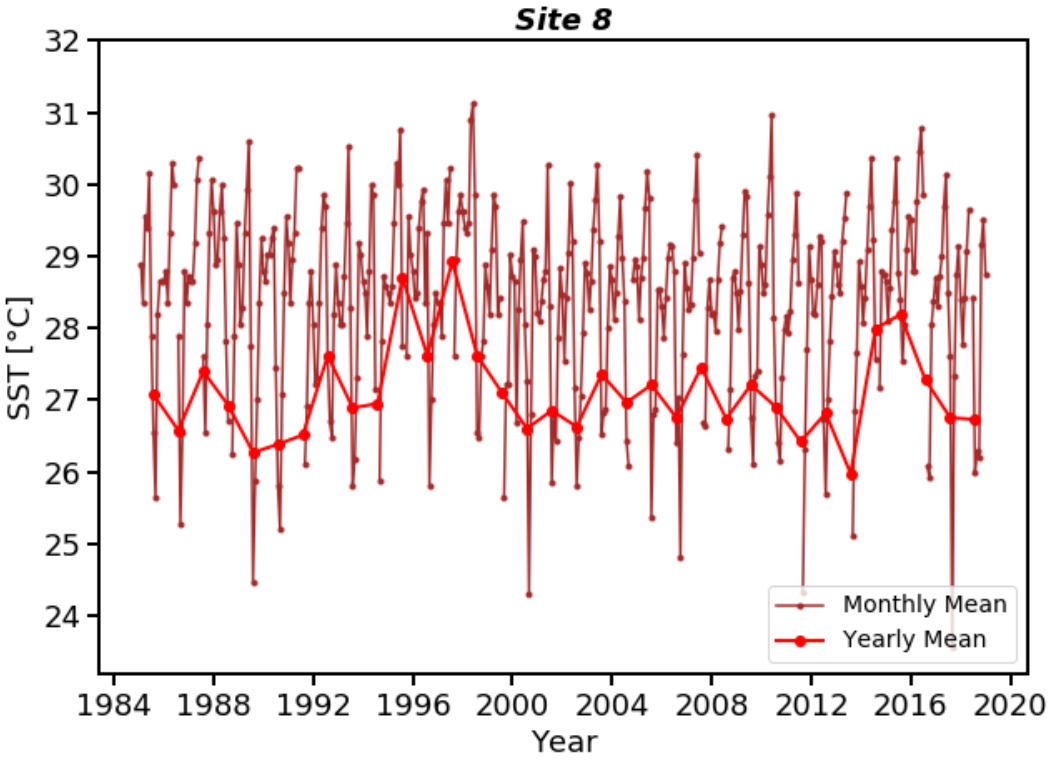

Figure 4.56.E. Monthly and yearly mean SST from 1985 to 2018 at Site 8

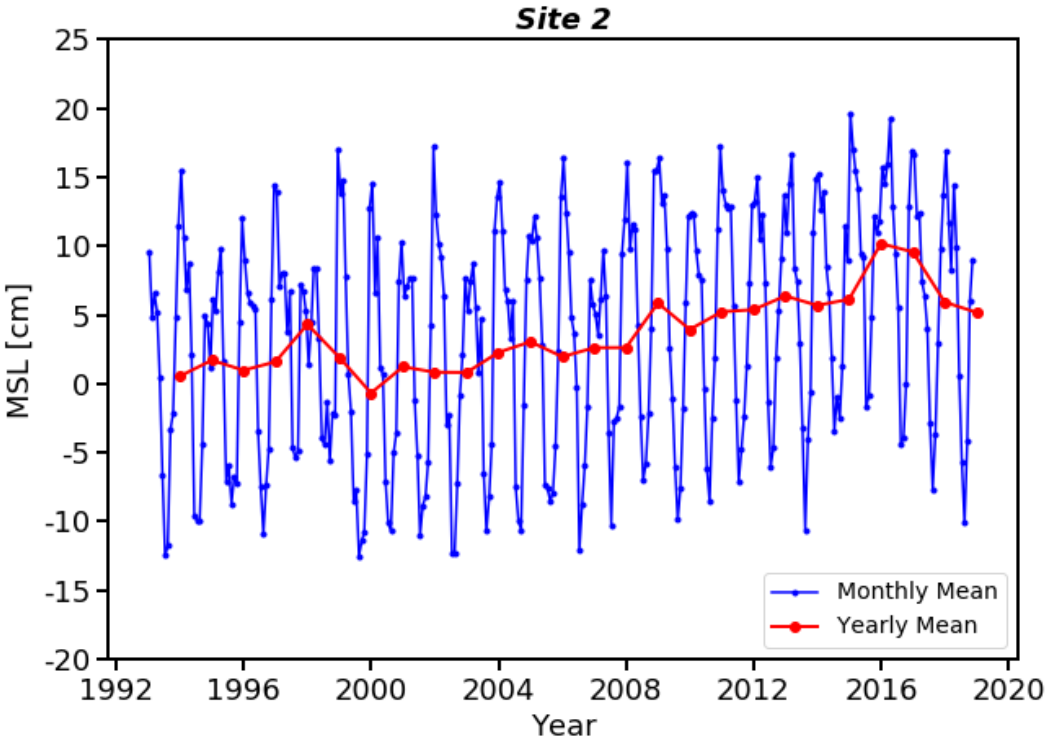

Figure 4.57. A. Monthly and yearly MSL from 1993 to 2018 at Site 2

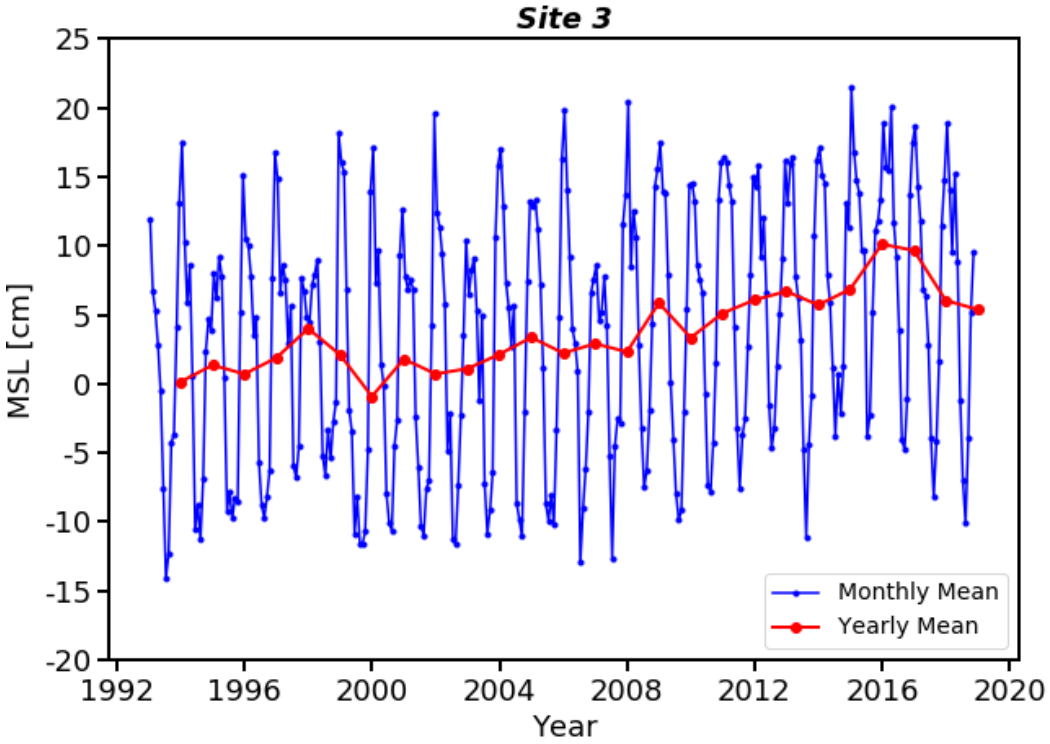

Figure 4.57. B. Monthly and yearly MSL from 1993 to 2018 at Site 3

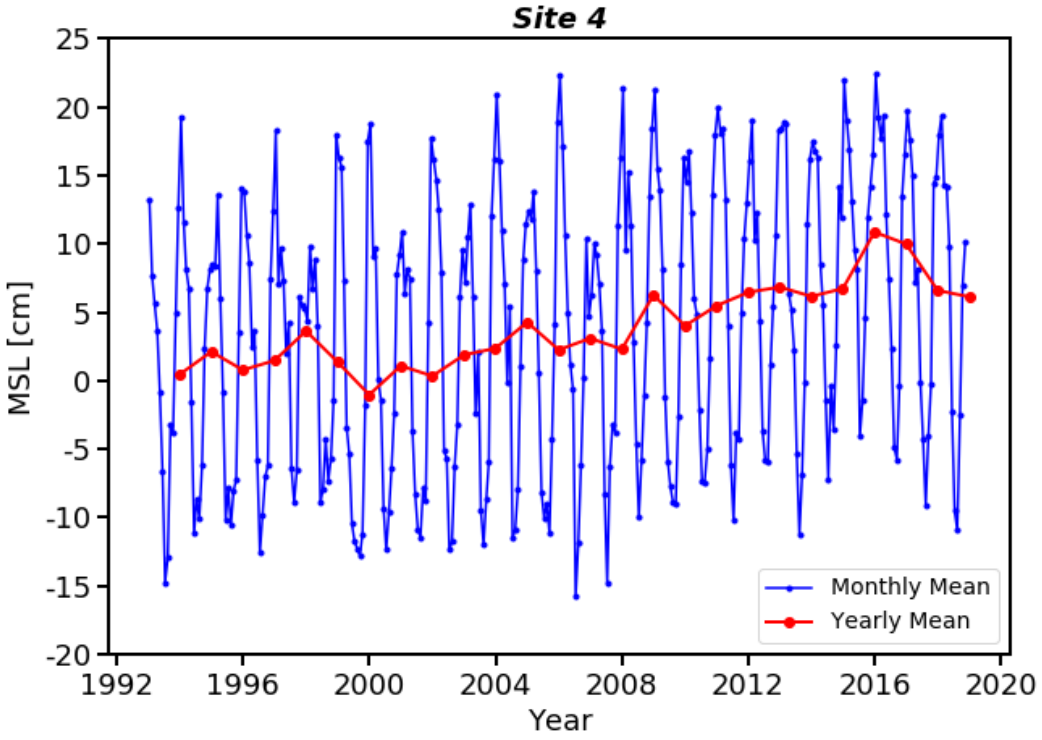

Figure 4.57. C. Monthly and yearly MSL from 1993 to 2018 at Site 4

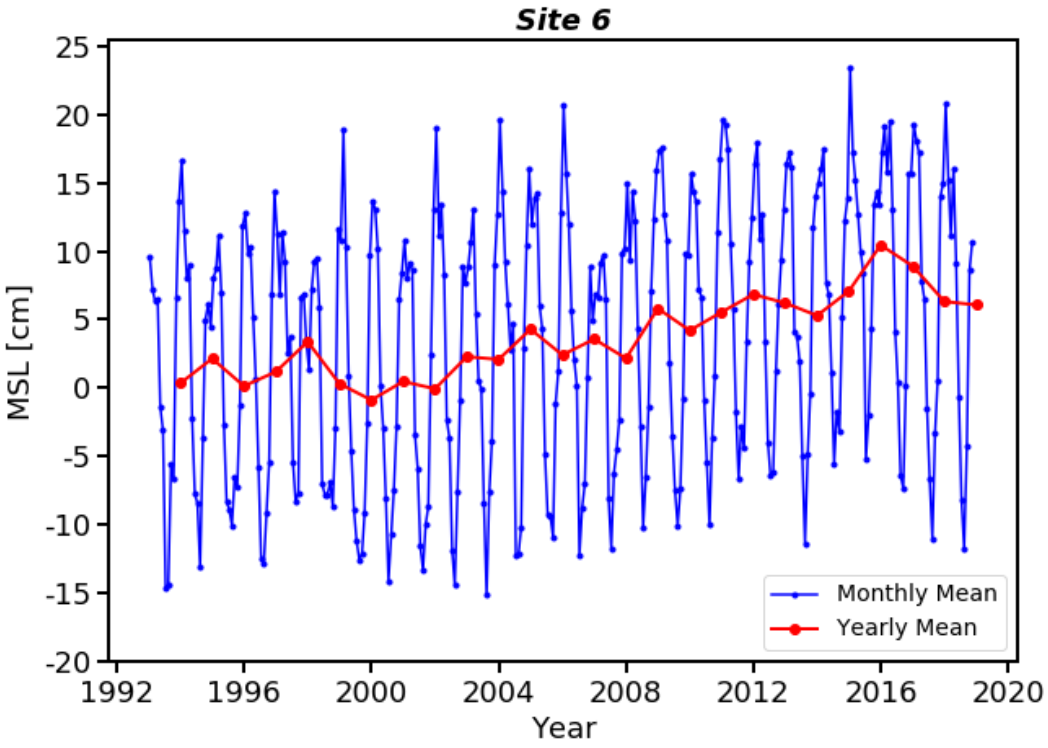

Figure 4.57. D. Monthly and yearly MSL from 1993 to 2018 at Site 6

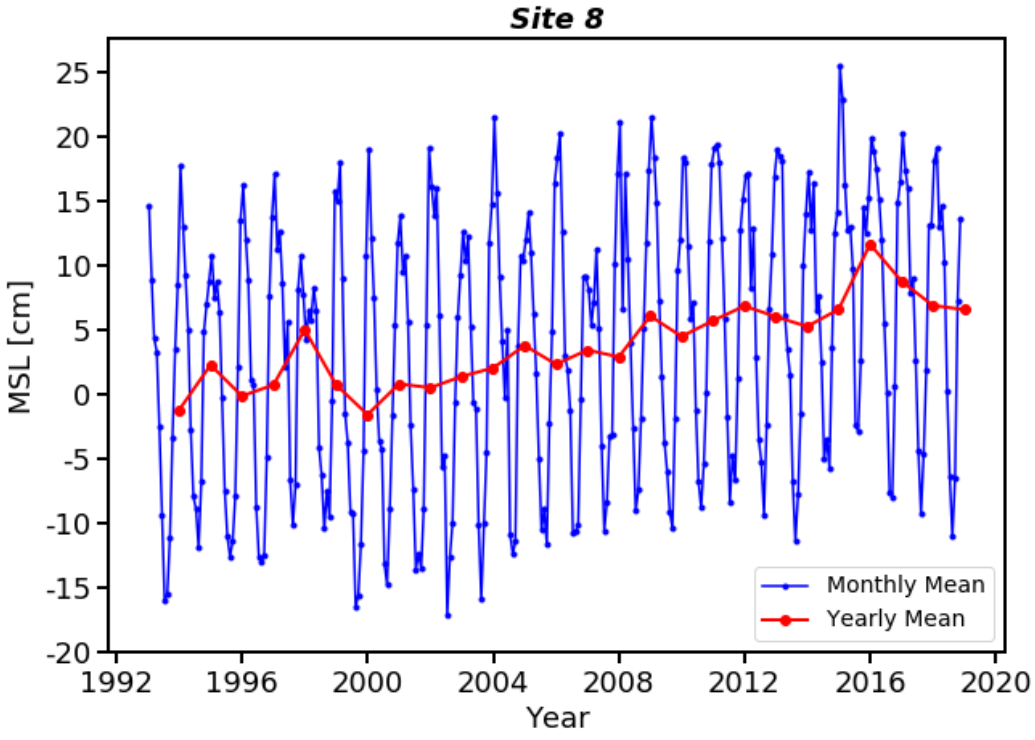

Figure 4.57. E. Monthly and yearly MSL from 1993 to 2018 at Site 8

CHAPTER 5

DISCUSSION

Along the southwest coast of India, coastal upwelling is observed to be an annually recurring phenomenon associated with the summer monsoon. Many studies showed that the climate change impacts regional and global oceanographic processes such as SST-wind pattern which can alter the upwelling dynamics. The study is focused on upwelling off the southwest coast of India. The model results prove the importance of wind in the southeast Arabian Sea upwelling. The long-term changes in the upwelling indices are analyzed and the major factors which influence the spatio-temporal variations in the upwelling along the coast are identified from the study.

5.1. WIND, THE PRIMARY INDUCER OF UPWELLING

The model output proves the importance of wind in southeast Arabian Sea upwelling. The cooling of the surface water during the monsoon season was found to be higher when compared with the results in the absence of wind. This proves that the upwelling off the southwest coast of India occurs as a result of wind-induced Ekman divergence. In fact, the model was simulated with and without wind condition only, all other parameters like, heat flux, precipitation, air temperature, open boundary forcing, humidity etc were included in the model. However, in the absence of wind, cooling of the coastal water is observed during June-September. But the extent of cooling was lower than that of the 'wind off' condition. This cooling can be attributed to the southwest monsoon precipitation during the period. Similarly, when looked at the vertical transect plot of water temperature at Kochi, the surfacing of 26°C isotherm is evident for 'wind on' condition while the uplifting of isotherms is negligible for 'wind off' condition. Similar results were proposed by Seena et al., (2019) which highlighted the influence of wind on the plume transport. The model was ran for 'with wind' and 'without wind' condition. In the presence of wind, the plume appeared to propagate to the north throughout the year irrespective of the seasons. When the effects of wind are nullified, the effect of the earth's rotation forced the plume to move to the right and the mixing of the plume with the oceanic water was considerably lower than the normal condition. The results from this study confirm that

the upwelling is primarily resulted from the wind-induced Ekman divergence but there may be some other parameters which support the uplifting of water. More experimental studies are required to discover the favorable parameters of upwelling phenomena.

5.2. CLIMATOLOGY OF THE SOUTHEAST ARABIAN SEA UPWELLING

Southwest coast of India features wind-induced upwelling, which is a well-known phenomenon with the availability of fish landings. During the southwest monsoon, the wind is south-westerly over the most parts of the Arabian Sea. Moving towards the southwest and southern coast of India, the direction changes to north-westerly and westerly respectively, which are almost parallel to the coast, thereby favoring upwelling along the region. The climatology of upwelling indices revealed that the upwelling along the southeast Arabian Sea coincides with the summer monsoon months (June-September) and is expected to commence in June, starting from the southern part of the coast, eventually spreading northward (McCreary, Kundu and Molinari, 1993; Smitha et al., 2008). The maximum upwelling is found to occur at the southern coast where the wind is the strongest which reaches up to 8-9 ms^{-1} and blows nearly tangential to the coast for most of the period. Upwelling intensity is decreasing towards the north with the direction of wind turning to be more westerly.

The wind along the coast starts to intensify from February onwards and the direction is mostly northerly along the southwest coast while it is north-easterly along the southern coast. The wind begins to blow from the northwest along the southwest coast from April onwards with the intensity of wind rising the following months. The strongest wind is usually observed during July-August after which it starts to weaken and so is the pattern of the offshore Ekman transport. This is in compliance with the upwelling pattern proposed by Gupta et al. (2016). The strongest upwelling is perceived at Site 3 of the study where the highest wind speed is observed and the wind was nearly parallel to the coast. The upwelling intensity is observed to be different at Site 2 and 4 even though the wind is stronger on either site. This confirms that upwelling intensity is influenced by the strength as well as the direction of the wind with respect to the coast. Along the southwest and southern coast of India, the upwelling favorable wind is north westerly and westerly respectively.

The upwelling will significantly affect the variation of SST as the bottom cooled water is piled up to the surface. The highest SST in the southeast Arabian Sea is observed in the month of

May. The SST along the coast begins to cool from May onwards which happens to coincide with the upwelling period. The spatio-temporal variation of the Ekman transport was similar to the SST, which initiates to cool off starting from the south, gradually spreading northward and the minimum SST is found to occur in August, after which the water starts to warm up again (McCreary et al., 1993). The climatology of MSL anomaly shows changes corresponding to the changes in SST. The LTA values also showed an increase starting from March onwards which suggests the cooling of coastal waters and the value is found to peak during July-August. The maximum anomaly is usually observed at Site 3, followed by Site 4 and these results are in compliance with that from the Ekman transport. But at Site 1 and Site 2, the LTA was observed to be usually negative during the monsoon season even though a rise is observed during the period. The LTA is also observed to be reducing northward but at Site 7, a slightly higher value is observed when compared to Site 5 and Site6. The reference isotherm (26°C), which is taken to be the base of the Mixed Layer, showed upward slopping during the monsoon period. This upslopping of isotherms is solely driven by the Ekman pumping. So the upwelling is the strongest where the upslopping is the most prominent. From the climatology of isotherms, the upwelling is observed to be more prominent within the 50 km distance from the coast. At Site 1 and Site 2, the isotherms were not clearly visible at 20 km distance from the coast and this can be attributed to the mixing of water due to wave and wind action at the region. This mixing would also affect the LTA values as it alters the SST of the region. The coastal and offshore SST at this region is observed to be almost similar due to the mixing, which is reflected in the LTA values also. The upslopping of isotherms becomes more prominent from Site 1 to Site 3 and the strongest upwelling signals are found at Site 3. At Site 4, the upwelling was stronger at 20 km distance from the coast but at 50 km distance, the upwelling signals were weaker when compared to Site 5. When looked from the south to north, a lag is observed for the isotherm to reach the minimum depth. This confirms that the upwelling starts from the southern coastal region and gradually progresses northwards. At Site 7, the upslopping was more prominent when compared to Site 5 and Site 6. Similar results are also observed from LTA. These spatial variations in the upwelling indices can be attributed to the varying bathymetry features along the southwest coast.

The climatology of NPP suggests an increase along the coast starting from May but the maximum value is observed during September after which it begins to decline. This lag can be attributed to the time taken for the primary production. Study conducted by Rajagopalan et al.

(1992) revealed that along the Cochin inshore waters, the most favorable condition for maximum NPP is observed to occur during the post-monsoon season. The study also confirmed that enhanced rainfall favors NPP to a certain level, beyond which the fresh water influx turns out to be unfavorable. They also suggested that the nutrients brought by coastal upwelling has significant role in primary productivity than that brought by fresh water discharge.

5.3. SPATIAL VARIATIONS

It can be understood from the windrose charts that the strongest wind is observed at Site 3, followed by Site 4 and Site 2. The strongest offshore Ekman transport is also observed along these sites. The Ekman transport is found to reduce northward. From Site 3 to Site 7, the wind speed is observed to reduce. This reduction in wind speed is also observed in the Ekman transport. From Site 7 to Site 9 an increase is noted in the wind speed but the Ekman transport is observed to decrease further. This reduction in the Ekman transport even though the wind is strengthening can be attributed to the change in the wind direction with respect to the coast. From the south to north, the wind becomes less parallel to the coast, with the wind direction still being similar, due to the inclination of the Indian coast of about 24° from the true north. At Site 10, the wind becomes almost westerly and nearly perpendicular to the coast.

Even though the Ekman transport at Site 2 shows higher values than that of Site 4, all the other upwelling indices imply that the highest upwelling intensity is observed at Site 3, followed by Site 4. The upwelling weakens from the south to north, that is, from Site 3 to Site 10. At Site 1 and Site 2, the LTA showed negative values during most of the years. This anomaly in the signals received from LTA might be due to the mixing of the water due to wind and wave action. Similar LTA values at both the offshore stations imply that the upwelling usually confines within the 1° distance. But the climatology of isotherms showed highest upwelling signals within 50 km to the offshore from the coast. Hence, it can be noted that the upwelling is confined within 50 km offshore from the coast but this upwelled water move further offshore, thereby affecting the SST further offshore. The movement of the upwelled water further offshore explains the similar SST at 1° and 2° distance from the coast.

In case of NPP, relatively higher values during June-September was found at Site 5 but the values show high temporal and spatial fluctuations, given that the climatology showed greatest NPP during the month of October. All the upwelling indices points out that the

maximum upwelling is observed at the southern coast of India which reduces towards the north. The upwelling signals become almost negligible at Site 10. So the upwelling extent along the southwest coast is confined within 7°N to 14°N latitudes (Smitha et al., 2014).

Figure 4.47 showed the monthly marine fish catch for each coastal districts of Kerala for the period of 2007 to 2018. From the figure, it can be observed that the reported marine fish landing is high along the coasts of Ernakulam, Kollam and Kozhikode and the lowest catch was reported along Kasargode coast throughout the period. The highest fish landing along the southwest coast of India is observed during the monsoon season. However, due to the existing trawl ban during the summer monsoon months, the actual fishery potential cannot be derived from the data.

5.4. LONG-TERM VARIATIONS IN UPWELLING INDICES

Bakun (1990) suggested an enhancement of offshore Ekman transport and the associated upwelling due to climate change and global warming which would result in the intensification of the upwelling favorable winds. This theory was later corrected by Hsieh and Boer (1992) who suggested that the impact of climate change on coastal upwelling varies regionally.

Figure 4.51 showed the monthly and yearly mean wind speed during 1979-2018. Even though inter-annual variations are visible, the wind speed along the coast did not show any significant trend for the past four decades. Similarly, no significant trend can be observed from the monthly and yearly mean SST along the coast. But during the very strong El Nino years of 1997-1998 and 2015-2016, a sudden increase in annual SST is observed. After these events, a reduction in SST is also observed for one or two years. Similar pattern is also visible in the annual MSL anomaly. But unlike the wind speed and SST, the MSL anomaly showed an increasing trend from 1993 to 2015 and afterwards, a continuous reduction is observed. Swapna et al. (2017) pointed out an increasing trend in the north Indian Ocean sea level during the last 3-4 decades, especially in the Arabian Sea, the reason for which is attributed to the enhanced heat storage due to reduced southward heat transport as a result of weakening monsoon circulation. The highest MSL anomaly is observed in 2015. After the sudden rise in MSL during 1997-1998 and 2015-2016 very strong El Nino event, a continuous reduction is noted for two or three consecutive years. The MSL also seems to rise during positive IOD events. According to the observed MSL pattern since 1993, a further rise in MSL can be expected in the future even

though a reduction is observed after 2015. When compared with the 1997-1998 El Nino event, this reduction in MSL might be temporary. The La Nina and negative IOD events do not seem to have particular impact on these parameters.

From the long-term analysis of the parameters, no significant trend is noted in the upwelling intensity along the southwest coast of India for the past 3-4 decades. But the study conducted by Manjusha et al. (2013) found nearly 50% increase in the coastal upwelling indices along the southwest coast of India during 1998-2007. Even though the MSL showed an increasing trend, it does not seem to impact the southeast Arabian Sea upwelling. Considerable inter-annual variations can be observed throughout the study period.

5.5. INTER-ANNUAL VARIATIONS IN UPWELLING INDICES

Table 4.1 showed ENSO years during 1979 to 2018. It can be seen from the table that most of the El Nino years are followed by La Nina events, whether weak, moderate or strong. The years 1982-1983, 1997-1998 and 2015-2016 experienced very strong El Nino events. The 1997-1998 El Nino was followed by a strong La Nina event which prolonged for three consecutive years. Most of the El Nino events are accompanied by an IOD event as strong El Nino is expected to trigger the development of IOD (Roxy et al., 2011). During 2006-2008, three consecutive positive IOD events were reported with the strongest one in 2006 (Iskandar et al., 2013). During this period, the LTA at Site 2 showed positive values indicating a stronger upwelling along the region. The MSL during the monsoon season showed an increase during these positive IOD years. No significant changes can be observed in other upwelling indices.

After a mature phase of El Nino, a basin-wide warming is expected to occur in the Indian Ocean (Nigam and Shen, 1993). It can be clearly seen from the figure 4.53 that the ENSO has an impact on the southeast Arabian Sea SST. The June to September mean SST tends to increase during an El Nino year while it tends to decrease during La Nina year. During the prolonged La Nina events of 1973-1976 and 1998-2001, the southwest tropical Indian Ocean showed maximum cooling (Singh et al., 2013). It can also be observed from the results that the SST showed continuous reduction during 1998-2001. D26 was observed to be deeper during the El Nino years, probably due to the rise in SST. The changes in the Indo-Pacific Walker circulation induced by the resulting SST variability in the western tropical Indian Ocean due to ENSO, delay

the Indian summer monsoon (Annamalai et al., 2005). This delay can probably affect the seasonal upwelling in the Indian Ocean.

El Nino induces anomalous anti-cyclonic circulation over the southeastern Indian Ocean which brings about some changes in the climatological winds (Roxy et al., 2011). The wind speed is found to decrease during El Nino and so is the upwelling. This is also evident from the reduction in LTA during 2015. There was a remarkable reduction in wind speed and Ekman transport during 1997 and 2015 which then strengthened the following year. The highest variation in the wind speed was observed at the southern region. Ekman transport during the period 2000-2018 was found to be the strongest in 2016. Figure 4.48 shows the wind speed variation with latitude for the entire study area. It can be seen from the figure that the strongest wind during June-September for the period was found during 2018 and 2013 and the wind intensity increases to the north. A reduction in the wind speed was also observed in 2017. This was soon after the MHW across northern Australia which might have influenced the SST over the Indian Ocean and thereby reduce the wind speed.

Study by Rao et al. (2010) revealed that the annual variations in equatorial zonal winds are expected to reflect in the MSL through the eastward propagating Kelvin waves. The ENSO events are observed to bring about changes in the equatorial zonal winds. The MSL is expected to be high during El Nino and low during La Nina corresponding to the SST changes. Even though MSL is observed to be high during El Nino years, it is not observed to fall during all the La Nina events. This deviation from the expected fall in MSL might be attributed to the precipitation and river discharge which compensate the decrease in MSL. As per the observed SST pattern during 2000-2018 summer monsoon months, the MSL is expected to show reduction from the previous year level in 2007 and 2011 since those were strong La Nina years, but instead, it is observed to rise or remain the same as that of the previous year. These years are reported to have positive deviation of precipitation from the normal and this might be considered as the reason for the variation in the expected sea level change. But the study conducted by Shetye (2016) stated that the sea level at Veraval, Marmagao and Cochin is observed to decrease during the monsoon period when the rainfall is considerably high which suggest that the contribution of rain water runoff to the sea level change is small. So, another possible reason for this deviation might be that the La Nina fails to cool the western Indian Ocean to the same extent

that the El Nino warms the western Indian Ocean as proposed by Roxy et al. (2016) which fails to reduce the sea level as expected.

The IOD is not observed to have significant influence on the upwelling indices except MSL. The MSL is found to rise during positive IOD years. When IOD coincide with an ENSO event, the impact of IOD is overcome by the influence of ENSO. 2012 was solely a positive IOD event and during that year, an increase in wind speed is noted. But this is not sufficient to conclude the effect of IOD on the upwelling off the southwest coast.

CHAPTER 6

SUMMARY AND CONCLUSION

Coastal upwelling along the southwest coast of India is an annually recurring phenomenon associated with the summer monsoon and is considered to have significant influence on the fishery potential of this region. The study confirms that the upwelling along the southwest coast of India is induced by wind-driven Ekman divergence during the monsoon season. The wind intensity as well as the direction of wind with respect to the coast turns out to be an important factor which influence the upwelling intensity. The wind along the southwest coast during summer monsoon is found to be north-westerly while it blows from the southwest over the rest of the Arabian Sea. The wind is westerly along the southern coast of India. This along-shore wind is the primary reason for the recurrence of upwelling along the coast. The phenomenon is observed to initiate with the onset of monsoon in June, peak by July-August and subside by September. The strongest upwelling along the coast is observed to occur at the southern latitudes where the wind speed is the highest and the wind is most parallel to the coast. The intensity is found to decrease northward. But a reduction in upwelling signals is observed between Kollam and Kochi coasts. This might be due to the variations in the bathymetry along the coast. The upwelling is confined within 50 km distance offshore from the coast but the upwelled water is found to move further offshore up to 2-3° offshore.

The analysis of upwelling indices for a period of 19 years, from 2000-2018 did not show any significant changes but showed considerable inter-annual variations. When the inter-annual variations in the upwelling indices are analyzed, it revealed that the wind speed over the southeastern Arabian Sea decreases during a strong El Nino event and so does the upwelling. But this reduction is found to recover during the succeeding year. So it can be noted that the El Nino has a temporary impact on the coastal upwelling in the southeast Arabian Sea. But there might be a possibility that the increased incidence of El Nino in the future can bring about permanent changes in the upwelling intensity. Further studies must be required to prove the exact impact of increased El Nino events. The La Nina and IOD events do not seem to particularly impact the upwelling intensity.

The maximum NPP is found to occur after the peak monsoon period and this time lag corresponds to the time taken for the primary production. The monthly marine fish landings along the Kerala coast showed higher landings during the monsoon season. But due to the existing trawl ban during this period, it is not possible to derive the exact fishery potential of the region from this data. The coasts of Kollam, Ernakulam and Kozhikode showed the highest fish landings. Most of the districts showed an increasing trend in the fish landings during the monsoon season from 2016 onwards.

The SST and wind speed during the summer monsoon months during the past 3-4 decades revealed no considerable variations, but the MSL is found to be on rise from 1993 to 2015. After 2015, a continuous reduction is observed. But when compared to the 1997-1998 very strong El Nino event, the continuous reduction in MSL after 2015-2016 El Nino event can be expected to be temporary. The MSL might continue to rise in the future. This rise in MSL does not seem to affect the upwelling intensity.

REFERENCES

Annamalai, H., Liu, P. and Xie, S. P., 2005. Southwest Indian Ocean SST variability: Its local effect and remote influence on Asian monsoons. *J. Clim.* 18(20), pp.4150-4167.

Bakun, A., 1990. Global climate change and intensification of coastal ocean upwelling. *Science*, *247*(4939), pp.198-201.

Bakun, A., Black, B.A., Bograd, S.J., Garcia-Reyes, M., Miller, A.J., Rykaczewski, R.R. and Sydeman, W.J., 2015. Anticipated effects of climate change on coastal upwelling ecosystems. *Curr. Clim. Chang. Reports*, *1*(2), pp.85-93.

Behrenfeld, M.J., Boss, E., Siegel, D.A. and Shea, D.M., 2005. Carbon-based ocean productivity and phytoplankton physiology from space. *Global biogeochemical cycles*, *19*(1).

Cadet, D.L., 1985. The southern oscillation over the Indian Ocean. *J. climatol.*, *5*(2), pp.189-212.

Central Marine Fisheries Research Institute. 2019. CMFRI Annual Report 2017-18.

Central Marine Fisheries Research Institute. 2019. CMFRI Annual Report 2018-19.

Chen, G., Han, W., Li, Y. and Wang, D., 2016. Interannual variability of equatorial eastern Indian Ocean upwelling: Local versus remote forcing. *J. of Physl Oceanogr. 46*(3), pp.789-807.

Cheung, W.W. and Frölicher, T.L., 2020. Marine heatwaves exacerbate climate change impacts for fisheries in the northeast Pacific. *Scientific reports*, *10*(1), pp.1-10.

Dong, L. and McPhaden, M.J., 2016. Interhemispheric SST gradient trends in the Indian Ocean prior to and during the recent global warming hiatus. *Journal of Climate*, *29*(24), pp.9077-9095.

Frölicher, T.L., Fischer, E.M. and Gruber, N., 2018. Marine heatwaves under global warming. *Nature*, *560*(7718), pp.360-364.

Garvine, R.W., 1971. A simple model of coastal upwelling dynamics. *J. of Phys Oceanogr. 1*(3), pp.169-179.

George, J.V., Nuncio, M., Chacko, R., Anilkumar, N., Noronha, S.B., Patil, S.M., Pavithran, S., Alappattu, D.P., Krishnan, K.P. and Achuthankutty, C.T., 2013. Role of physical processes in chlorophyll distribution in the western tropical Indian Ocean. *Journal of Marine Systems*, *113*, pp.1-12.

Grunseich, G., Subrahmanyam, B., Murty, V.S.N. and Giese, B.S., 2011. Sea surface salinity variability during the Indian Ocean Dipole and ENSO events in the tropical Indian Ocean. *Journal of Geophysical Research: Oceans*, *116*(C11).

Gupta, G.V.M., Sudheesh, V., Sudharma, K.V., Saravanane, N., Dhanya, V., Dhanya, K.R., Lakshmi, G., Sudhakar, M. and Naqvi, S.W.A., 2016. Evolution to decay of upwelling and associated biogeochemistry over the southeastern Arabian Sea shelf. *Journal of Geophysical Research: Biogeosciences*, *121*(1), pp.159-175.

Hidaka, K., 1954. A contribution to the theory of upwelling and coastal currents. *Eos, Transactions American Geophysical Union*, *35*(3), pp.431-444.

Hsieh, W.W. and Boer, G.J., 1992. Global climate change and ocean upwelling. *Fisheries Oceanography*, *1*(4), pp.333-338.

Iskandar, I., Irfan, M. and Saymsuddin, F., 2013. Why was the 2008 Indian Ocean Dipole a short-lived event?. *Ocean Science Journal*, *48*(2), pp.149-160.

Iskandar, I., Sasaki, H., Sasai, Y., Masumoto, Y. and Mizuno, K., 2010. A numerical investigation of eddy-induced chlorophyll bloom in the southeastern tropical Indian Ocean during Indian Ocean Dipole—2006. *Ocean Dynamics*, *60*(3), pp.731-742.

Jayaram, C., Chacko, N., Joseph, K.A. and Balchand, A.N., 2010. Interannual variability of upwelling indices in the southeastern Arabian Sea: a satellite based study. *Ocean Sci. J. 45*(1), pp.27-40.

Manjusha, U., Jayasankar, J., Remya, R., Ambrose, T.V. and Vivekanandan, E., 2013. Influence of coastal upwelling on the fishery of small pelagics off Kerala, south-west coast of India. *Indian Journal of Fisheries*, *60*(2), pp.37-42.

Manyilizu, M., Penven, P. and Reason, C.J.C., 2016. Annual cycle of the upper-ocean circulation and properties in the tropical western Indian Ocean. *African Journal of Marine Science*, *38*(1), pp.81-99.

McCreary Jr, J.P., Kundu, P.K. and Molinari, R.L., 1993. A numerical investigation of dynamics, thermodynamics and mixed-layer processes in the Indian Ocean. *Prog. Oceanogr. 31*(3), pp.181-244.

Meyers, G., McIntosh, P., Pigot, L. and Pook, M., 2007. The years of El Niño, La Niña, and interactions with the tropical Indian Ocean. *J. Clim. 20*(13), pp.2872-2880.

Miyakawa, T., Yashiro, H., Suzuki, T., Tatebe, H. and Satoh, M., 2017. A Madden-Julian Oscillation event remotely accelerates ocean upwelling to abruptly terminate the 1997/1998 super El Niño. *Geophysical Research Letters*, *44*(18), pp.9489-9495.

Narayan, N., Paul, A., Mulitza, S. and Schulz, M., 2010. Trends in coastal upwelling intensity during the late 20th century. *Ocean Sci. Discussions*, *7*(1).

Nigam, S. and Shen, H.S., 1993. Structure of oceanic and atmospheric low-frequency variability over the tropical Pacific and Indian Oceans. Part I: COADS observations. *Journal of climate*, *6*(4), pp.657-676.

Oliver, E.C., Donat, M.G., Burrows, M.T., Moore, P.J., Smale, D.A., Alexander, L.V., Benthuysen, J.A., Feng, M., Gupta, A.S., Hobday, A.J. and Holbrook, N.J., 2018. Longer and more frequent marine heatwaves over the past century. *Nature communications*, *9*(1), pp.1-12.

Praveen, V., Ajayamohan, R.S., Valsala, V. and Sandeep, S., 2016. Intensification of upwelling along Oman coast in a warming scenario. *Geophysical Research Letters*, *43*(14), pp.7581-7589.

Price, J.F., Weller, R.A. and Schudlich, R.R., 1987. Wind-driven ocean currents and Ekman transport. *Science*, *238*(4833), pp.1534-1538.

Rahmstorf, S. and Coumou, D., 2011. Increase of extreme events in a warming world. *Proceedings of the National Academy of Sciences*, *108*(44), pp.17905-17909.

Rajagopalan, M.S., Thomas, P.A., Mathew, K.J., Selvaraj, G.D., George, R.M., Mathew, C.V., Naomi, T.S., Kaladharan, P., Balachandran, V.K. and Antony, G., 1992. Productivity of the Arabian Sea along the southwest coast of India. *CMFRI Bulletin*, *45*, pp.9-37.

Rao, R.R., Kumar, M.G., Ravichandran, M., Rao, A.R., Gopalakrishna, V.V. and Thadathil, P., 2010. Interannual variability of Kelvin wave propagation in the wave guides of the equatorial Indian Ocean, the coastal Bay of Bengal and the southeastern Arabian Sea during 1993–2006. *Deep Sea Research Part I: Oceanographic Research Papers*, *57*(1), pp.1-13.

Rao, S.A., Dhakate, A.R., Saha, S.K., Mahapatra, S., Chaudhari, H.S., Pokhrel, S. and Sahu, S.K., 2012. Why is Indian Ocean warming consistently?. *Climatic change*, *110*(3-4), pp.709-719.

Roxy, M., Gualdi, S., Drbohlav, H.K.L. and Navarra, A., 2011. Seasonality in the relationship between El Nino and Indian Ocean dipole. *Climate dynamics*, *37*(1-2), pp.221-236.

Roxy, M.K., Modi, A., Murtugudde, R., Valsala, V., Panickal, S., Prasanna Kumar, S., Ravichandran, M., Vichi, M. and Lévy, M., 2016. A reduction in marine primary productivity driven by rapid warming over the tropical Indian Ocean. *Geophysical Research Letters*, *43*(2), pp.826-833.

Roxy, M.K., Ritika, K., Terray, P. and Masson, S., 2014. The curious case of Indian Ocean warming. *J. Clim. 27*(22), pp.8501-8509.

Saji, N.H., Goswami, B.N., Vinayachandran, P.N. and Yamagata, T., 1999. A dipole mode in the tropical Indian Ocean. *Nature*, *401*(6751), pp.360-363.

Shetye, S.R. and Almeida, A.M., 1985. An examination of the factors that influence the monthly-mean sea level along the coast of India. In *IOC/Unesco workshop on regional co-operation in marine science in the central Indian ocean and adjacent seas and gulfs, Colombo, Sri Lanka, IOC workshop reports* (Vol. 37, pp. 87-104).

Singh, P., Chowdary, J.S. and Gnanaseelan, C., 2013. Impact of prolonged La Niña events on the Indian Ocean with a special emphasis on southwest Tropical Indian Ocean SST. *Glob. and planet. change*, *100*, pp.28-37.

Smitha, A., Joseph, K.A., Jayaram, C. and Balchand, A.N., 2014. Upwelling in the southeastern Arabian Sea as evidenced by Ekman mass transport using wind observations from OCEANSAT–II Scatterometer. *Indian J. Geomarine. Sci. 43*(1), pp.111-116.

Smitha, B.R., 2010. Coastal upwelling of the South Eastern Arabian sea: an integrated approach.

Smitha, B.R., Sanjeevan, V.N., Vimalkumar, K.G. and Revichandran, C., 2008. On the upwelling off the southern tip and along the west coast of India. *J. Coast. Res. 24*(sp3), pp.95-102.

Sreenivas, P., Gnanaseelan, C. and Prasad, K.V.S.R., 2012. Influence of El Niño and Indian Ocean Dipole on sea level variability in the Bay of Bengal. *Global and Planetary Change*, *80*, pp.215-225.

Swapna, P., Jyoti, J., Krishnan, R., Sandeep, N. and Griffies, S.M., 2017. Multidecadal weakening of Indian summer monsoon circulation induces an increasing northern Indian Ocean sea level. *Geophysical Research Letters*, *44*(20), pp.10-560.

Tozuka, T., Nagura, M. and Yamagata, T., 2014. Influence of the reflected Rossby waves on the western Arabian Sea upwelling region. *Journal of physical oceanography*, *44*(5), pp.1424-1438.

Varela, R., Álvarez, I., Santos, F., DeCastro, M. and Gómez-Gesteira, M., 2015. Has upwelling strengthened along worldwide coasts over 1982-2010?. *Scientific reports*, *5*(1), pp.1-15.

Wang, J. and Yuan, D., 2015. Roles of western and eastern boundary reflections in the interannual sea level variations during negative Indian Ocean dipole events. *Journal of Physical Oceanography*, *45*(7), pp.1804-1821.

Westberry, T., Behrenfeld, M.J., Siegel, D.A. and Boss, E., 2008. Carbon-based primary productivity modeling with vertically resolved photoacclimation. *Global Biogeochemical Cycles*, *22*(2).

XIE, L. and HSIEH, W.W., 1995. The global distribution of wind-induced upwelling. *Fish. Oceanogr. 4*(1), pp.52-67.

Xie, S.P., Annamalai, H., Schott, F.A. and McCreary Jr, J.P., 2002. Structure and mechanisms of South Indian Ocean climate variability. *J. Clim. 15*(8), pp.864-878.

Yuan, D., Wang, J., Xu, T., Xu, P., Hui, Z., Zhao, X., Luan, Y., Zheng, W. and Yu, Y., 2011. Forcing of the Indian Ocean dipole on the interannual variations of the tropical Pacific Ocean: roles of the Indonesian throughflow. *Journal of Climate*, *24*(14), pp.3593-3608.

ABSTRACT

Upwelling along the southwest coast of India is an annually recurring phenomenon associated with the summer monsoon. The study was conducted to understand the long-term changes in the southeastern Arabian Sea upwelling and to identify the factors that influence the spatio-temporal variation in upwelling intensity. Finite Volume Community Ocean Model (FVCOM) has run for two conditions, 'wind on' and 'wind off' condition. The model results prove that the upwelling off the southwest coast of India is a classical wind-driven upwelling system. The analysis of upwelling indices for a period of 19 years, from 2000 to 2018 did not show any noticeable trend but showed considerable inter-annual variations. The spatial variations in the upwelling along the coast can be attributed to the variations in the bathymetry. The southeast Arabian Sea upwelling is affected by El Nino, but the La Nina and IOD events does not appear to influence the upwelling significantly. The long-term analysis of Sea Surface Temperature (SST) and wind speed during the past 3-4 decades has not shown any significant trend. The Mean Sea Level (MSL) during June-September showed a rising trend during the past two decades. But this rise in MSL does not seem to affect the upwelling off the southwest coast of India.